AD_____

AWARD NUMBER: W81XWH-08-1-0357

TITLE: MR-Guided Near Infrared Spectroscopy for Reducing Breast Cancer False Positives

PRINCIPAL INVESTIGATOR: Colin Carpenter

CONTRACTING ORGANIZATION: Dartmouth College
Hanover, NH 03755

REPORT DATE: September 2009

TYPE OF REPORT: Annual Summary

PREPARED FOR: U.S. Army Medical Research and Materiel Command
Fort Detrick, Maryland 21702-5012

DISTRIBUTION STATEMENT: Approved for Public Release;
Distribution Unlimited

REPORT DOCUMENTATION PAGE

Form Approved
OMB No. 0704-0188

1. REPORT DATE	2. REPORT TYPE	3. DATES COVERED
1 September 2009	Annual Summary	1 May 2008- 31 Aug 2009

4. TITLE AND SUBTITLE

MR-Guided Near Infrared Spectroscopy for Reducing Breast Cancer False Positives

5a. CONTRACT NUMBER

5b. GRANT NUMBER
W81XWH-08-1-0357

5c. PROGRAM ELEMENT NUMBER

6. AUTHOR(S)

Colin Carpenter

E-Mail: colincarpenter@stanford.edu

5d. PROJECT NUMBER

5e. TASK NUMBER

5f. WORK UNIT NUMBER

7. PERFORMING ORGANIZATION NAME(S) AND ADDRESS(ES)

Dartmouth College
Hanover, NH 03755

8. PERFORMING ORGANIZATION REPORT NUMBER

9. SPONSORING / MONITORING AGENCY NAME(S) AND ADDRESS(ES)
U.S. Army Medical Research and Materiel Command
Fort Detrick, Maryland 21702-5012

10. SPONSOR/MONITOR'S ACRONYM(S)

11. SPONSOR/MONITOR'S REPORT NUMBER(S)

12. DISTRIBUTION / AVAILABILITY STATEMENT
Approved for Public Release; Distribution Unlimited

13. SUPPLEMENTARY NOTES

14. ABSTRACT

This project investigated the relationship between optical and magnetic resonance (MR) breast imaging, with the goal of reducing false positives resulting from MR mammography. MR-guided Diffuse Optical Imaging (MRg-DOI), which combines the high sensitivity of breast MR with quantitative images of tissue physiology, may improve differentiation between benign and malignant lesions. This work developed a unique MR breast coil-coupled fiber interface to improve data quality and increase the adjustability of fiber positioning. This platform enabled multi-planar, patient-specific fiber arrangements to optimize data quality. To correct for the deficiencies of optical photodetectors in quantifying water, MR water/fat (DIXON) imaging was used to reduce hemoglobin/water crosstalk and improve hemodynamic quantification by at least 20%. Next, this study investigated the correlation between hemodynamics determined both optical imaging and MRI. This work was the first demonstration of optical tomography and Blood Oxygen Level Dependent (BOLD) MRI in the breast. Results showed significant correlation in a study population of 13 women ($p<0.05$) when the appropriate respiratory challenge was used. Additionally, the respiratory challenge showed promise in imaging tumor vasculature characteristics in breast cancers. To comprehensively merge the MR data and optics, a combined optical/MR image reconstruction model was developed. This formulation provides a foundation to characterize breast lesions with higher temporal, spatial, and functional information than was previously available. In case studies, the MR-guided optical system correctly characterized malignant lesions, and in one case, correctly assessed a tissue region that was incorrectly identified by MRI as malignant.

15. SUBJECT TERMS
BREAST CANCER, IMAGING, HEMODYNAMICS, MR, CHEMOTHERAPY MONITORING, WATER FAT IMAGING, BOLD

16. SECURITY CLASSIFICATION OF:			17. LIMITATION OF ABSTRACT	18. NUMBER OF PAGES	19a. NAME OF RESPONSIBLE PERSON
a. REPORT	b. ABSTRACT	c. THIS PAGE			USAMRMC
U	U	U	UU	90	19b. TELEPHONE NUMBER *(include area code)*

Table of Contents

INTRODUCTION

The aim of this research project was to improve optical breast cancer imaging by merging advanced magnetic resonance imaging (MRI) sequences into optical imaging. This multimodality technique, known as Magnetic Resonance (MR)-guided Diffuse Optical Imaging (MRg-DOI), combines the high sensitivity of breast MR with images of tissue physiology, including blood content, oxygen saturation, and water fraction, which help differentiate benign and malignant lesions. This information has been shown to be highly specific to breast cancer with a standalone (non-MR guided) device [1, 2]. Since MR mammography has been shown to have a high false-positive rate, leading to unneeded invasive biopsy procedures [3], this project developed the foundations and methodology for combining these imaging modalities to achieve a highly sensitive, highly specific breast MR system.

One of the difficulties in MRg-DOI is integrating the optical fibers into the MR breast coil. Because of space limitations in the bore of the MRI and the different shapes of breast coils, coupling optical fibers to the breast tissue can be difficult. To improve fiber/breast coupling, a highly adaptive fiber positioning interface was constructed to improve data quality of MR-guided optics. This interface was built to mate to 3 different coils, including a custom designed MR breast coil that was developed in conjunction with Philips Medical Systems. Results from this slab geometry reveal an increase in useful data as compared to a circular geometry, and 16% greater contrast recovery in phantom experiments.

Optical imaging involves spectrally separating the light absorption effects caused by oxyhemoglobin, deoxyhemoglobin, and water. Insufficient spectral sampling, due either to inadequate photodetectors, or the desire to increase temporal resolution, can introduce errors in quantification. Often times, these errors arise in oxyhemoglobin, as oxyhemoglobin and water have similar spectral features. In this study, the photomultiplier photodetectors had inherent limitations in spectral sensitivity due to the wavelength dependent quantum efficiency of the photocathodes. With these detectors, SNR is insufficient for optical imaging in deep tissue above ~850nm. This results in significant cross-talk because the resulting water quantification is poor. To improve optical quantification, MR water/fat imaging was incorporated into the image reconstruction. Incorporating the water content improved the quantification of blood content and oxygen saturation by as much as 20% in experiments.

Optical tomography was correlated to Blood Oxygen Level Dependent (BOLD) MRI in the breast. This study addressed the inherent limitations of each of these modalities; although optical tomography is hampered by limited spatial (~5mm) and temporal (~3min) resolution, it is able to image both oxy and deoxyhemoglobin, which is not possible with BOLD MR. To enable this comparison, the system was modified to have a 6-fold reduction in imaging time. Results of this system in 13 women showed significant correlation ($p<0.05$) to BOLD, as long as the appropriate respiratory challenge was used. This correlation enables the possibility of integrating the high temporal and spatial BOLD data into optical imaging. This study also revealed new contrast possibilities for optical tomography, as the ability to image vasculature functional characteristics were demonstrated in healthy tissue and in breast cancers.

To merge these MR and optical contrasts, a comprehensive image formation model was developed to incorporate MR water/fat imaging, MR BOLD imaging, and MR anatomical. This methodology provides a foundation for quantitatively accurate physiological images with high temporal and spatial resolution.

These techniques were investigated in 5 cases: three lesions were malignant invasive ductal carcinomas (IDCs), one was a benign fibroadenoma, and one was an IDC that was pathologically determined to have fully responded to neoadjuvant chemotherapy. In one case, MRg-DOI was able to correctly assess a tissue region that was incorrectly identified by MRI as malignant.

The techniques developed in this pre-doctoral training program demonstrate the potential of MR-guided optics to characterize breast cancer, and to aid the understanding of MR contrasts. This project provided essential tools for a career in breast cancer research, including medical imaging software and hardware design, training in multimodality instrumentation and experimentation, and experience in the development of novel markers for cancer detection and therapy monitoring. The final outcomes from this work were a Ph.D. degree awarded in the Engineering Sciences, 2 peer-reviewed journal publications, 3 articles in preparation, 4 invited oral presentations, 2 co-authored journal articles, 6 conference proceedings, and a postdoctoral fellowship position attained at Stanford University.

BODY

The work completed during this fellowship completed the following aims:

Aim 1: The MRg-DOI fiber interface was redesigned to enable better fiber coupling to the tissue and higher data quality, in the breast coils of several manufacturers. This interface allows volumetric optical images of the breast to be captured without distorting the breast tissue boundary. A custom optical/MR breast coil was developed with Philips Medical Systems to provide optimal flexibility.

Aim 2: Spectroscopic (MR Water/Fat) and functional (Blood Oxygen Level Dependent) MR images were incorporated into the image reconstruction to improve optical quantification, and verify MR contrasts. BOLD contrast was used instead of VASO (Vascular Space Occupancy) contrast because the technique was more established and accepted in the MR community. This work lead to the investigation of vascular functional contrasts, which are new to breast DOI.

Aim 3: This aim was reduced to concentrate on the novel findings of Aim 2. Five subjects with abnormal mammograms were imaged during this study, and the results are presented below. Interaction with the pathologist and radiologists provided a more thorough understanding of the data, and the limitations of common practice. Additionally, a patient undergoing neoadjuvant chemotherapy was monitored with MRg-DOI, and the results are promising.

1. Advances in the optical fiber / MR coil interface

The first aim in this work was to improve data quality through advancements in patient interface design. The circular geometry that was originally developed for this instrument, shown in Figure 1a, was changed to a slab geometry, shown in Figure 1b, to improve upon several limitations of the circular geometry in optical imaging in the MR. The advantages of the slab geometry include better optical and

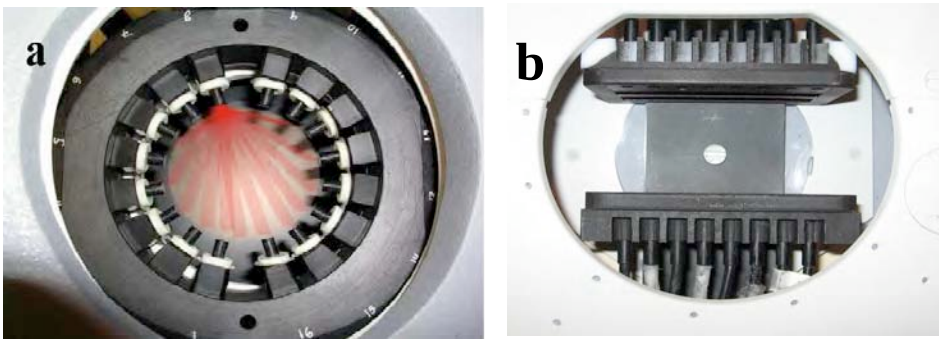

Figure 1: (a) Circular and (b) slab patient optical interface attached to MR breast coils with simulated optical overlays.

MR data quality, a more common clinical orientation, a more adaptable system to fit in different MR coils, and the ability to image multiple planes without distorting the breast shape. A 3D rapid

prototyping machine was used to print out grids from non-metallic plastic which were customizable for a specific fiber arrangement. These grids were painted black to avoid reflection of stray light within the interface.

The higher data quality is due to the slight compression utilized in the slab geometry, which is applied to conform the breast to the parallel plates. This geometry results in shorter optical pathlengths which corresponds to less signal loss. Thus this geometry increases the amount of data above the noise floor. For example, data from a tissue-mimicking phantom and a healthy subject showed that 20% more data may be used with the slab geometry. Most importantly, in the slab geometry, the optical pathlengths that pass through the region of interest have higher signal to noise. These source-detector pairs are critical to obtain accurate quantification in the region-of-interest. Investigating this issue further in tissue mimicking phantoms, this study revealed that the recovered error in optical properties was 16% lower in this slab geometry compared to the circular geometry.

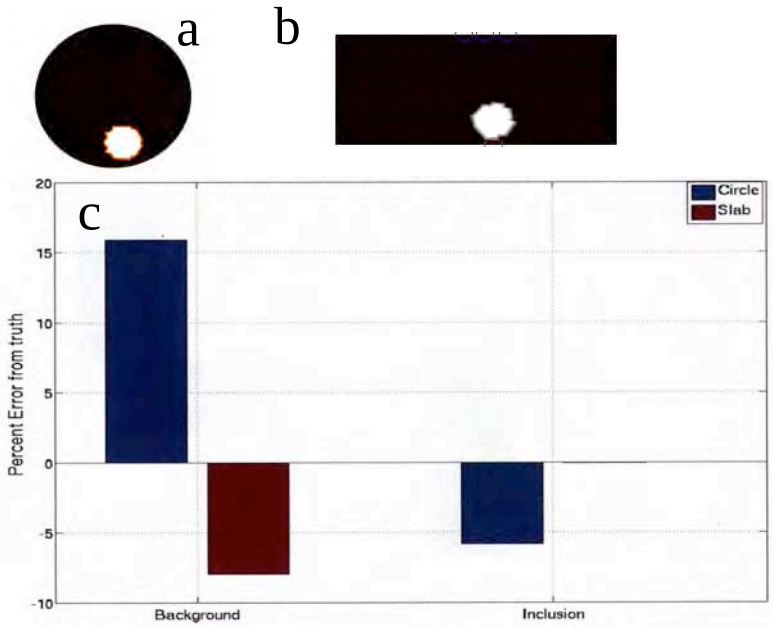

Figure 2: (c) Percent errors in contrast recovery between identical inclusions in the (a, blue) circular, and (b, red) slab geometries of resin phantoms. In the slab case, contrast recovery in the inclusion was accurate within 1%.

Another important issue in using the slab geometry is the ease in fiber positioning. By immobilizing the breast with a grid, fibers can be moved to probe several regions of interest without changing the breast shape. This allows image reconstructions with multiple planes of data without the expense and bulk of adding more planes of fibers to the interface. This advantage is critical in patient imaging because many lesions will not be located with MR until the contrast agent is administered, and any changes in breast volume after the injection will hinder accurate coregistration between the altered breast shape and the contrast enhanced MR dataset. Additionally, since breast immobilization is becoming more common in new breast coil designs, due to the reduction in patient motion, this design is more clinically viable than the circular design.

This geometry was shown to be more adaptable to breast coils from different manufacturers. The parallel-plate geometry was integrated into Philips and GE magnets by coupling the interface to coils made by Invivo and USA Instruments, respectively. Photographs are shown in Figure 3. The slab geometry was especially critical in coupling to the USA Instruments coil (Figure 3b) because access was possible in the sagittal plane only. This coil would not permit circular geometries.

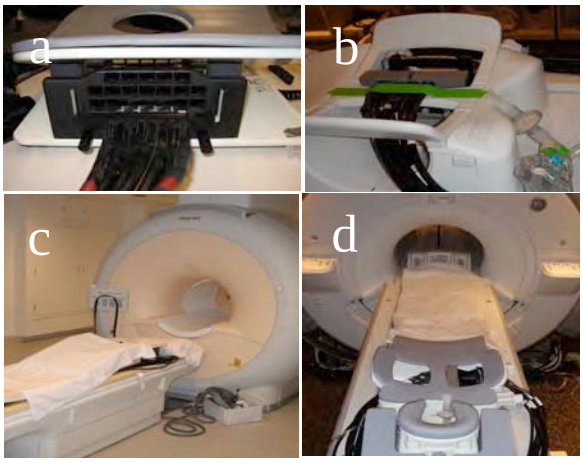

Figure 3: (a) Fiber interface integrated into an Invivo breast coil in a (b) Philips scanner, and (b) a USA Instruments coil in a (d) GE scanner.

Finally, to fully integrate this geometry into a coil, a custom MR breast coil was designed in collaboration with Philips Medical Systems, (Hamburg, GER) to facilitate optimal fiber positioning. This coil alleviated the space constraints in most commercial MR breast coils. The new breast coil, shown in Figure 4, moved the supports to the periphery to increase open space within the coil. A simple circular insert supports the optical holder and allows arbitrary rotation. We believe this new coil will offer the best opportunity to image suspect lesions in future exam sessions.

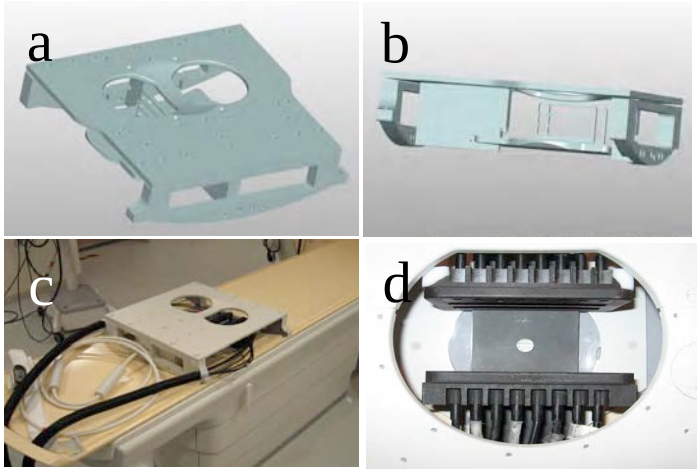

Figure 4: (a,b) Sketches (courtesy of Philips Medical Systems, Hamburg, GER) and (c,d) photographs of the optical/MR breast coil.

Aim 1 of this project resulted in a change from the circular geometry to the slab geometry. This geometry was found to be more adaptable, and improved data quality both for optical imaging and MR imaging (data not shown). The conclusion from this work is that slab geometries are more suitable for coupling to an MR coil. A fully integrated MR coil/fiber interface was constructed to carry out future studies.

2. Incorporating Spectroscopic and Functional MR

2a. Improving optical imaging through MR water/fat separation

Quantitative accuracy in optical imaging is greatly improved when using wavelengths that are most sensitive to the spectral features of the tissue chromophores [4]. However, wavelength choice is often

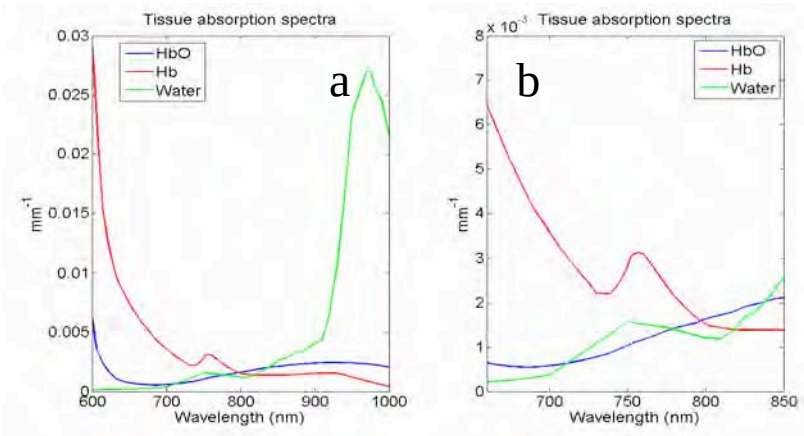

Figure 5: (a) Tissue absorption spectra for tissue optical properties of 20μM oxy-, 20μM deoxyhemoglobin, and 60% water. (b) Tissue absorption spectra within the sensitivity region of the PMTs. Note the spectral similarity between oxyhemoglobin and water.

limited by the spectral sensitivity of the photodetectors, or if higher temporal resolution is desired. These limitations may introduce crosstalk between different spectral contents, which introduces errors in quantification with optical imaging. In this study, the photomultiplier photodetectors used because of their high dynamic range, were insensitive to light above 850nm. Unfortunately, the spectral features of water in the near infrared are most pronounced above 850nm (with a spectral peak at ~975nm), shown in Figure 5. This lack of longer wavelengths will lead to errors in water quantification. Since the water spectrum overlaps with oxyhemoglobin in the spectral region of these photomultiplier tubes, there will be significant crosstalk, leading to quantification errors in total hemoglobin and oxygen saturation.

To improve quantification accuracy, this study used the MR's ability to accurately quantify water and fat to reduce the effects of crosstalk. By utilizing the quantitative images of water and fat, provided by the IDEAL MR sequence [5], hemoglobin recovery was shown to be at least 20% more accurate. Specifically, two reconstruction approaches were developed to incorporate the water and fat information. The *Direct Substitution* method was formulated to directly substitute the value of water and fat determined from the MR images into the optical reconstruction. In this method, it was assumed that the MR water and fat information were perfectly accurate. An alternative approach, the *Joint Weighted Estimation* (JWE) method, relaxed the assumption that the MR information was perfect. This approach was adopted because of the potential error in MR water/fat quantification, due to effects from T1 relaxation, inhomogeneous Rf excitation, and spectral deviations from the assumed spectral signatures [6].

The JWE approach used the Generalized Least Squares approach to the reconstruction [7], which includes a weighting term to account for the accuracy of the MR scanner in determining water and fat images. The advantage of this method is that it is robust to errors in MR quantification. This invariance to MR water errors is due to the fact that this method used both the MR and the optical data simultaneously to recover the water and fat properties. The weighting function was set based on the accuracy of the MR scanner used in this study.

These methods were tested in a 86mm diameter gelatin phantom, shown in Figure 6, with porcine blood added to mimic the optical properties of breast tissue. 2:1 contrast in oxyhemoglobin was added to a 15mm inclusion to simulate a breast tumor mass. Figure 6b shows the reconstructed errors in hemoglobin recovery when using 3 wavelengths in the reconstruction vs. using 6 wavelengths. The bars to the left of Figure 6b indicate reconstructions without MR water quantification, while the bars to the right incorporate MR water. These results show that using 3 wavelengths yields poorer recovered values of hemoglobin than using 6 wavelengths. This is expected, due to spectral undersampling. However,

when MR water is used to guide the water contrast, errors in hemoglobin recovery are significantly reduced, especially when only 3 wavelengths are used, as errors decrease by at least 20% in all cases. In one case (yellow bars), the non MR-water guided reconstruction recovers a 225% error due to its reliance on the 849nm wavelength, which is nearly beyond the sensitivity capabilities of the detectors. This finding has significant implications for optical imaging, as faster systems incorporating fewer wavelengths may be used without suffering from errors in quantification if water/fat separation is incorporated into the optical reconstruction.

These studies were also verified *in vivo* with a patient diagnosed with breast cancer. These techniques increased the contrast between the tumor and the healthy background, due to the crosstalk between water and oxyhemoglobin. Contrast improvement was greater than 40% between the tumor and the background (see attached paper for full investigation).

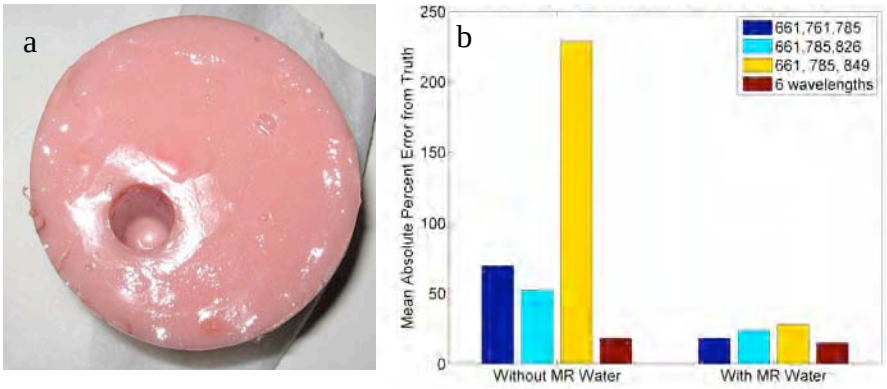

Figure 6: (a) Gelatin phantom with porcine blood added for optical contrast. 2:1 contrast was added to the inclusion. (b) Mean absolute errors in quantifying oxyhemoglobin. Shown are the cases where 3 wavelengths and 6 wavelengths of data are incorporated into the standard (bars to the left) and MR water-aided (bars to the right) reconstructions.

As multimodality instruments become more common in clinical trials, it will likely be important that they compliment one and other and provide synergistic information. Combining MR and optical provides such benefits to each modality. While MR can improve on the inherent limitations of optical imaging, optical contrasts may improve the information content of MR. Imaging of water and fat quantities more accurately is a good example of this type of synergy.

This section summarized the results from Aim 2a. MR fat/water was successfully incorporated into the optical imaging reconstruction, and improved quantification accuracy. After the choice of the most accurate MR water/fat sequence, MR water was incorporated into the reconstructions. This foundation provides a more accurate recovery of tissue properties. This study resulted in a manuscript, "MR Water Quantitative Priors Improves the Accuracy of Optical Breast Imaging," which is attached to this report.

2b. Correlating BOLD MR and optical tomography

Blood Oxygen Level Dependent (BOLD) MR imaging is beneficial to research and the clinic because of its ability to measure brain activation-induced changes in deoxyhemoglobin and blood flow. The physiological differences of blood oxygenation in normal vs. diseased tissue suggests that BOLD images could also have significant clinical benefit in other tissues, such as the breast. This study investigated the correlation between BOLD and optical breast imaging. The benefit of combining BOLD and optics is the ability to utilize the high temporal resolution (<1 sec) and the high spatial resolution (<1mm) of BOLD MR. To investigate the relation between BOLD and optical imaging, a respiratory breathing scheme was developed to induce hemodynamic changes in the breast. This contrast could additionally

be used to examine vascular function, and the potential of this contrast to identify tumors was also investigated.

Vascular function was modulated by introducing oxygen, or carbon dioxide into the vasculature through gas breathing. Specifically, gases containing 100% oxygen, carbogen, a 95% O_2:5% CO_2 mixture, and air, were introduced into a breathing circuit, shown in Figure 7. Three periodic stimuli were chosen from these gases: Oxygen/Carbogen (referred to as O_2/CO_2), Air/Oxygen (referred to as Air/O_2), and Air/Carbogen (referred to as Air/CO_2). These gases were alternated every 2 minutes. BOLD and optical images were acquired simultaneously. A protocol consisting of 4 breathing cycles (2 min carbogen, 2 min oxygen per cycle) was used to obtain data from 13 healthy volunteers. The first cycle was dropped to account for transient changes from previous breathing states. An oxycapnograph (Datex Capnomac Ultima, Helsinki, Finland) was used to ensure subject compliance.

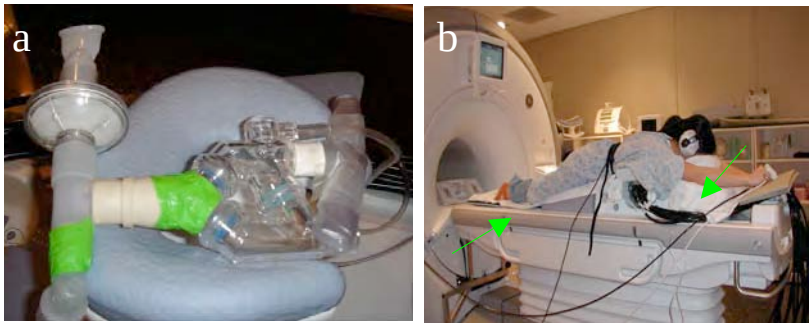

Figure 7: (a) The breathing circuit used to control respiratory gases (shown on the face pillow). (b) Subject prepared on the MRI system bed. Green arrows indicate the pulse oximeter and respiratory belt which were used to de-noise the BOLD MR signal.

Optical data was reconstructed to form a temporal signal response to the breathing stimulus. This response was cross-correlated to the periodic respiratory stimulus to form a strength of correlation and a phase delay between the measured signals and the stimulus, for each subject, for each gas stimulus. Figure 8 shows the delay between the measured response and the stimulus for each gas combination. During stimuli with carbogen (both the air/carbogen and oxygen/carbogen stimuli), total hemoglobin significantly varied with oxygenation. During the air/oxygen stimulus, oxygen saturation and total hemoglobin showed no correlation.

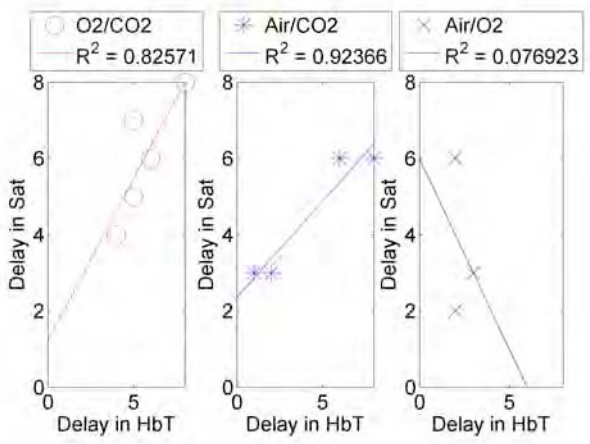

Figure 8: Time lag comparison of oxygen saturation (Sat) vs. total hemoglobin (HbT) for the three gas stimuli. A positive correlation indicates that total hemoglobin was increasing as oxygenation was increasing, and vice versa. This was the case for the stimuli containing carbogen. Alternately, a Air/oxygen gave a poor correlation between total hemoglobin and oxygenation, indicating no relationship.

The difference between time lag of total hemoglobin and oxygen saturation, shown in Figure 8, indicates a significant correlation between total hemoglobin and oxygen saturation for oxygen/carbogen

(O_2/CO_2, $R^2 = 0.825$, $p = 0.0018$, N=8) and air/carbogen (Air/CO_2, $R^2 = 0.923$, $p = 0.0039$, N=4). This data is consistent with the theory that carbogen induces an increase in blood flow. During carbogen stimulus, the vasodilation brings freshly oxygenated arterial blood (~98-100% oxygenated) into the tissue, washing out deoxygenated blood from the vasculature, and increasing oxygen saturation[8]. Thus, total hemoglobin and oxygenation are expected to vary together. In the air/oxygen (air/O_2) stimulus, oxygen saturation changes may be independent of total hemoglobin changes (as the variation in HbT is not explained by the variation on oxygen saturation ($p = 0.82$, N=3). Thus, other factors besides vasomotor control contribute substantially to the regulation of the hemodynamic response during the air/O_2 stimulus. These changes are most likely due changes in pO_2, which induce changes in the loading and unloading of oxygen onto hemoglobin. Without a pO_2 probe, this effect can not be explained with confidence.

The strength of correlation for these gases is shown in Figure 9. In order to consider the effects of physiological noise, a signal to noise (SNR) measure was calculated for total hemoglobin and oxygen saturation, which compared the relative magnitude of the maximum correlations between gas stimulus and air control breathing. SNR was calculated as:

$$SNR = \frac{\max(Corr_{Gas})}{\max(Corr_{Air})} \quad (1)$$

An SNR < 1 indicated that the gas did not induce a meaningful change in breast physiology.

These results show that many cases had SNR < 1. Of the three stimuli, oxygen/carbogen induced a response in oxygen saturation which was significantly stronger than the control ($p = 0.02$, two-sample t-test, N=11). The response in total hemoglobin strongly suggested a greater correlation than the control, although this claim is not significant ($p = 0.06$ two-sample t-test, N=11). Because of these strong physiological changes, O_2/CO_2 exhibits the most promise compared to the other stimuli for inducing consistently strong responses in breast tissue. In comparison, Air/CO_2 was not significantly greater than the control for either total hemoglobin ($p = 0.30$ two-sample t-test, N=4) or oxygen saturation ($p = 0.25$ two-sample t-test, N=4). Air/O_2 was also not significantly greater than the control for either total hemoglobin ($p = 0.49$ two-sample t-test, N=7) or oxygen saturation ($p = 0.33$ two-sample t-test, N=7).

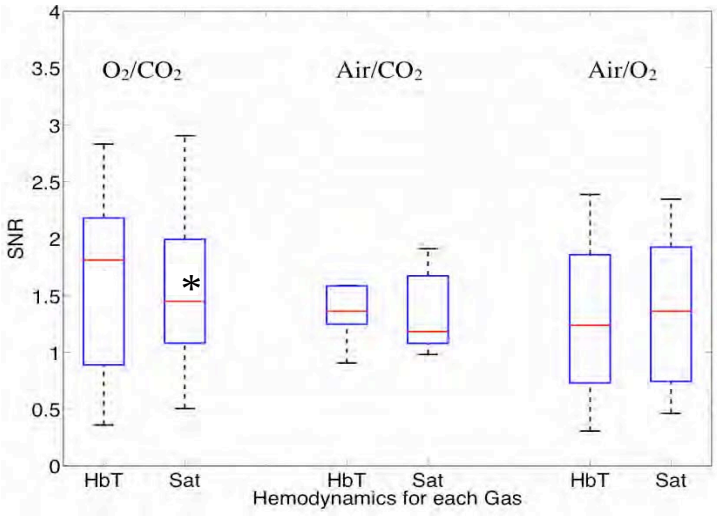

Figure 9: Signal to noise ratio for hemodynamic measures for each stimulus shows that O_2/CO_2 induces the strongest response compared to the air control. (* denotes significance)

The gas breathing stimulus contrast was investigated in its ability to separate tumors and healthy tissue. The oxygen/carbogen stimulus was examined because it induced the largest response in the

breast tissue. Tumors were identified by CE-MR and segmented with the aid of a radiologist. The subjects in this study all provided informed consent, following the procedures approved by the Institutional Review Board at the Stanford University School of Medicine.

Relative changes in tumor vascular function are identified in Figure 10 by plotting the Signal to Noise Ratio of the tumor tissue compared to the normal surrounding tissue, as a way of gauging the relative magnitude of the change with respect to normal air variations which are from biological noise. There is a substantial separation in SNR between the normal and tumor tissue in HbT, from 1.8 in the tumor to 2.8 in normal tissue. This SNR change is due to a weaker correlation in the tumor tissue response to the gas stimulus in both cases. These results could be explained by a lack of adequate smooth muscle cells to allow proper vasodilatory response.

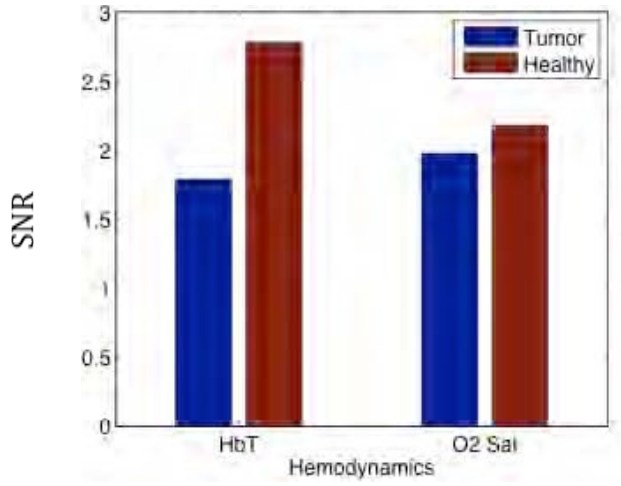

Figure 10: The magnitude of the change for gas to air as a ratio is plotted for total hemoglobin (HbT) at left, and oxygen saturation (O2 Sat) at right. In tumor tissue the HbT change is significantly lower than the background fibroglandular tissue (p-value = 0.018). The difference is not significant in O_2 Sat values.

These vascular responses were compared to BOLD MR. A comparison of the phase (related to time) lag of BOLD compared to deoxyhemoglobin (Hb) is shown for the 11 healthy subjects in Figure 11. Figure 11b utilized the Gas to Air ratio, which compared the correlation of the deoxyhemoglobin response during the gas stimulus to the correlation between the stimulus and air breathing. The air breathing time course data was acquired prior to the gas stimulus. Figure 11b does not include four subjects who had a Gas to Air ratio less than 1, which indicated that the gas stimulus did not induce a significant response.

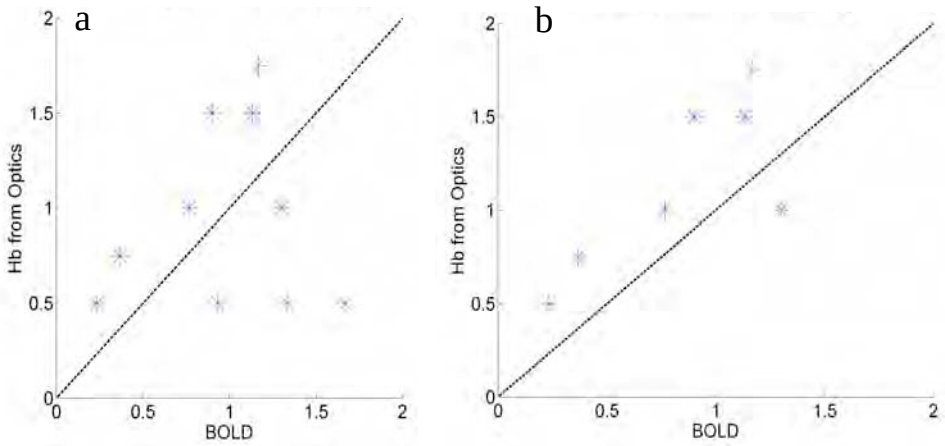

Figure 11: Temporal cycle delay (in units of pi) for BOLD response relative to the optical deoxyhemoglobin response for (a) all subjects, and (b) all subjects who had a greater response from the gas breathing than during air breathing. When controlling for non-responders, BOLD and optical responses correlate significantly $r = 0.76$, $p = 0.048$.

The results from this work indicate that BOLD and optically-determined deoxyhemoglobin signals correlate significantly in the breast with an oxygen/carbogen respiratory stimulus, as long as only subjects that exhibit a significant response are included. This use of control measurement as a baseline is needed to account for subjects who do not exhibit sufficient hemodynamic change in response to the inspired gas stimulus due to larger variations in their natural physiological processes.

2c. Combining MR Contrasts and Optical Tomography

The water/fat and BOLD contrasts were combined into a comprehensive model for MRg-DOI. This procedure aims to provide improved quantification, speed, and resolution, than optical imaging alone. An outline of the procedure is shown in Figure 12. In this method, T1-weighted anatomical MR images, BOLD images, and MR water images are incorporated into the optical reconstruction.

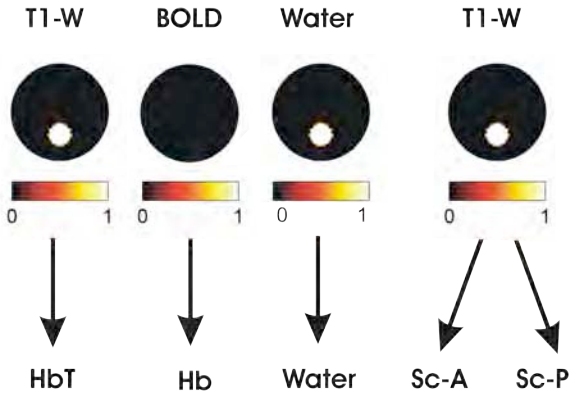

Figure 12: MR maps included into the MRg-DOI reconstruction. Anatomical structures, deoxyhemoglobin, and water maps are incorporated into the reconstruction.

For the MRg-optical reconstruction the objective function is:

$$\Omega = \delta^T W_d \delta + \mu^T W_\mu \mu \quad (2)$$

In this model-based image reconstruction, the tissue properties are fit to a model for light propagation in breast tissue. The data/model misfit, , is minimized along with controls for system noise, W . This formulation recovers the tissue properties:

$$\mu = \{\{Hb + HbO\} \quad \{Hb\} \quad \{H_2O\} \quad \{Sc \quad A\} \quad \{Sc \quad P\}\} \quad (3)$$

The parameter weight matrix is:

$$W_\mu = \begin{bmatrix} \operatorname{cov}(Hb + HbO) & \operatorname{cov}(Hb + HbO, Hb) & & & & \\ \operatorname{cov}(Hb, Hb + HbO) & \operatorname{cov}(Hb) & & & & \\ & & \operatorname{cov}(H_2O) & & & \\ & & & \operatorname{cov}(Sc - A) & & \\ & & & & \operatorname{cov}(Sc - P) & \end{bmatrix}^{-1} \quad (4)$$

where oxyhemoglobin, deoxyhemoglobin, Water, Scattering Amplitude, and Scattering Power are *HbO, Hb, H_2O, Sc-A, and Sc-P*, respectively. Thus, this reconstruction algorithm can combine MR water/fat, MR BOLD, and MR anatomical information into the optical reconstruction.

Aim 2 of this project resulted in the incorporation of MR contrasts into optical breast imaging. MR water and fat were added through the use of a DIXON technique. Respiratory modulation was used to induce hemodynamic changes in the breast. In a cohort of 13 healthy women, carbogen was shown to induce a vasodilatory response, which confirms long established findings in the vasculature[9]. These changes were shown to correlate to BOLD MR in the breast when the oxygen/carbogen stimulus was used, and the SNR was larger than one. A reconstruction model was developed to incorporate these contrasts into the optical contrast recovery.

3. Tumor characterization using MR guided optics

3a. Breast Cancer Characterization

This work will present several case studies demonstrating the potential for image-guided optical tumor characterization and treatment monitoring. First, we report on the results from five patients. Two patients were imaged prior to the start of neoadjuvant chemotherapy, two patients were imaged during the late stages of chemotherapy, and one patient was imaged during a call-back for a mammographically

determined suspicious lesion (the end-result being the identification of a benign fibrocystic lesion). All subjects provided informed consent and were imaged according to study protocols approved by the Institutional Review Board at Dartmouth Hitchcock Medical Center. These images were reconstructed using anatomical maps provided from MR.

The results (only total hemoglobin presented) suggest that total hemoglobin is the only consistent delineator between the malignant tissue and the benign and responding tissue. This differentiation is likely due to the increase in vascular content in malignant tumors. These results are summarized in Figure 13, which shows a comparison of the total hemoglobin in the region of interest vs the background tissue for all subjects. Since tumor tissue is a sub-region of the fibroglandular tissue, fibroglandular tissue is designated as the background in this analysis. Malignant tumors in subjects 3, 4, and 5 clearly have higher hemoglobin than the background fibroglandular tissue, whereas the normal / benign and responding cases show comparable or less total hemoglobin than the background.

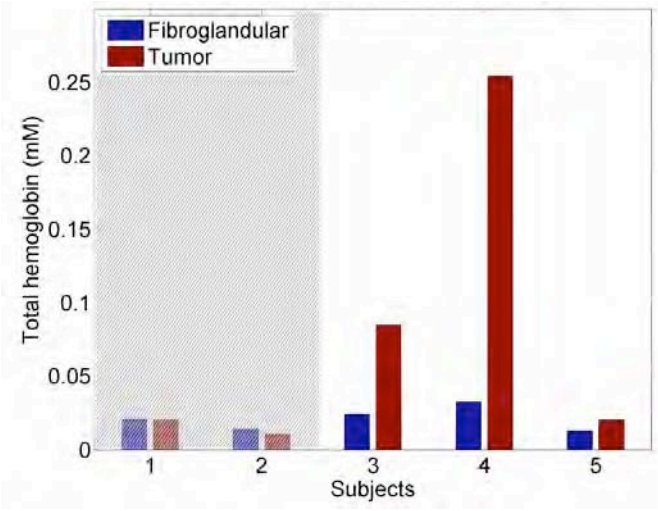

Figure 13: Comparison of (suspect) tumor to fibroglandular total hemoglobin across all subjects. The subjects denoted in the non-shaded region, subjects 3, 4 and 5, had known malignant lesions. The shaded region consisted of subject 1, who had a benign/normal lesion, and subject 2, who fully responded to chemotherapy. Total hemoglobin is higher than the background fibroglandular tissue in the known malignant tumors.

3b. Breast Cancer Treatment Monitoring

The use of neoadjuvant chemotherapy to manage breast cancer treatment is increasing because it has been shown to be as effective as post-operative adjuvant chemotherapy, while enabling the option of breast conserving surgery in some cases [10]. Imaging tumor response has the potential to gauge the effectiveness of the therapy, allowing the possibility of tailoring a drug regimen to the individual, or determining survival outcomes. Because of its potential, imaging disease response to neoadjuvant chemotherapy has become a significant topic of interest in the literature.

Optical imaging has been shown to be an effective way to monitor chemotherapy response in the breast. Cerussi et al. [11] demonstrated in eleven subjects that NIRS could perfectly separate chemotherapy responders vs. non-responders within the first week of treatment via monitoring the absolute concentration of total hemoglobin and relative differences in deoxyhemoglobin and water. Jiang et al. [12] confirmed the trend of decreasing total hemoglobin in four responding patients vs three patients who showed incomplete response. These results are expected to improve with MRg-DOI because of the merits of adding MR to optics. Thus, there is potential for using MR guided optical imaging to monitor chemotherapy.

One subject was scheduled for seven imaging sessions during neoadjuvant chemotherapy. Table 1 displays the timeline of all imaging exams. The MRg-DOI imaging results for session 1 are shown in Figure 14.

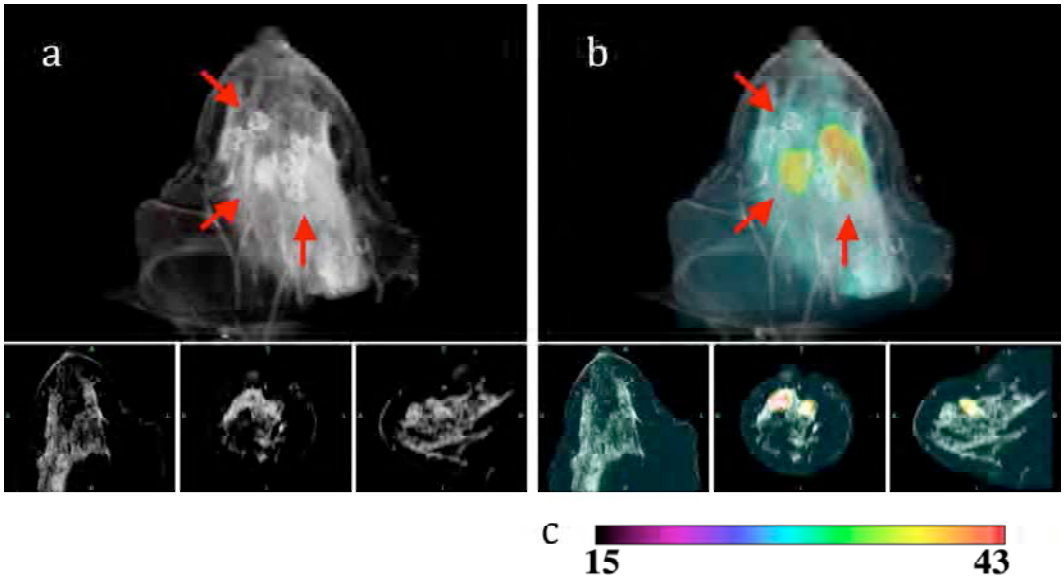

Figure 14: a) DCE MR images of a subject with an IDC taken 1 day prior to chemotherapy shows slight enhancement of 1 main node with 3 satellite lesions. b) MR-NIR images overlaid on a). The lesions in the plane of the optical fibers of the MR-NIR instrument show increased hemoglobin over the background. c) The colorbar used for quantitative analysis of hemoglobin in b).

A 3cm invasive ductal carcinoma and three satellite lesions fully responded to chemotherapy, according to pathologist assessment at the end of the treatment. Session 3 was cancelled because of a malfunctioning cable in the MR breast coil. Session 2 was not analyzed because the fibers did not intersect with the plane of the contrast enhancing tumors. Sessions 6 and 7 were not analyzed because the tumors were not visible in the MR, most likely due to full chemotherapy response.

Imaging Session	Treatment	Notes
1	Pre	
2	2 days post Cycle 1	Fibers out of tumor plane
3		Cancelled
4	2 days post cycle 2	
5	2 days post cycle 3	
6		No visible tumor in MR
7		No visible tumor in MR

Table 1: Overview of imaging sessions for the subject monitored during neoadjuvant chemotherapy.

Lesions were identified from the dynamic breast MR images with the aid of 2 radiologists that had 15 and 10 years of experience, respectively.

Optically recovered total hemoglobin, oxygen saturation, and water are shown below in Figure 15. The anterior satellite lesion was consistently located in the optical fiber plane in each of the 3

successful imaging exams, and its values were used for analysis. Optical imaging indicates a decrease in total hemoglobin over the course of the treatment. Total hemoglobin decreased from ~ 0.038 mM to ~ 0.020 mM between cycle 1 to cycle 2, due to the reduction in the tumor size, and likely the minimization of tumor vasculature. Tumor total hemoglobin did not change significantly between cycle 2 and cycle 3. Oxygen saturation also decreased, likely because of destruction of functioning tumor vasculature, which

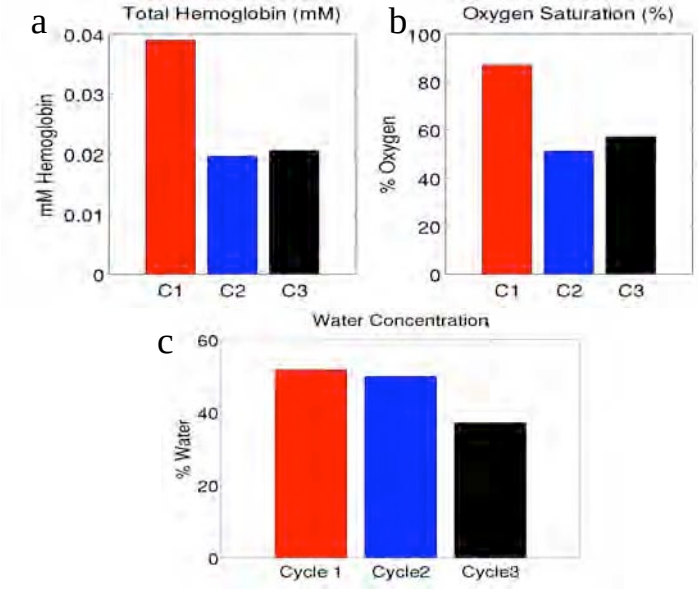

Figure 15: Quantitative Comparison of (a) total hemoglobin, (b) oxygen saturation, and (c) water content in an invasive ductal carcinoma over 3 cycles of chemotherapy in a complete responder.

restricted tumor perfusion. Water diminished in this lesion from about 52% to 38%, most likely because of the reduction in functional vascular tissue in the tumor.

This section described results towards the goals of Aim 3. It is shown that MR-guided optics shows promise for breast cancer imaging, both for diagnostics and for physiological therapy monitoring. More patients are needed to investigate the true impact of this technique.

Key Research Accomplishments

- Advanced patient interface which allowed more flexible fiber positioning and better data quality
- Incorporated MR water sequence into image reconstruction which improved quantification by at least 20% in tissue-simulating phantoms.
- Examined respiratory stimulus contrast to evaluate vascular function. Determined that oxygen/carbogen induced the largest, most consistent response.
- Examined the vascular functional contrast between normal and tumor tissue. Found a substantial difference in total hemoglobin changes in tumor tissue in case studies.
- Correlated optical imaging with breast BOLD. Found significant correlation with oxygen/carbogen when the SNR was greater than one.
- Developed a comprehensive reconstruction model to incorporate MR and optical contrasts.
- Imaged 5 patients with suspect lesions. Correctly assessed pathology in all subjects. Demonstrated > 50% contrast in all known malignancies.
- Monitored response of chemotherapy and showed ability of MR guided optics to successfully monitor therapy response.

Reportable Outcomes

This period of funding resulted in 2 peer-reviewed journal publications, 3 articles in preparation, 4 invited oral presentations, 2 co-authored journal articles, and 6 conference proceedings.

Publications:

Carpenter, CM. et. al. "Inducing and Monitoring Hemodynamic Changes in the Healthy Breast," *in preparation.*

Carpenter, CM. et. al. "Measuring vascular function in tumors with MR-guided Diffuse Optical Imaging: A Pilot Study," *in preparation.*

Carpenter, CM. et. al. "MR water/fat imaging improves quantification accuracy in diffuse optical tomography," *in preparation.*

Srinivasan, S., **Carpenter, CM**, et al. "Sensitivity of Hemoglobin Concentration on Optical Probe Positioning in Image-Guided Near Infrared Spectroscopy," IEEE Engineering in Medicine and Biology Conference, Mineapolis, MN, September 2009.

Srinivasan, S., **Carpenter, CM**, et al. "Optimization of 3-D image-guided near infrared spectroscopy using boundary element method," IEEE International Symposium on Biomedical Imaging, Boston, MA, 2009.

Carpenter CM., et al. "MRI-guided near infrared spectroscopy of breast tumors," Medicamundi **53**:1, 2009.

Jiang S., Pogue BW **Carpenter CM,** et al. "Evaluation of breast tumor response to neoadjuvant chemotherapy with Tomographic Diffuse Optical Spectroscopy: Case studies of tumor Region of Interest changes," Radiology, 231, 551-560, 2009.

Carpenter CM., et al.. "Examination of the synergy of near-infrared spectroscopy guided by advanced MR sequences in vivo," Proceedings of the International Society for Optical Engineering, San Jose, CA, January 2009.

Carpenter CM., et al.. "3D optical contrast-recovery in MR guided diffuse optical spectroscopy," Proceedings of the International Society for Optical Engineering, San Jose, CA, January 2009.

Srinivasan S. **Carpenter CM.,** et al Image-guided near infrared spectroscopy using boundary element method: phantom validation," Proceedings of the International Society for Optical Engineering, San Jose, CA, January 2009.

Carpenter CM., Srinivasan S., Pogue BW., and Paulsen KD. "Methodology Development for three-dimensional MR-Guided Near Infrared Spectroscopy of Breast Tumors," Optics Express, 16:22, 2008.

Carpenter CM., "Breast Cancer Characterization with Optical Spectroscopy integrated into an MR Breast Biopsy Plate," in Breast Cancer (Clinical Studies), Proc. Of International Society of Magnetic Resonance in Medicine, 2008.

Srinivasan S., Pogue BW., **Carpenter CM.,** and Paulsen KD. "Image-Guided Near Infrared Spectroscopy Using Boundary Element Method: Pilot Results in the Breast," Medical Physics, submitted.

Oral Presentations:

Carpenter, CM. "MR guided Optical Imaging for Breast Cancer Diagnosis." Presentation for the Department of Radiation Oncology, Stanford University Medical School, Oct. 25th, 2009.

Carpenter CM., et al.. "Examination of the synergy of near-infrared spectroscopy guided by advanced MR sequences in vivo," Presented at Multimodal Biomedical Imaging IV, International Society for Optical Engineering, San Jose, CA, January 2009.

Carpenter CM., et al.. "3D optical contrast-recovery in MR guided diffuse optical spectroscopy," Presented at Optical Tomography and Spectroscopy of Tissue VIII, International Society for Optical Engineering, San Jose, CA, January 2009.

Carpenter, CM. "Breast Cancer Imaging with Light in MRI." Presentation for the Radiological Sciences Laboratory at Stanford University, Nov. 19th, 2008. *Invited.*

CONCLUSIONS

The work developed in during this grant introduced a more synergistic MRg-DOI instrument. All aspects of the system were studied. A more flexible, improved fiber interface and MR breast coil slowed for better fiber positioning capabilities, and better data quality. MR water/fat and BOLD were imaging were investigated and incorporated into the optical image reconstruction. Results show improved hemodynamic quantification, and pave the way for incorporating breast BOLD into optical imaging for higher temporal and spatial resolution. Vascular contrast was examined with a respiratory stimulus. It was determined that oxygen/carbogen gave the largest and most consistent changes. Results in 5 patients and 1 patient undergoing chemotherapy show promise for MR-guided optics in imaging breast cancer.

REFERENCES

1. S. P. Poplack, T. D. Tosteson, W. A. Wells, B. W. Pogue, P. M. Meaney, A. Hartov, C. A. Kogel, S. K. Soho, J. J. Gibson, and K. D. Paulsen, "Electromagnetic Breast Imaging: Results of a Pilot Study in Women with Abnormal Mammograms," Radiology **243**, 350-9 (2007).
2. R. Choe, S. D. Konecky, A. Corlu, K. Lee, T. Durduran, D. R. Busch, B. Czerniecki, J. Tchou, D. L. Fraker, A. DeMichele, B. Chance, E. Putt, M. D. Schnall, M. A. Rosen, and A. G. Yodh, "Differentiation of benign and malignant breast lesions by in-vivo three-dimensional diffuse optical tomography," Cancer Research **69**, 102S-102S (2009).
3. S. G. Orel and M. Schnall, "MR Imaging of the Breast for Detection, Diagnosis, and Staging of Breast Cancer," Radiology **220**, 13-30 (2001).
4. A. Corlu, R. Choe, T. Durduran, K. Lee, M. Schweiger, S. R. Arridge, E. M. Hillman, and A. G. Yodh, "Diffuse optical tomography with spectral constraints and wavelength optimization," Applied Optics **44**, 2082-93 (2005).
5. S. Reeder, N. Pelc, M. Alley, and G. Gold, "Multi-coil Dixon chemical species separation with an iterative least squares method," Magnetic Resonance in Medicine **51**, 35-45 (2004).
6. G. H. Glover and E. Schnieder, "Three-point dixon technique for true water/fat decomposition with B0 inhomogeneity correction," Magnetic Resonance in Medicine **18**, (1991).
7. Lynch, D., Numerical Partial Differential Equations for Environmental Scientists and Engineers: a first practical course, ed. (Springer, New York, 2005).
8. Guyton, A. & Hall, J., Textbook of Medical Physiology, 11 ed. (Elsevier, Philadelphia, 2006).
9. R. Alonzi, A. R. Padhani, R. J. Maxwell, N. J. Taylor, J. J. Stirling, J. I. Wilson, J. A. d'Arcy, D. J. Collins, M. I. Saunders, and P. J. Hoskin, "Carbogen breathing increases prostate cancer oxygenation: a translational MRI study in murine xenografts and humans," British Journal of Cancer **100**, 644-648 (2009).
10. B. Fisher, J. Bryant, N. Wolmark, E. Mamounas, A. Brown, E. R. Fisher, D. L. Wickerham, M. Begovic, A. DeCillis, A. Robidoux, R. G. Margolese, A. B. Cruz, J. L. Hoehn, A. W. Lees, N. V. Dimitrov, and H. D. Bear, "Effect of preoperative chemotherapy on the outcome of women with operable breast cancer," Journal of Clinical Oncology **16**, 2672-2685 (1998).
11. A. Cerussi, D. Hsiang, N. Shah, R. Mehta, A. Durkin, J. Butler, and B. J. Tromberg, "Predicting response to neoadjuvant chemotherapy using diffuse optical spectroscopy," PNAS **104**, (2007).
12. S. Jiang, B. W. Pogue, C. M. Carpenter, S. P. Poplack, W. A. Wells, C. A. Kogel, J. Forero, L. S. Muffly, G. N. Scwartz, K. D. Paulsen, and P. A. Kaufman, "Evaluating tumor response to neoadjuvant chemotherapy with Diffuse Optical Spectroscopic Tomography: Case studies of tumor Region of Interest changes," Radiology **252**, 330 (2009).

APPENDIX

See attached.

Monitoring of Hemodynamic Changes Induced in the Healthy Breast through Inspired Gas Stimuli with MR-guided Diffuse Optical Imaging

CM Carpenter[1], R Rakow-Penner[2], S. Jiang[1], BW Pogue[1], GH Glover[2], and KD Paulsen[1]

[1]Thayer School of Engineering, Dartmouth College, Hanover, NH, USA
[2]Department of Radiology, School of Medicine, Stanford University, Stanford, CA, USA
(Email: colincarpenter@stanford.edu)

Purpose: The modulation of tissue hemodynamics has important clinical value in medicine for both oncology and radiology. As an oncological tool, increasing tissue oxygenation via modulation of inspired gas has been proposed as a method to improve cancer therapy and determine radiation sensitivity. As a radiological tool, inducing changes in tissue total hemoglobin has been proposed as a means to detect and characterize malignant tumors by providing information about tissue vascular function. The ability to change and measure tissue hemoglobin and oxygenation concentrations in the healthy breast during administration of three different types of modulated gas stimuli – oxygen / carbogen, air / carbogen, and air / oxygen – was investigated.

Methods: Subjects breathed combinations of gases which were modulated in time. MR-guided diffuse optical tomography measured total hemoglobin and oxygen saturation in the breast every 30 seconds during the 16 minute breathing stimulus. Metrics of maximum correlation and phase lag were calculated by cross correlating the measured hemodynamics with the stimulus. These results were compared with an air/air control to determine the hemodynamic changes compared to the baseline physiology.

Results: This study demonstrated that a gas stimulus consisting of alternating oxygen / carbogen induced the largest and most robust hemodynamic response in healthy breast parenchyma relative to the changes that occurred during the breathing of room air. This stimulus caused increases in total hemoglobin and oxygen saturation during the carbogen phase of gas inhalation, and decreases during the oxygen phase. These findings are consistent with the theory that oxygen acts as a vasoconstrictor, while carbogen acts as a vasodilator. However, difficulties in inducing a consistent change in tissue hemoglobin and oxygenation were observed because of variability in inter-subject physiology, especially during the air/oxygen or air/carbogen modulated breathing protocols.

Conclusions: MR-guided diffuse optical imaging is a unique tool that can measure tissue hemodynamics in the breast during modulated breathing. This technique may have utility in determining the therapeutic potential of pre-treatment tissue oxygenation, or in investigating vascular function. Future gas modulation studies in the breast should use a combination of oxygen and carbogen as the functional stimulus. Additionally, control measures of subject physiology during air breathing are critical for robust measurements.

1. Introduction

Tumor oxygenation has been a major area of interest in oncology research for decades because of its known links to disease severity and treatment outcome [1]. Since hypoxic tumors are more aggressive, resistant to therapy, and prone to metastatic growth [2], the ability to increase their oxygenation has been investigated as a way to improve outcomes in acute treatments such as radiotherapy [3, 4, 5], hyperthermia [6], and photodynamic [7] therapy. Methods to alter tumor tissue oxygenation and/or to measure the induced changes would be powerful aids in the oncologic management of cancers.

One simple way to increase tissue oxygenation is to administer pure (100%) oxygen or carbogen (95% O_2, 5% CO_2) through a respiration mask. Unfortunately, the complexity of the body's physiological response to the administration of these gases presents challenges to successful implementation. For example, although the delivery of 100% oxygen leads to an increase in blood pO_2 (as compared to breathing room air) [8], the increased concentration of O_2 causes the smooth muscle cells lining the vasculature to contract due to the lack of carbon dioxide in the blood [9]. This condition, known as hypocapnia, causes the vascular resistance to increase, which decreases blood flow due to increased vascular constriction in the peripheral vascular bed [10, 11]. This decrease in blood flow may induce local areas of hypoxia [11] counteracting the desired oxygenation change.

To compensate for the loss in vascular tone during oxygen breathing, carbogen gas, which contains a large percentage of O_2 mixed with a small amount of CO_2, can be used to limit vascular constriction [12, 9]. Carbogen has been shown to increase both tissue blood flow [8, 13] and tissue oxygenation [14, 15, 16]. Increased tissue pO_2 due to carbogen has been reported in the cerebrum [13], liver, spleen, paraspinal muscle, subcutaneous fat [17], and head and neck tumors [18].

In tumors, conflicting reports have appeared in the literature on the vascular effects of carbogen breathing [19, 20, 21]. These inconsistencies are likely attributable to the heterogeneity in tumor vascular density and function, due to such factors as vasoconstriction of feeding vasculature [22], anemic tumor vessels [23], and increased vascular permeability [1]. These factors are inherent to neoplastic tissue and may account for poor oxygen delivery to the tumor during a respiratory stimulus.

74 However, measurement inconsistencies may also contribute to the conflicting results
75 found in the literature. For example, physiological variations between individuals may
76 account for amplitude and time differences in tissue response. In some cases, the inspired
77 gas may cause immeasurable changes to oxygenation and blood flow even in healthy
78 tissue. Oxygen microelectrodes or laser Doppler flow meters, the instrumentation
79 commonly used to measure oxygenation and blood flow, measure point samples of tissue.
80 Because tissues (especially tumors) are highly heterogeneous, these point measurements
81 often give inconsistent results, which are not necessarily indicative of the overall
82 volumetric response. Diffuse optical techniques, on the other hand, produce more
83 consistent results [16, 24] because they sample a much larger volume of tissue. For example,
84 Kim et al. [25] measured consistent increases in tissue oxygenation in prostate tumors with
85 Near Infrared Spectroscopy (NIRS), while measuring inconsistent changes in pO_2
86 recorded by microelectrodes and F^{19} Magnetic Resonance (MR) when rats were
87 challenged with a carbogen stimulus.
88 The goal of this study was to investigate whether a significant hemodynamic response
89 in the healthy breast could be induced through control of inspired gas, and subsequently
90 measured reliably with MR-guided diffuse optical imaging. The administration of three
91 gas combination pairs – Air/Carbogen (Air/Cb), Air/Oxygen (Air/Ox) and
92 Oxygen/Carbogen (Ox/Cb)– was compared in order to determine if a consistently strong
93 response could be measured. The responses to these gas stimuli were related to a control
94 experiment involving the inhalation of room air (in an identical Air/Air delivery protocol)
95 to assess the normal physiological variations of each subject. By determining the gas
96 combination that produced the most robust changes, these results could serve as a

baseline for studies of modulated gas breathing to characterize tumor vasculature or monitor oxygenation changes during treatment evaluation. To the best of our knowledge, this paper reports the first systematic study of the volumetric response of total hemoglobin and oxygen saturation to externally controlled gas stimuli in the healthy human breast.

3. **Methods**

3.1 MR-Guided Diffuse Optical Imaging

Diffuse optical imaging is a relatively new imaging modality that can be used to produce images of oxyhemoglobin, deoxyhemoglobin, water fraction, and lipid content in breast tissue [26, 27]. These concentrations are determined by fitting maps of light absorption at multiple wavelengths in the near infrared (NIR) to known chromophore spectra [28]. To accurately quantify tissue properties, the effects of light absorption and scatter on photon migration must be separated by either time or frequency domain measurements[29, 30]. By operating within an MR scanner, images may be formed with increased accuracy and spatial resolution [31] through the incorporation of prior knowledge of tissue boundaries, similarly to one way in which Computed Tomography (CT) has aided PET by providing structural details [32].

The MR-guided optical imaging instrument used in this work is shown in Figure 1. This system coupled 16 optical fibers to the breast tissue through a custom-built non-metallic interface [33]. Light signals emitted from laser diodes at three wavelengths (661nm, 785nm, and 826nm) were modulated at unique frequencies and combined at the source fiber, which was sequentially translated to 16 positions around the breast. Light was subsequently detected with photomultiplier tubes through the other 15 fibers. The

details of the data acquisition scheme are described in more detail in Jiang et al. [34] and McBride et al.[35]. Measurements of AC amplitude and phase shift were input into an iterative model-based reconstruction [36, 37] to obtain images of breast hemodynamics in a single anatomically coronal slice every 30 seconds. This algorithm utilized the tissue boundaries defined by MR to influence the spatial distribution of contrast [38]. The overall performance of the system is described more fully in Brooksby et al. [39]. In this study, a region-based method was used to determine hemodynamic properties in the adipose and fibroglandular tissue [38] which were identified through an MR water/fat separated image [40]. Previous studies have determined that the spatial resolution of this system is about 5mm for typical tumor contrasts[41].

3.2 Modulated Gas Breathing Stimulus

The hemodynamics of breast tissue were monitored in eleven (11) healthy volunteers during the modulation of three different inspired gas compositions: oxygen(100% O_2) / carbogen(95% O_2, 5% CO_2), carbogen / air(~21% O_2), and oxygen / air. Air / air was used as a control measure. We chose a four minute (1/240 = 0.042 Hz) period for the breathing stimulus, alternating between the paired gas mixtures every two minutes, for a total of four complete cycles (16 minute total acquisition). The gas stimulus combinations are shown in Figure 2. Each image acquisition period was started within 1 minute of the conclusion of the previous recording. The image data from the first alternating gas period was dropped after the gas combination pair was switched to ensure that lingering effects from the previous stimulus were minimized. All gas stimuli were not used with all volunteers because of MR scan-time limitations. The number of

subjects who participated in the breathing experiments with a given gas stimulus is listed in Table 1.

For the oxygen and carbogen gas stimuli, medical gases (Praxair) were directed from holding tanks into a respiratory circuit that controlled the source of inhaled gas while preventing the re-breathing of expired gases. As shown in Figure 3, when the inlet valve from the gas tanks was opened, positive pressure from the feeding gas line closed the room air valve (preventing the breathing of room air). During the room air stimulus, the inlet valve from the gas tanks was closed (lack of inlet pressure from the gas tanks opened the room air valve). The switching of gases was controlled through a valve driven by a computer running Eprime software (Psychology Software Tools, Inc.). Flow rates were maintained at 9 liters/min and were monitored by flow meters attached to the tanks.

Expired O_2 and CO_2 concentrations were continuously monitored during image acquisition to ensure subject compliance. A gas line attached to the breathing mask just below the mouthpiece led to an oxycapnograph (Capnomac Ultima, Helsinki, Finland), sampling the expired gas at 100 ml/min. Analog signals from the oxycapnograph (CO_2 and O_2) were acquired using a data logger recording at 100 Hz (Measurement Computing, Norton, MA). All subjects had their noses sealed to ensure breathing only occurred through the mouthpiece.

All study participants provided informed consent and procedures were performed according to the protocol approved by the Institutional Review Board at Stanford University Medical Center.

3.3 Data Processing

Each point in the time series of data collection consisted of one optical image reconstruction. The data was calibrated with the first time point in a given stimulus series in order to reduce experimental noise from changes in fiber coupling, fiber attenuation, and other systematic errors[42]. The calibrated data at the nth time point, Φ_{CB}^{n}, was calculated as:

$$\Phi_{CB}^{n} = \Phi_{M}^{n} - (\Phi_{M}^{1} - \Phi_{C}^{1}) \quad (1)$$

where Φ_{M}^{n} is the measured data at the nth time point and Φ_{M}^{1} and Φ_{C}^{1} are the measured and calculated data (from a numerical fit of the optical properties to the data) from the 1st time point, respectively. This calibration routine is essentially the same as the one described in McBride et al.[43] except that the reference recordings result from data collected at the initial timepoint in the breathing protocol (rather than from a phantom). Data below the system noise floor was eliminated. The first breathing (4 minute) period of each gas stimulus was also disregarded to remove physiological contributions from earlier gas stimuli. Thus, a full temporal dataset consisted of 23 image acquisitions (2 images/minute x 4 minutes/period x 3 periods – 1 calibration image).

Cross correlations between the gas stimulus and the measured hemodynamic response in the breast were performed on the healthy fibroglandular tissue. Gas modulation was modeled with a sine wave at the stimulus frequency, shown in Figure 2b – an approximation which is reasonable because the vasculature acts as a temporal low pass filter [44, 45]. The time course of the induced tissue response was median filtered and de-trended before data processing. Cross correlation analyses were used to provide robust measures of the strength of correlation and the time lag between the gas stimulus and

tissue response. The time lag at maximum correlation represented the lag in time between the gas stimulus and the tissue response and was calculated for total hemoglobin and oxygen saturation for each subject in this study.

To measure the strength of response in the breast due to the gas stimulus compared to each subject's normal physiology, a signal to noise (SNR) metric was calculated for total hemoglobin and oxygen saturation. The SNR was the ratio of the magnitude of the maximum correlation with the gas stimulus, to the maximum correlation with room air/air breathing sequence:

$$SNR = \frac{\max\left(Corr_{Gas}\right)}{\max\left(Corr_{Air}\right)} \quad (2)$$

This measure yielded a method to determine which gas pair induced the strongest change and also served as a means to exclude data from the analysis when certain subjects did not measurably respond to a given gas stimuli. An SNR < 1 was assumed to indicate that the gas stimulus did not induce a measurable change in breast physiology that was greater than the natural variations which occur during a particular subject's breathing of normal room air.

4. Results

4.1 System stability

During the course of data collection, the optical system was tested for stability to ensure the acquisition of high quality images. These measurements were performed on a static, homogenous tissue simulating phantom. Figure 4 shows the oxy- and deoxy-hemoglobin concentrations recorded for this phantom. The system caused fluctuations of less than 0.25% in its estimates of both of these quantities.

213

214 *4.2 Time response in the healthy breast*

215 A comparison of the total hemoglobin changes over time for a typical subject due to the
216 oxygen/carbogen stimulus (Figs 5a,b) relative to the air/air control (Fig. 5c,d) when SNR
217 > 1 are shown in Figure 5. The corresponding oxygen saturation changes appear in
218 Figure 6. Compared to the control measurements, the oxygen/carbogen gas stimulus
219 induced a tissue response in total haemoglobin and oxygen saturation at the stimulus
220 frequency (see Figs. 5b and 6b relative to Figs 5d and 6d) which was greater than the
221 physiological background in this subject. However, in some subjects, the physiological
222 noise was greater than or equal to the induced gas response (i.e, SNR < 1) as described in
223 more detail in Section 4.4.

224

225 *4.3 Time lag response in healthy breast tissue*

226 Time lag responses are shown in Figure 7. These data are plotted in terms of phase lag
227 ranging from 0 to 2 . Zero phase lag indicates a positive response to Gas 1 with no delay
228 whereas a phase lag of indicates a positive response to Gas 2 (see Figure 2). Cases
229 were excluded from the analysis (3 with oxygen/carbogen, 1 with the air/carbogen, and 4
230 with the air/oxygen) when the tissue response to the stimulus was less than the air control
231 (i.e, SNR < 1).

232 The time lags between total hemoglobin and oxygen saturation demonstrate a
233 significant correlation for the oxygen/carbogen ($R^2 = 0.83$, $p = 0.0018$, $N=8$) and
234 air/carbogen ($R^2 = 0.92$, $p = 0.0039$, $N=4$) stimuli which is consistent with the
235 assumption that carbogen induces vasodilation. Since vasodilation increases blood flow,
236 the freshly oxygenated arterial blood (~98-100% oxygenated) washes its deoxygenated

counterpart out of the vasculature increasing oxygen saturation [46]. In the air/oxygen case, oxygen saturation changes were independent of changes in total hemoglobin (as the variation in HbT was not explained by the variation on oxygen saturation, $p = 0.82$) although the numbers (N=3) are small. Thus, other factors besides vasomotor control appear to contribute substantially to the regulation of the hemodynamic response during the air/oxygen stimulus. These changes are most likely due to variations in pO_2, which induce changes in the loading and unloading of oxygen onto hemoglobin. Overall, these results indicate that the time delay in response is subject-dependent for both total hemoglobin and oxygen saturation which may be attributed to the physiological differences between each subject, as inter-subject cardiac and vascular status influences blood gas delivery and exchange [47].

4.4 Noise considerations in the healthy breast

The body's normal low frequency hemodynamic fluctuations are a confounding factor in the analysis of the data produced during this study. In some cases, these fluctuations had stronger spectral amplitude than the tissue response to the stimulus. By measuring the signal to noise ratio (SNR) between the response from the gas stimulus compared to the room air delivery, the gas stimuli can be evaluated for its effectiveness in inducing changes in breast vascular hemodynamics. Indeed, without properly accounting for the response of tissue during the room-air breathing control, natural oscillations in hemodynamics could be mistakenly attributed to the gas stimuli.

These physiological fluctuations are frequency dependent. Previous investigators have noted that significant oscillations in blood flow and blood pressure exist between 0 Hz and 0.5Hz [48]. The frequency used in this study, 0.0042 Hz, coincides with the "very-

low" frequency range evaluated in spectral analyses of hemodynamics, which has been attributed to fluctuations in tissue metabolism [49].

Box plots of the SNR for total hemoglobin concentration and oxygen saturation for each gas stimulus for all subjects are shown in Figure 8. These results indicate that multiple subjects had SNR < 1. Of the three stimuli, the oxygen/carbogen gas pair induced a response in oxygen saturation which was significantly stronger than the control ($p = 0.02$, two-sample t-test, N=11). The response in total hemoglobin suggested a greater correlation than the control, although the result was not significant ($p = 0.06$ two-sample t-test, N=11). In comparison, air/carbogen was not significantly greater than the control for either total hemoglobin ($p = 0.30$ two-sample t-test, N=4) or oxygen saturation ($p = 0.25$ two-sample t-test, N=4). Air/oxygen was also not significantly greater than the control for either quantity (H_bT: $p = 0.49$ two-sample t-test, N=7; Sat: $p = 0.33$ two-sample t-test, N=7).

To compare the strength in correlation for all stimuli, SNR was compared for the four subjects who underwent all tests. Figure 9 shows that the mean SNR for the oxygen/carbogen stimulus was higher than the other stimuli, although not significantly. The lack of significance is most likely due to the small sample size in the face of relatively large inter-subject variation, especially during the air/oxygen stimulus.

5. Discussion

This study investigated the feasibility of inducing a measurable hemodynamic response in normal breast parenchyma during the breathing of controlled gas mixtures. The complex physiological changes that occur during the breathing of oxygen and carbogen were observed. The results obtained with diffuse optical imaging confirm the expectation

that the response to a gas stimuli with carbogen is dominated by changes in vasomotor control. These changes appear to override the effects of changes in pCO_2 when the gas is switched to carbogen from air or oxygen (the latter would cause an opposite and negative change in oxygen saturation independent of total hemoglobin concentration due to the rightward shift in the oxygen dissociation curve [46]). In contrast, the response to an air/oxygen stimulus is not dominated by vasomotor changes. Effects such as the change in oxygen saturation due to the change in pO_2, which oppose the expected changes due to vasomotor control, seem to play a greater role in the modulation of total hemoglobin and oxygen saturation.

An important consideration in using any respiratory stimulus for either a diagnostic or a prognostic exam is choosing the optimal gas stimulus and/or modulation frequency. These results show that significant changes can be induced in healthy breast tissue with an oxygen/carbogen stimulus. Intuitively, the oxygen/carbogen induced changes would be larger than those resulting from oxygen and room air or carbogen and room air because oxygen and carbogen induce opposing changes in vascular tone. Thus, a larger range in response would be expected from the pairing of oxygen/carbogen as the gas stimulus. Our results support the expectation of an increase in SNR – the ratio between the hemodynamic response to the gas stimulus and the response during the breathing of room air. The responses to the oxygen/carbogen stimulus were stronger than to air in both total hemoglobin ($p = 0.06$) and oxygen saturation ($p < 0.05$). In comparison, responses from the other gas stimuli did not demonstrate significant SNR ($p > 0.2$). Overall, SNR > 1 was generated in 81% of the subjects breathing the oxygen/carbogen

combination, 80% of the volunteers breathing the air/carbogen pair of gases and only 64% of participants breathing the air/oxygen stimulus.

Efforts to elevate tissue oxygen levels for improved therapy sensitivity through the controlled breathing of gas mixtures has been under investigation for over 50 years [50]. The ability to determine the sensitivity of a subject to these respiratory stimuli would have a significant impact on radiation treatment. In practice, the method described here could be used to screen for patients who would benefit from gas breathing to increase tissue oxygenation for therapy. For tumor detection, abnormal blood flow and oxygenation are known to be hallmarks of cancer [51]. The modulation of respiratory gases may be a technique to probe tissue functional maturity.

5. Conclusions

This study presents the first reported measures of significant respiratory changes in the breast resulting from a respiratory stimulus. The data suggest that consistent physiological changes can be induced with the appropriate gas breathing stimulus – specifically, oxygen/carbogen. Subjects who breathed the oxygen/carbogen stimulus showed consistent ($p < 0.05$) and significant ($p < 0.05$) responses in total hemoglobin concentration and oxygen saturation determined via MR-guided diffuse optical tomography.

However, the data also indicate that these respiratory measurements can be affected by physiological noise. Even with the breathing stimulus having the strongest response signal, specifically, the oxygen/carbogen gas pair, 19% of healthy volunteers had SNR < 1. The results highlight both the need for correct choice of breathing stimulus and the importance of monitoring normal physiological fluctuations as a control. If the technique

is to be used for further proof of concept studies in tumor imaging or treatment response, use of the oxygen/carbogen gas stimulus is recommended.

Acknowledgements

The authors would like to sincerely thank the funding sources: the Department of Defense Predoctoral Training Fellowship 503298, the National Cancer Institute grants 5P01CA080139 and 2R01CA069544, and the Center for Advanced Magnetic Resonance Technology at Stanford, P41 RR009784. The authors would also like to thank the generous efforts of Anne Sawyer, Dr. Bruce Daniel, and Dr. Brian Hargreaves.

References

[1]P. Vaupel, F. Kallinowski, and P. Okunieff, “Blood Flow, Oxygen and Nutrient Supply, and Metabolic Microenviroment of Human Tumors: A Review,” Cancer Res **49**, pp. 6449-6465 (1989).

[2]D. M. Brizel, S. P. Scully, J. M. Harrelson, L. J. Layfield, J. M. Bean, L. R. Prosnitz, and M. W. Dewhirst, “Tumor oxygenation predicts for the likelihood of distant metastases in human soft tissue sarcoma,” Cancer Res **56** (5), pp. 941-3 (1996).

[3]M. Nordsmark, S. M. Bentzen, V. Rudat, D. Brizel, E. Lartigau, P. Stadler, A. Becker, M. Adam, M. Molls, J. Dunst, D. J. Terriis, and J. Overgaard, “Prognostic value of tumor oxygenation in 397 head and neck tumors after primary radiation therapy. An international multi-center study,” Radiother Oncol **77** (1), pp. 18-24 (2005).

[4]N. T. S. Evans and P. F. D. Naylor, “The Effect of Oxygen Breathing and Radiotherapy Upon the Tissue Oxygen Tension of Some Human Tumours,” British J Radiol **36** (426), pp. 418-425 (1963).

[5]J. M. Henk, “Late Results of a Trial of Hyperbaric-Oxygen and Radiotherapy in Head and Neck-Cancer - a Rationale for Hypoxic Cell Sensitizers,” Int J Radiat Oncol **12** (8), pp. 1339-1341 (1986).

[6]H. Frank, R. Loewe, C. Loewe, G. Oberhuber, B. Schwaighofer, K. Huber, and R. Weissleder, “Efficacy of thrombolytic therapy in pulmonary embolism determined by MION-enhanced MRA: an experimental study in rabbits,” Invest Radiol **33** (12), pp. 853-7 (1998).

[7]T. H. Foster and L. Gao, “Dosimetry in Photodynamic Therapy - Oxygen and the Critical Importance of Capillary Density,” Radiat Res **130** (3), pp. 379-383 (1992).

[8]O. Thews, D. K. Kelleher, and P. Vaupel, “Dynamics of tumor oxygenation and red blood cell flux in response to inspiratory hyperoxia combined with different levels of inspiratory hypercapnia,” Radiother Oncol **62** (1), pp. 77-85 (2002).

[9]Guyton, A. & Hall, J., Textbook of Medical Physiology, 11 ed. (Elsevier, Philadelphia, 2006).

[10]G. W. N. Eggers, J. V. Warren, H. W. Paley, and J. J. Leonard, “Hemodynamic Responses to Oxygen Breathing in Man,” J Appl Physiol **17** (1), pp. 75 (1962).

[11]T. F. Floyd, J. M. Clark, R. Gelfand, J. A. Detre, S. Ratcliffe, D. Guvakov, C. J. Lambertsen, and R. G. Eckenhoff, “Independent cerebral vasoconstrictive effects of hyperoxia and accompanying arterial hypocapnia at 1 ATA,” J Appl Physiol **95** (6), pp. 2453-2461 (2003).

[12]Brown, S., Miller, W., & Eason, J., Exercise Physiology: Basis of Human Movement in Health and Disease, 1 ed. (Lippincott Williams & Wilkins, Philadelphia, 2006).

[13]M. Ashkanian, P. Borghammer, A. Gjedde, L. Ostergaard, and M. Vafaee, “Improvement of Brain Tissue Oxygenation by Inhalation of Carbogen,” Neuroscience **156** (4), pp. 932-938 (2008).

[14]B. A. Berkowitz, “Adult and newborn rat inner retinal oxygenation during carbogen and 100% oxygen breathing - Comparison using magnetic resonance imaging Delta P-O-2 mapping,” Invest Ophth Vis Sci **37** (10), pp. 2089-2098 (1996).

[15]B. F. Jordan, G. O. Cron, and B. Gallez, “Rapid monitoring of oxygenation by 19F magnetic resonance imaging: Simultaneous comparison with fluorescence quenching,” Magn Reson Med **61** (3), pp. 634-8 (2009).

[16]G. M. Palmer, R. J. Viola, T. Schroeder, P. S. Yarmolenko, M. W. Dewhirst, and N.

Ramanujam, “Quantitative diffuse reflectance and fluorescence spectroscopy: tool to monitor tumor physiology in vivo,” J Biomed Opt **14** (2), pp. 024010 (2009).

[17]J. O'Connor, A. Jackson, G. Buonaccorsi, D. Buckley, C. Roberts, Y. Watson, S. Cheung, D. McGrath, J. Naish, C. Rose, P. Dark, G. Jayson, and G. Parker, “Organ-Specific Effects of Oxygen and Carbogen Gas Inhalation on Tissue Longitudinal Relaxation Times,” Magn Reson Med **58**, pp. 490-496 (2007).

[18]L. Martin, E. Lartigau, P. Weeger, P. Lambin, A. M. Le Ridant, A. Lusinchi, P. Wibault, F. Eschwege, B. Luboinski, and M. Guichard, “Changes in the Oxygenation of Head and Neck Tumors during Carbogen Breathing,” Radiother Oncol **27** (2), pp. 123-130 (1993).

[19]M. E. Powell, S. A. Hill, M. I. Saunders, P. J. Hoskin, and D. J. Chaplin, “Effect of carbogen breathing on tumour microregional blood flow in humans,” Radiother Oncol **41** (3), pp. 225-31 (1996).

[20]T. J. Dunn, R. D. Braun, W. E. Rhemus, G. L. Rosner, T. W. Secomb, G. M. Tozer, D. J. Chaplin, and M. W. Dewhirst, “The effects of hyperoxic and hypercarbic gases on tumour blood flow,” Brit J Cancer **80** (1-2), pp. 117-26 (1999).

[21]J. L. Lanzen, R. D. Braun, A. L. Ong, and M. W. Dewhirst, “Variability in blood flow and pO2 in tumors in response to carbogen breathing,” Int J Radiat Oncol **42** (4), pp. 855-9 (1998).

[22]S. Dische, “What Have We Learnt from Hyperbaric-Oxygen,” Radiother Oncol **20**, pp. 71-74 (1991).

[23]A. Rojas, F. A. Stewart, K. A. Smith, J. A. Soranson, V. S. Randhawa, M. R. Stratford, and J. Denekamp, “Effect of Anemia on Tumor Radiosensitivity under Normo and

Hyperbaric Conditions," Int J Radiat Oncol **13** (11), pp. 1681-1689 (1987).

[24]H. L. Liu, Y. L. Song, K. L. Worden, X. Jiang, A. Constantinescu, and R. P. Mason, "Noninvasive investigation of blood oxygenation dynamics of tumors by near-infrared spectroscopy," App Optics **39** (28), pp. 5231-5243 (2000).

[25]J. G. Kim, D. W. Zhao, Y. L. Song, A. Constantinescu, R. P. Mason, and H. L. Liu, "Interplay of tumor vascular oxygenation and tumor pO(2) observed using near-infrared spectroscopy, an oxygen needle electrode, and F-19 MR pO(2) mapping," J Biomed Opt **8** (1), pp. 53-62 (2003).

[26]T. O. McBride, B. W. Pogue, E. Gerety, S. Poplack, U. L. Osterberg, and K. D. Paulsen, "Spectroscopic diffuse optical tomography for quantitatively assessing hemoglobin concentration and oxygenation in tissue," Appl Optics **38** (25), pp. 5480-90 (1999).

[27]B. W. Pogue, S. P. Poplack, T. O. McBride, W. A. Wells, O. K. S., U. L. Osterberg, and K. D. Paulsen, "Quantitative Hemoglobin Tomography with Diffuse Near-Infrared Spectroscopy: Pilot Results in the Breast," Radiology **218** (1), pp. 261-6 (2001).

[28]A. Li, Q. Zhang, J. Culver, E. Miller, and D. Boas, "Reconstructing chromosphere concentration images directly by continuous-wave diffuse optical tomography," Opt Lett **29** (3), pp. 256-8 (2004).

[29]M. S. Patterson, J. D. Moulton, B. C. Wilson, K. W. Berndt, and J. R. Lakowicz, "Frequency-Domain Reflectance for the Determination of the Scattering and Absorption Properties of Tissue," Appl Optics **30** (31), pp. 4474-4476 (1991).

[30]E. Gratton, W. W. Mantulin, M. J. van de Ven, J. B. Fishkin, M. B. Maris, and B. Chance, "A novel approach to laser tomography," Bioimaging **1**, pp. 40-46 (1993).

[31]B. Brooksby, S. Jiang, H. Dehghani, B. W. Pogue, K. D. Paulsen, J. B. Weaver, C. Kogel, and S. P. Poplack, "Combining near infrared tomography and magnetic resonance imaging to study in vivo breast tissue: implementation of a Laplacian-type regularization to incorporate MR structure," J Biomed Opt **10** (5), pp. 050504-1-10 (2005).

[32]X. Ouyang, W. H. Wong, V. E. Johnson, X. Hu, and C. T. Chen, "Incorporation of correlated structural images in PET image reconstruction," IEEE T Med Imaging **13** (4), pp. 627-40 (1994).

[33]C. M. Carpenter, S. Srinivasan, B. W. Pogue, S. Jiang, H. Dehghani, and K. D. Paulsen, in *Biomedical Optics*, OSA Technical Digest (CD) , (Optical Society of America, St. Petersberg, FL, 2008), pp. BSuB4.

[34]S. Jiang, B. Pogue, A. Laughney, C. Kogel, and K. Paulsen, "Measurement of pressure-displacement kinetics of hemoglobin in normal breast tissue with near-infrared spectral imaging," Appl Opt **48** (10), pp. D130-D136 (2009).

[35]T. O. McBride, B. W. Pogue, S. Jiang, U. L. Osterberg, and K. D. Paulsen, "A parallel-detection frequency-domain near-infrared tomography system for hemoglobin imaging of the breast in vivo," Rev Sci Instrum **72** (3), pp. 1817-1824 (2001).

[36]S. R. Arridge, M. Scheiger, and D. T. Delpy, in *Inverse Problems in Scattering and Imaging*, (SPIE, San Diego, 1992), pp. 372-383.

[37]K. D. Paulsen and J. H., "Spatially varying optical property reconstruction using a finite element diffusion equation approximation," Med Phys **22** (6), pp. 691-701 (1995).

[38]H. Dehghani, B. W. Pogue, J. Shudong, B. Brooksby, and K. D. Paulsen, "Three-dimensional optical tomography: resolution in small-object imaging," Appl Optics **42** (16), pp. 3117-28 (2003).

[39]B. Brooksby, S. Jiang, H. Dehghani, B. W. Pogue, K. D. Paulsen, C. Kogel, M. Doyley, J. B. Weaver, and S. P. Poplack, "Magnetic Resonance-Guided Near-Infrared Tomography of the Breast," Rev Sci Instrum **75** (12), pp. 5262-5270 (2004).

[40]S. Reeder, N. Pelc, M. Alley, and G. Gold, "Multi-coil Dixon chemical species separation with an iterative least squares method," Magn Reson Med **51**, pp. 35-45 (2004).

[41]B. W. Pogue, "Image analysis methods for Diffuse Optical Tomography," J Biomed Opt **11** (3), pp. 33001 (2006).

[42]H. Xu, R. Springett, H. Dehghani, B. W. Pogue, K. D. Paulsen, and J. F. Dunn, "Magnetic-resonance-imaging--coupled broadband near-infrared tomography system for small animal brain studies," Appl Opt **44** (10), pp. 2177-2188 (2005).

[43]T. O. McBride, B. W. Pogue, U. L. Osterberg, and K. D. Paulsen, "Strategies for absolute calibration of near infrared tomographic tissue imaging," Adv Exp Med Biol **530**, pp. 85-99 (2003).

[44]R. B. King, A. Deussen, G. M. Raymond, and J. B. Bassingthwaighte, "A vascular transport operator," Am J Physiol **265** (6 Pt 2), pp. H2196-208 (1993).

[45]B. R. Rosen, J. W. Belliveau, J. M. Vevea, and T. J. Brady, "Perfusion Imaging with Nmr Contrast Agents," Magn Reson Med **14** (2), pp. 249-265 (1990).

[46]West, J., Respiratory Physiology: The Essentials, 8 ed. (Lippincott Williams & Wilkins, Philadelphia, 2008).

[47]M. J. Brischetto, R. P. Millman, D. D. Peterson, D. A. Silage, and A. I. Pack, "Effect of Aging on Ventilatory Response to Exercise and Co2," J Appl Physiol **56** (5), pp. 1143-1150 (1984).

[48]T. B. J. Kuo, C. M. Chern, W. Y. Sheng, W. J. Wong, and H. H. Hu, "Frequency domain analysis of cerebral blood flow velocity and its correlation with arterial blood pressure," J Cerebr Blood F Met **18** (3), pp. 311-318 (1998).

[49]L. Yan, Y. Zhuo, Y. Ye, S. Xie, J. An, G. Aguirre, and J. Wang, "Physiological Origin of Low-Frequency Drift in Blood Oxygen Level Dependent (BOLD) Functional Magnetic Resonance Imaging (fMRI)," Magn Reson Med **61**, pp. 819-827 (2009).

[50]F. Urbach and W. K. Noell, "Effects of Oxygen Breathing on Tumor Oxygen Measured Polarographically," J Appl Physiol **13** (1), pp. 61-65 (1958).

[51]C. Kuhl, "The Current Status of Breast MR Imaging Part I, Choice of Technique, Image Interpretation, Diagnostic Accuracy, and Transfer to Clinical Practice," Radiology **244** (2), pp. 356-378 (2007).

Tables

	Gas 1	Gas2	Number of Subjects
Stimulus 1	Air	Air	11
Stimulus 2	Oxygen	Carbogen	11
Stimulus 3	Air	Carbogen	5
Stimulus 4	Air	Oxygen	7

Table 1: The number of volunteers monitored with each gas stimulus pair.

	Ox/Cb : Control	Air/Cb : Control	Air/Ox : Control
HbT	**p = 0.062, N=11**	**p = 0.297, N=4**	**p = 0.489, N=7**
O2 Sat	**p = 0.035, N=11**	**p = 0.251, N=4**	**p = 0.33, N=7**

Table 2: Comparison of the correlation while breathing a gas stimulus compared to the correlation while breathing only room air (control). Shown are the significance values resulting from two-sample t-tests, determining if the means were significantly different.

Figures

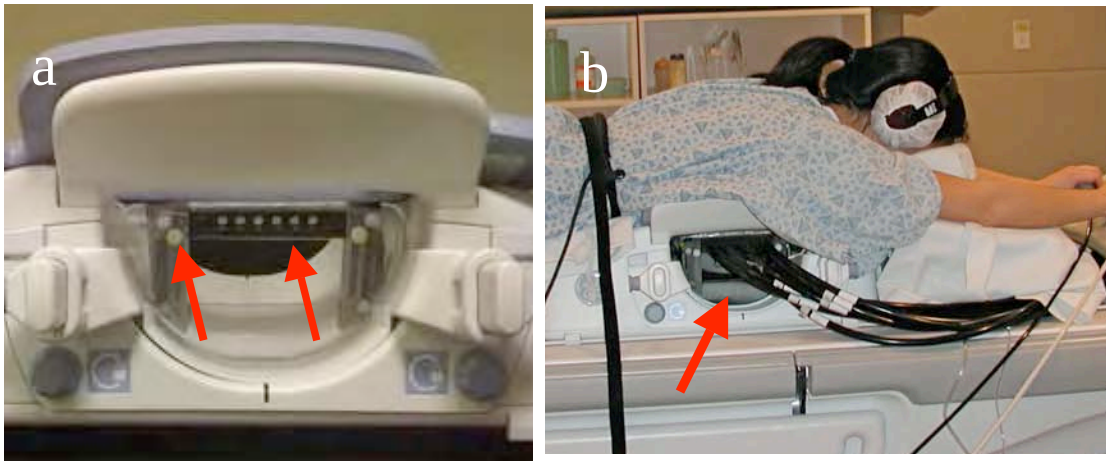

Figure 1 (a) Photograph of the optical fiber holder incorporated into a biopsy attachment for an 8-channel breast coil (USA Instruments). Slots in the optical fiber holder allowed for vertical positioning of the optical fibers, while the biopsy attachment allowed positioning in the medical/lateral direction. These degrees of freedom in the fiber interface enabled the optical fibers to maintain contact with the breast. Arrows indicate the fiber holder and the vertical adjustment. (b) Photograph of a healthy subject with fibers attached to the MR coil. The arrow shows the fibers attached to the fiber holder.

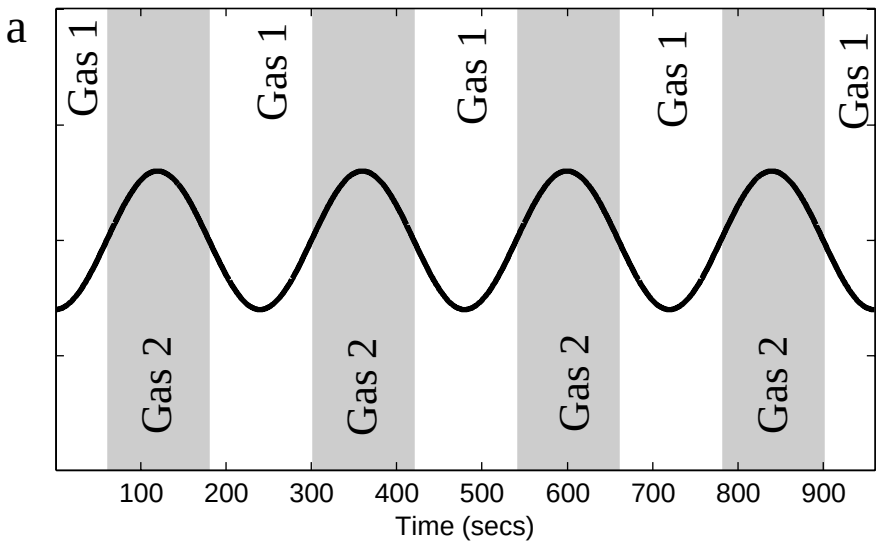

Figure 2: Gas time series for the stimuli combinations in Table 1. (a) Timing diagram indicating duration of each gas stimulus. (b) The true timing of each gas, shown in blue, was modeled by a sine wave, shown in red, for data processing. The shading behind the modeled stimulus indicates the active gas.

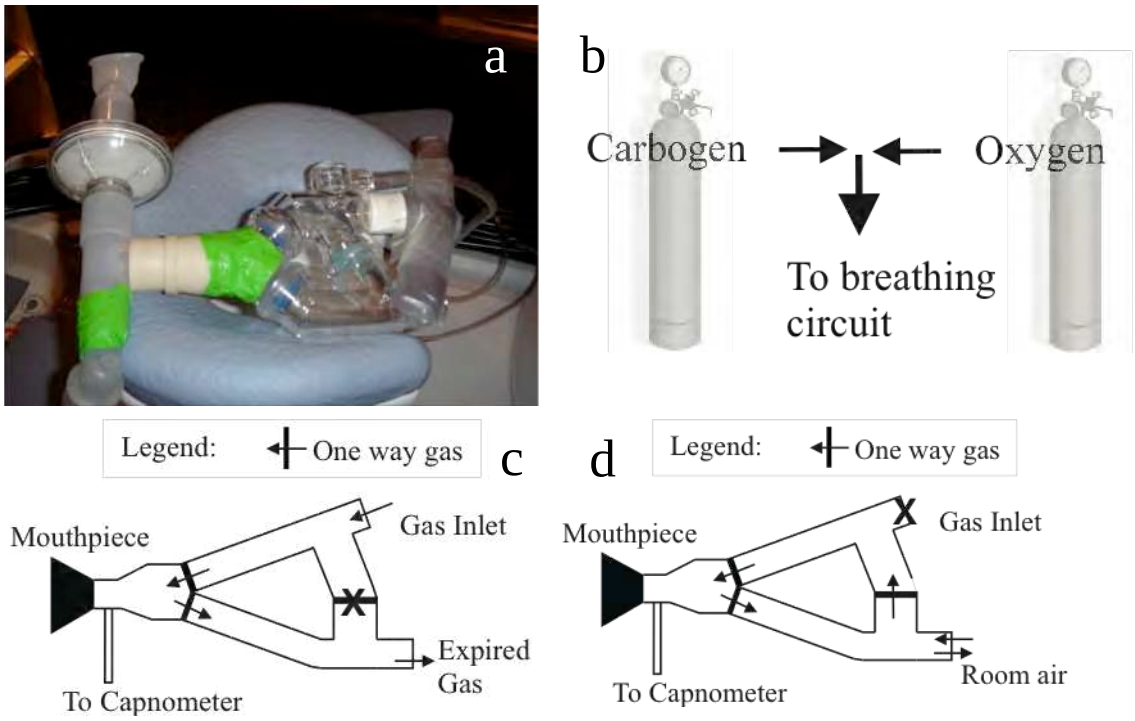

Figure 3 (a) Photograph of the gas breathing circuit placed on the MR table. (b) Schematic indicating that the carbogen and oxygen gases were controlled with a custom computer-controlled valve which was synchronized via software to maintain the desired modulation rate. (c) Diagram of circuit operation during gas stimulus. During oxygen or carbogen breathing, pressure from the inlet closes the valve to room air, preventing room air from entering the circuit. All valves were one-way. A fan in the MR bore was turned on to prevent re-breathing of expired gases. (d) Diagram of circuit operation during air stimulus. During air stimulus, the lack of pressure from the inlet opened the room air valve, allowing room air to be drawn into the circuit. A small tube was inserted near the mouthpiece to channel a small amount of expired air to an oxycapnometer to monitor exhaled gas concentrations.

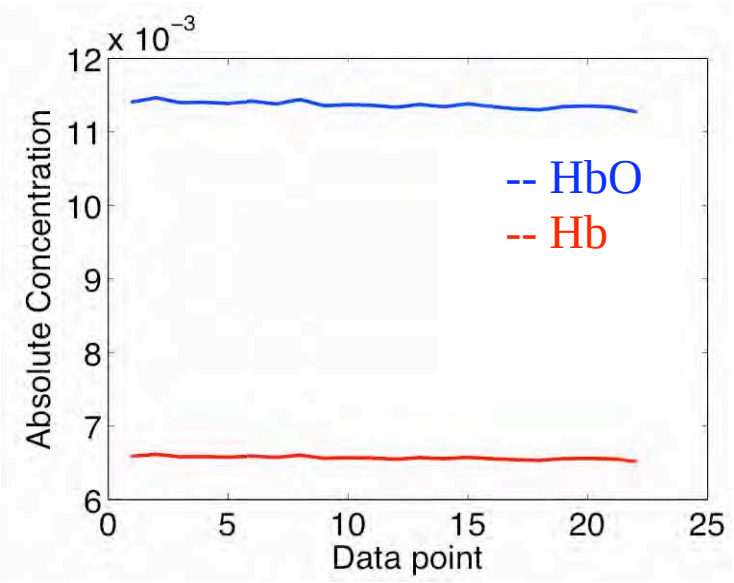

Figure 4: Instrumentation related fluctuations in hemoglobin concentration recordings in a tissue-simulating phantom. Standard deviation in fitted deoxy-hemoglobin is 0.19% of its amplitude while standard deviation in fitted oxy-hemoglobin (HbO) is 0.22% of its amplitude.

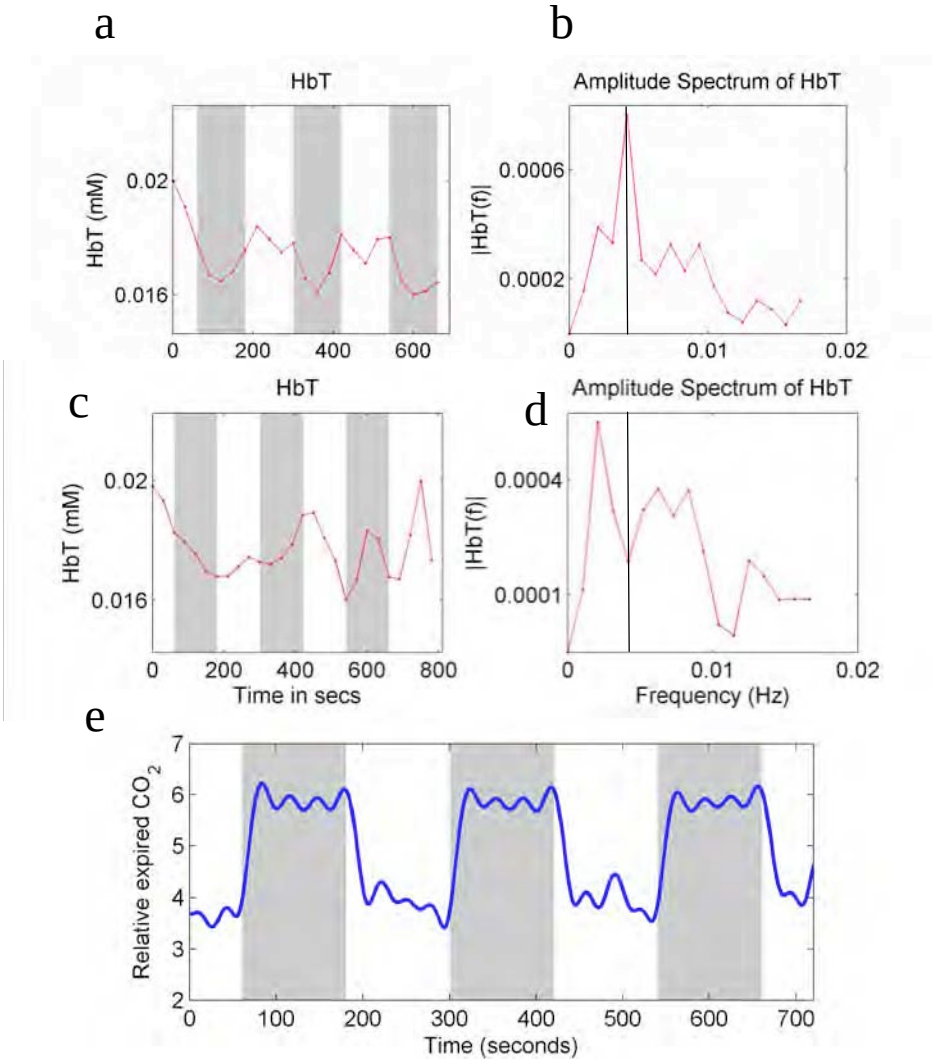

Figure 5: Temporal and frequency response of total haemoglobin (HbT) for oxygen/carbogen gas stimulus compared to an air control in a typical subject when SNR > 1. In (a), white bars indicate delivery of the O_2 stimulus and gray bars symbolize carbogen administration whereas in (c), both bars indicate the breathing of room air. Total hemoglobin oscillations during gas stimulus show a significantly larger peak at 0.0042 Hz , the stimulus frequency, than the air control (compare b vs. d), indicating the tissue response to the stimulus was larger than the physiological noise. Oscillations in CO_2 measured with the oxycapnograph during the oxygen/carbogen stimulus shown in (e) demonstrate subject compliance during the experimental protocol.

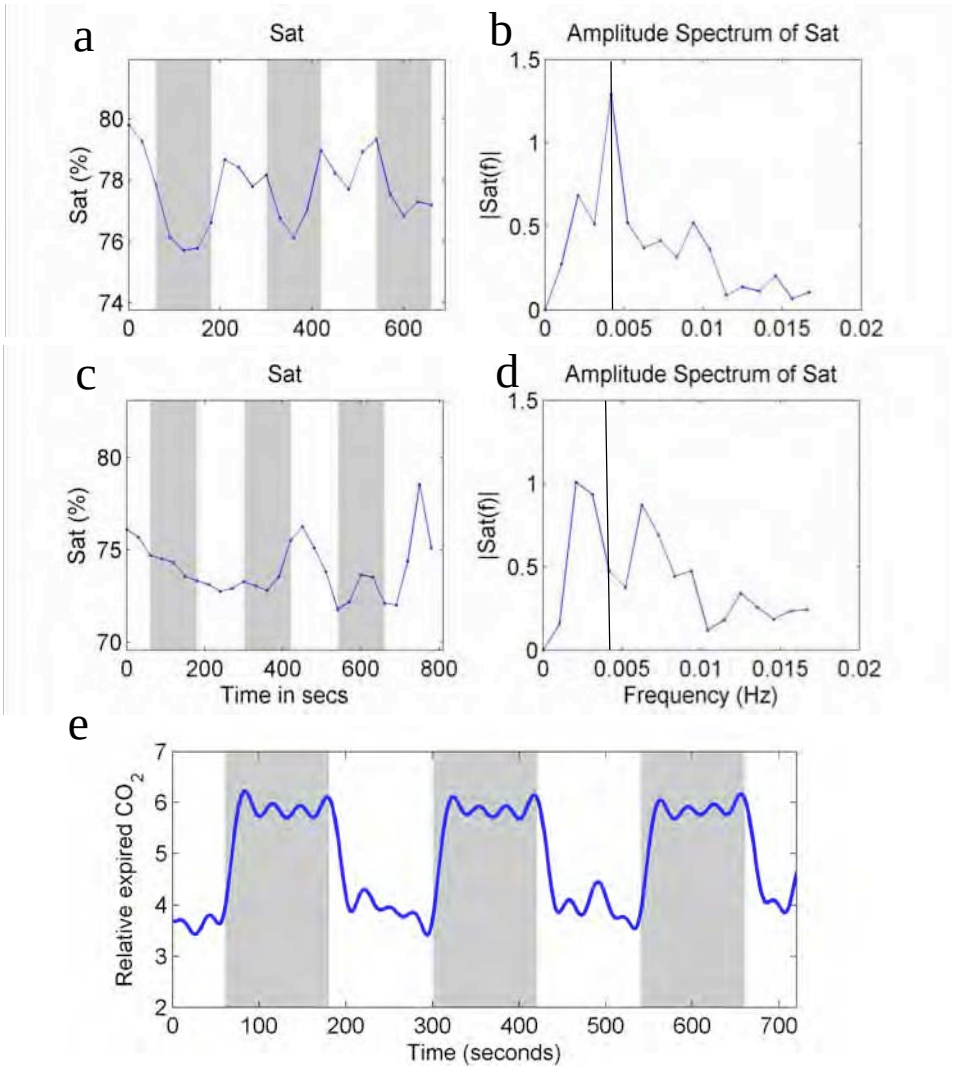

Figure 6: Same as Figure 5 for oxygen saturation.

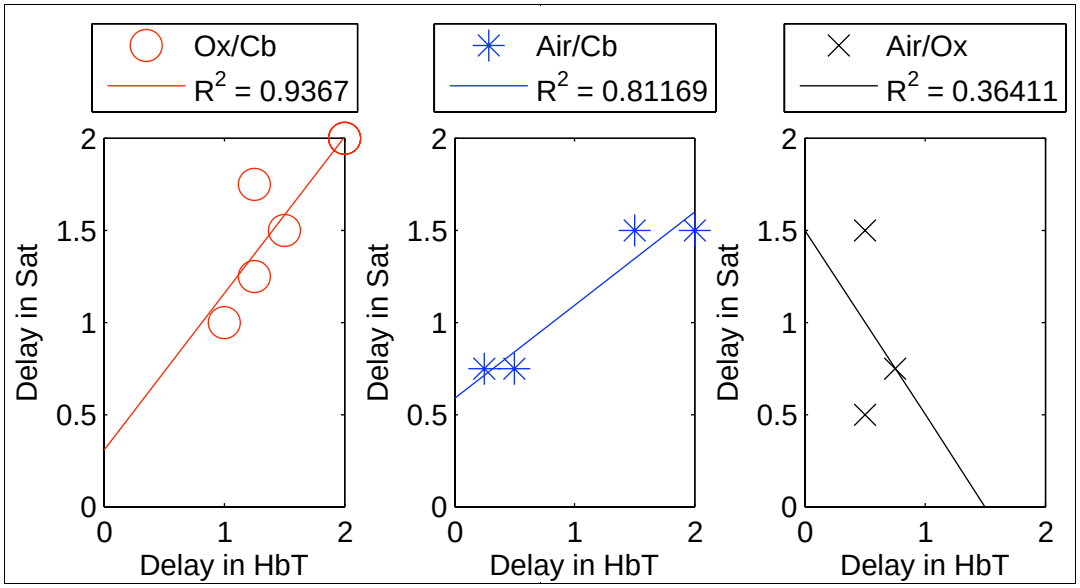

Figure 7: Time lag comparison of oxygen saturation (Sat) vs total haemoglobin (HbT) for the three gas stimuli (in units of). The stimuli with carbogen demonstrate vasodilation, a response that allows highly oxygenated blood to enter the breast tissue, thus washing out deoxygenated hemoglobin and increasing oxygen saturation. Oxygen saturation and total hemoglobin during air/oxygen stimulus is not dominated by changes in vascular tone. Instead, these changes may be influenced by changes in pO_2.

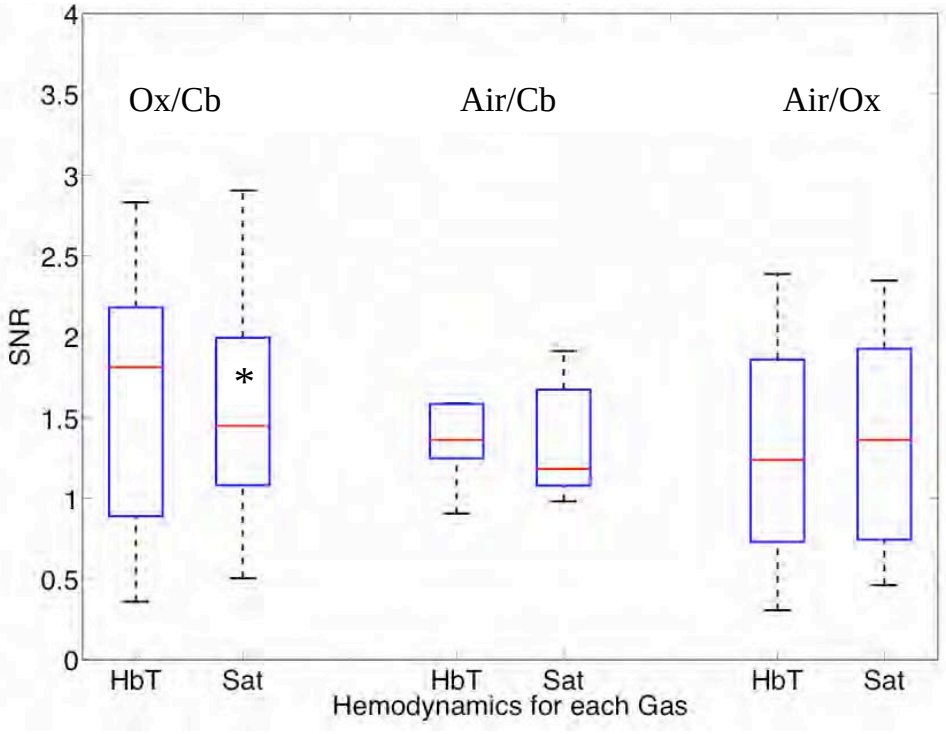

Figure 8: Signal to noise ratio (SNR) in total hemoglobin concentration (HbT) and oxygen saturation (Sat) for each gas stimulus in fibroglandular tissue (FG). (*) denotes statistical significance. P-values and number of subjects in each group are given in Table 2.

687

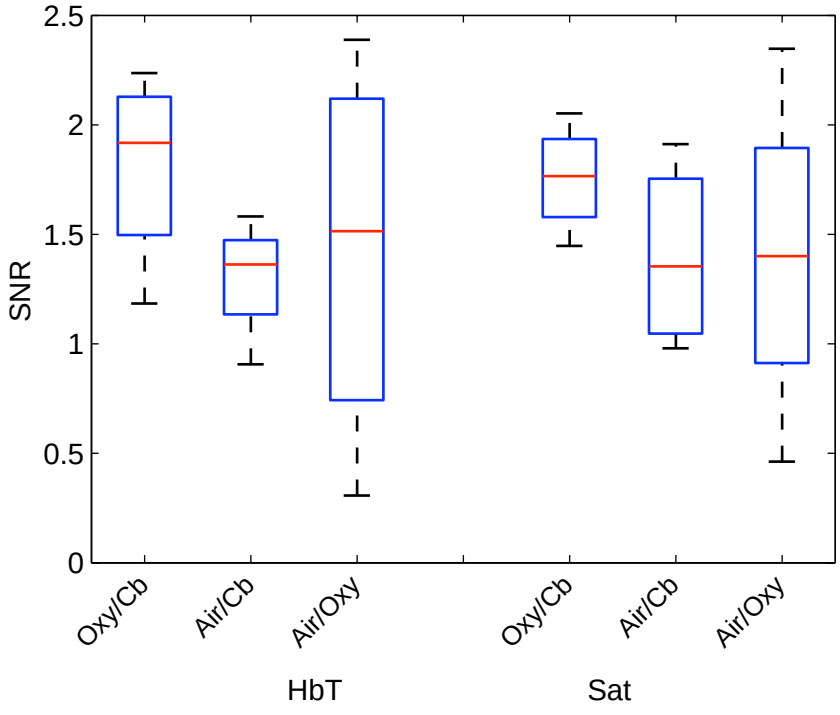

688

689 **Figure 9: Average signal to noise ratio (SNR) for total hemoglobin (HbT) and**

690 **oxygen saturation (Sat) for the 4 subjects who received all three gas stimuli. Error**

691 **bars indicate the standard deviation in SNR for each gas combination.**

Inspired gas induced vascular change in tumors with MR-guided Near-Infrared Imaging: A Human Breast Pilot Study

CM Carpenter[1], R Rakow-Penner[2], S. Jiang[1], BL Daniel[2], BW Pogue[1], GH Glover[2], and KD Paulsen[1]

[1]Thayer School of Engineering, Dartmouth College, Hanover, NH, USA
[2]Department of Radiology, School of Medicine, Stanford University, Stanford, CA, USA
(Email: colincarpenter@stanford.edu or Keith.Paulsen@dartmouth.edu, Tel:(603) 646-1110, Fax:(603) 646-3856)

1. Abstract

This study investigated the differences in the response of breast tumor tissue vs healthy fibroglandular tissue to inspired gases. Cycles of carbogen and oxygen gas were administered while measuring the changes with Magnetic Resonance guided (MRg) Near-Infrared (NIR) imaging in a pilot study of breast cancers in vivo. The results show that the overall vaso-response observed in the total hemoglobin level of healthy tissue had approximately twice the modulation amplitude of the tumor region. The cross correlation between the vascular tissue and the modulated gas stimulus, controlled for background physiological changes, showed that the correlation in tumor tissue was approximately 36% lower than that of the healthy surrounding fibroglandular tissue. This data supports the hypothesis that tumor vasculature has a poorly functioning vaso-dilatory mechanism, most likely caused by dysfunctional smooth muscle cells lining the vasculature. This study provides the first quantitative analysis of inspired gas changes in human breast tumors with MRg-NIR.

2. Introduction

The high sensitivity of magnetic resonance (MR) breast imaging has encouraged the development of adjunct techniques which aim to improve tumor specificity. These techniques can leverage knowledge of the location of a suspect lesion (provided by MR) to improve information content by examining other properties of breast cancer. For example, chemical metabolites can be imaged with MR Spectroscopy [1]; cellular packing density can be imaged with MR Diffusion Weighted Imaging [2]; structural architecture can be imaged with MR-based elastography[3] and optical imaging [4]; and hemodynamic information such as total hemoglobin and hypoxia can be determined with optical imaging [5]. This study reports on the contrast derived from measuring the vascular compliancy between normal and diseased tissue, which may have promising clinical utility in increasing imaging specificity.

Tumor vasculature is known to lack proper motor function because of the deficiency in smooth muscle cells lining the endothelial cells[6]. Thus, tumors are expected to respond differently to changes in the local environment than normal tissue. These changes may be induced by modulated gas breathing of oxygen and/or carbogen (95% oxygen, 5% carbon dioxide) [7]. Additionally, this contrast may also have the potential to identify tissues that are less susceptible to therapy, due to their poor vascular response to changes in oxygenation[8]. By determining the magnitude of vascular changes due to a respiratory stimulus, potential subjects who might respond more successfully to therapy may be identified. This study had a goal of characterizing breast tumors by measuring the impaired vasomotor function in tumor vasculature with MR-guided NIR imaging.

3. Methods

3.1 MR-guided NIR Imaging

NIR tomography produces quantitative images of oxyhemoglobin, deoxyhemoglobin, water content, and lipid content by sampling the absorption properties of light in the near infrared spectral range of 650-950 nm. These absorption properties are spectrally fit using known tissue absorption spectra to determine the tissue contents[5]. This technique has been successfully applied to a number of tissues, most notably the breast [5, 9] and brain[10].

In this study, data were acquired with an optical imaging instrument that collected data simultaneously within a breast coil in a 3T MRI (Discovery MR750, GE Medical Systems, Waukesha, WI). The optical instrument used three wavelengths (661, 785, 826nm) of light which were intensity modulated at unique frequencies and jointly coupled to a source illumination fiber; this technique is described in more detail in Jiang et al[11]. Light was sequentially transmitted to sixteen locations around the breast and detected by fifteen photomultiplier tubes acquiring data in parallel, to sample breast optical properties every 30 seconds. The performance of this system is described in more detail in a previous work[12]. The 3T anatomical (water/fat separated DIXON sequence) MR images were used to separate the fibroglandular from the adipose tissue, and were input into an MR-derived reconstruction to recover hemodynamic parameters[13]. These experiments were carried out simultaneously with a BOLD acquisition sequence (BOLD results in preparation).

3.2 Human Respiratory Breathing Experiments

Hemodynamics were dynamically modulated by introducing oxygen (100% O_2) and carbogen (95%O_2:5%CO_2) into the breathing circuit shown in Figure 1d. Subjects breathed through a mouthpiece and had their noses sealed to prevent inadvertent breathing of room air. The oxygen and carbogen gases (Praxair) were computer-controlled to switch between oxygen and carbogen every two minutes for a total of four cycles. Flow rates were set at 9 liters/min and were monitored by flowmeters attached to the tanks. Gas from the respiratory circuit was sampled with an oxycapnograph (Capnomac Ultima, GE Healthcare, Waukesha, WI) to monitor expired CO_2, O_2, and respiratory rate to ensure breathing compliance.

Oxygen and carbogen breathing leads to complex changes in blood flow and hemoglobin oxygen saturation because of the interplay between pO_2, pCO_2, and vascular function. However, it was recently shown that the total hemoglobin and oxygen saturation in the breast during oxygen and carbogen modulation are dominated by changes in the vasomotor function. We have also shown that some subjects do not exhibit significant changes in hemodynamics during this stimulus of gas breathing [14]. This is probably due to the variability in metabolism, which may cause a substantial modulation of physiology independent of the respiratory stimulus [15]. Thus, a Gas-to-Air Ratio (GAR), shown in equation (1), is calculated as a quantitative metric to determine how large the modulation due to gas is compared to the background physiological modulation during air breathing.

$$GAR = \frac{\max\left(Corr_{Gas}\right)}{\max\left(Corr_{Air}\right)} \tag{1}$$

In (1), the GAR is computed by finding the ratio of the maximum correlation of the gas to the stimulus to the maximum correlation of the all air control.

3.3 Data Analysis

The characteristics of the breast tissue response were calculated for each time point in the respiratory stimulus. Measurements of the AC amplitude and phase of the detected light intensity were calibrated by fitting measurements from the first time point to a homogeneous model for absorption and scatter[16]. This method, also known as differential imaging, provides measurements of optical property changes which are free from fiber coupling noise[17]. The resulting data were fit via an iterative least squares algorithm to a diffusion model for light propagation in tissue[18]. Tissue adipose, fibroglandular, and suspect lesion boundaries were defined by MRI and input into the image reconstruction to determine tissue properties of these regions[10, 19]. This procedure provides reconstructed tissue properties that are robust to system noise[20].

The resulting images of total hemoglobin were mean filtered in time, and cross correlated to the gas stimulus time series, which was modeled with a sinusoid with a frequency of 0.042Hz. This approximation was made because respiratory physiology acts as a low-pass filter to vascular contrast[21, 22]. The first period of data was dropped to account for respiratory changes due to the switch from room air to the gas stimulus.

The cross correlation metric provides measures of correlation and time lag between the tissue response and the gas stimuli. The time lag at maximum correlation represents the lag in time between the gas stimulus and the response in the tissue, whereas the

correlation at this time lag represents the degree to which the vasculature is affected by the gas stimulus. Correlation and time lags were calculated for healthy fibroglandular tissue and tumor tissue. Tumors were identified by contrast-enhanced MRI (CE-MRI) and segmented with the aid of the radiologist (B.D). The subjects in this study all provided informed consent, following the procedures approved by the Institutional Review Board at Stanford Medical Center.

4. Results and Discussion

An example of the vascular response to the gas stimulus for both the healthy fibroglandular and the tumor tissue is shown in Figure 2b,d, respectively. The response during an air/air control for healthy and tumor vasculature is shown in Figure 2a,c, respectively. MRg optical data points are plotted as open circles. Overlaid in black (with data points labelled as closed circles) are the best fit sinusoids that match the data. These sinusoids are phase shifted to match the time lag of the tissue response, and normalized to the amplitude of the response. These curves allow a visual comparison of the cross correlation between the tissue response and the modeled gas stimulus. Clearly, the response during air/air breathing, shown in Figure 2a,c, has lesser correlation to the sinusoidal stimulus than that of oxygen/carbogen breathing, shown in Figure 2b,d (0.7 vs. 0.27 in healthy tissue, and 0.65 vs. 0.21 in tumor tissue). Additionally, the response during the air/air control had a lower modulation amplitude.

Comparing healthy and tumor tissue during the gas breathing stimulus, the correlation for the healthy tissue was 0.70, while the correlation for the tumor tissue was lower, at 0.65. The modulation amplitude of response in this case also showed a

difference, as the healthy tissue varied by approximately 8% of the average total hemoglobin value, whereas the tumor tissue varied by approximately 4%.

Since the vascular changes induced during gas breathing can be insignificant in some subjects, the Gas to Air (GAR) ratio was computed. This metric provides a means to gauge the relative magnitude of the change with respect to normal air variations which are from biological noise. These results are shown for two patients in Figure 3.

The tumor regions of interest for these cases are identified by CE-MRI. These images are shown in Figure 3a,c. The sequences used to collect CE-MRI data were 3D T1-weighted Gradient echo images (TR/TE/flip angle = 30/8/40°) collected on a 1.5T MR system (Signa Excite, GE Medical Systems, Waukesha, WI). These images show regions of contrast enhancement which were histologically confirmed invasive ductal carcinomas. The optical data was collected in the plane indicated by the vertical lines in the CE-MRI images. Data from these planes were used to form images of the maximum correlation of the breast tissue to the respiratory stimulus compared to the air control.

The Gas to Air ratio for total hemoglobin of the tumor tissue compared to the normal surrounding fibroglandular tissue is shown in Figure 3b,d. There is a substantial separation in the average GAR between the normal and tumor tissue, which is on average 1.8 in tumor tissue, to 2.8 on average in normal tissue. This GAR change is due to a weaker correlation in the tissue response to the gas stimulus in these cases. These results could be explained by a lack of adequate smooth muscle cells to allow proper vasodilatory response.

These results are predicted based on histological studies in tumors which reveal inadequate smooth muscle cells lining the vasculature[6]. Without proper functioning

smooth muscle cells to control vascular tone, blood volume changes are expected to be smaller. For example, in healthy tissue, the breathing of carbogen would normally lead to vascular dilation due to the lack of oxygen in the blood. The lack of smooth muscle cells in tumor tissue would prevent the vasculature from dilating, resulting in a smaller or inconsistent change upon the introduction of carbogen. Conversely, the switch to oxygen gas from carbogen would lead to vascular constriction in normal healthy tissue. Again, the lack of proper functioning vasocontrol in a tumor would result in a smaller or inconsistent response to the stimulus, and thus less vascular constriction. These changes can be determined with the cross correlation metric, which provides a quantification of the agreement of the measured tissue response to the gas stimulus.

Interestingly, the phase of the vascular change in the tumor tissue, shown in Figure 2d, is different than that of the healthy tissue, shown in Figure 2b. This indicates a time lag between the tissue and the gas stimulus. This lag could be explained by a delay in the blood arriving in the tumor due to poor tissue perfusion, a well-documented characteristic of tumors[23].

5. Conclusions

The search for increased specificity in breast cancer continues in the radiology community due to inadequate biomarkers of malignancy. Vascular deficiency has been noted as one of the key hallmarks of breast cancer, but until recently, tools to measure it have been inadequate. Breathing oxygenated gases is a common method to induce and measure changes in tissue vascular function. This technique has been predominantly used in investigating brain tissue using Blood Oxygen Level Dependent (BOLD) MR

Imaging. However, the ability to monitor this contrast has been limited in the breast, due to the difficulty in inducing and measuring changes in hemodynamics. In this study, BOLD changes in the breast were simultaneously collected, and are the subject of another study. The use of MRg NIR allows the effects from oxygen saturation and blood content (total hemoglobin) to be separated.

Here, a pilot study was carried out using an oxygen/carbogen breathing protocol to produce hemodynamic changes. The functional changes in the tumor regions were compared to the surrounding healthy tissue, by cross correlating the measured response with the modeled breathing stimulus. This method provided self-referenced maps of the magnitude and time delay of vascular response of a region of interest detected during breast MR mammography. It is important to highlight that the changes shown in Figure 3 are the ratios between the induced stimulus and the background physiology, as monitoring background hemodynamic changes are an important control in measuring vascular function due to gas stimulus.

To summarize, the relative total hemoglobin variation was about two times higher in healthy tissue than tumor tissue. Additionally, the magnitude of the cross correlation between the tumor tissue during inspired gas compared to an air-air control was 36% less than that of the fibroglandular tissue compared to the control. Although this is a preliminary pilot study, this study shows the potential of using hemodynamic modulation as a tissue biomarker for diagnostic potential. Alternately, this metric could be used as a means to measure vascular function to determine sensitivity to therapy.

6. Acknowledgements

The authors would like to acknowledge the generous help of Anne Sawyer, Sandra Rodriguez, and Dr. Brian Hargreaves from the Stanford Department of Radiology. We also gratefully acknowledge the funding sources: the Department of Defense Predoctoral Training Fellowship 503298, the National Cancer Institute grants 5P01CA080139 and 2R01CA069544, and the Center for Advanced Magnetic Resonance Technology at Stanford P41 RR009784.

References:

1. R. Katz-Brull, P. T. Lavin, and R. E. Lenkinski, “Clinical utility of proton magnetic resonance spectroscopy in characterizing breast lesions,” J Natl Cancer Inst **94**, 1197-1203 (2002).

2. R. Woodhams, K. Matsunaga, S. Kan, H. Hata, M. Ozaki, K. Iwabuchi, M. Kuranami, M. Watanabe, and K. Hayakawa, “ADC mapping of benign and malignant breast tumors,” Magn Reson Med Sci **4**, 35-42 (2005).

3. D. B. Plewes, J. Bishop, A. Samani, and J. Sciarretta, “Visualization and quantification of breast cancer biomechanical properties with magnetic resonance elastography,” Phys Med Biol **45**, 1591-610 (2000).

4. X. Wang, B. W. Pogue, S. J. Jiang, H. Dehghani, X. Song, B. A. Brooksby, K. D. Paulsen, C. Kogel, S. P. Poplack, and W. A. Wells, “Image Reconstruction of effective Mie scattering parameters of breast tissue in vivo with near-infrared tomography,” J Biomed Opt **11**, 041106 (2006).

5. B. W. Pogue, S. P. Poplack, T. O. McBride, W. A. Wells, O. K. S., U. L. Osterberg, and K. D. Paulsen, “Quantitative Hemoglobin Tomography with Diffuse Near-Infrared Spectroscopy: Pilot Results in the Breast,” Radiology **218**, 261-6 (2001).

6. A. A. Gilad, T. Israely, H. Dafni, G. Meir, B. Cohen, and M. Neeman, “Functional and molecular mapping of uncoupling between vascular permeability and loss of vascular maturation in ovarian carcinoma xenografts: The role of stroma cells in tumor angiogenesis,” Int J Cancer **117**, 202-211 (2005).

7. A. Rauscher, J. Sedlacik, M. Barth, E. M. Haacke, and J. R. Reichenbach,

"Noninvasive assessment of vascular architecture and function during modulated blood oxygenation using susceptibility weighted magnetic resonance imaging," Magn Reson Med **54**, 87-95 (2005).

8. S. Dische, M. I. Saunders, R. Sealy, I. D. Werner, N. Verma, C. Foy, and S. M. Bentzen, "Carcinoma of the cervix and the use of hyperbaric oxygen with radiotherapy: a report of a randomised controlled trial," Radiother and Oncol **53**, 93-98 (1999).

9. R. Choe, S. D. Konecky, A. Corlu, K. Lee, T. Durduran, D. R. Busch, B. Czerniecki, J. Tchou, D. L. Fraker, A. DeMichele, B. Chance, E. Putt, M. D. Schnall, M. A. Rosen, and A. G. Yodh, "Differentiation of benign and malignant breast lesions by in-vivo three-dimensional diffuse optical tomography," Cancer Res **69**, 102S-102S (2009).

10. M. Schweiger and S. R. Arridge, "Optical tomographic reconstruction in a complex head model using a priori region boundary information," Phys Med Biol **44**, 2703-21 (1999).

11. S. Jiang, B. Pogue, A. Laughney, C. Kogel, and K. Paulsen, "Measurement of pressure-displacement kinetics of hemoglobin in normal breast tissue with near-infrared spectral imaging," Appl Optics **48**, D130-D136 (2009).

12. B. Brooksby, S. Jiang, H. Dehghani, B. W. Pogue, K. D. Paulsen, C. Kogel, M. Doyley, J. B. Weaver, and S. P. Poplack, "Magnetic Resonance-Guided Near-Infrared Tomography of the Breast," Rev Sci Instr **75**, 5262-5270 (2004).

13. C. M. Carpenter, B. W. Pogue, S. J. Jiang, H. Dehghani, X. Wang, K. D. Paulsen, W. A. Wells, J. Forero, C. Kogel, J. B. Weaver, S. P. Poplack, and P. A. Kaufman, "Image-guided spectroscopy provides molecular specific information in vivo: MRI-guided spectroscopy of breast cancer hemoglobin, water, and scatterer size," Opt Lett **32**, 933-

935 (2007).

14. C. M. Carpenter, R. Rakow-Penner, S. Jiang, B. W. Pogue, G. H. Glover, and K. D. Paulsen, "Inducing and Monitoring Hemodynamic Changes in the Healthy Breast," *in preparation*.

15. M. J. Brischetto, R. P. Millman, D. D. Peterson, D. A. Silage, and A. I. Pack, "Effect of Aging on Ventilatory Response to Exercise and Co2," J Appl Phys **56**, 1143-1150 (1984).

16. T. O. McBride, B. W. Pogue, U. L. Osterberg, and K. D. Paulsen, "Strategies for absolute calibration of near infrared tomographic tissue imaging," Adv Exp Med Biol **530**, 85-99 (2003).

17. H. Xu, R. Springett, H. Dehghani, B. W. Pogue, K. D. Paulsen, and J. F. Dunn, "Magnetic-resonance-imaging--coupled broadband near-infrared tomography system for small animal brain studies," Appl Opt **44**, 2177-2188 (2005).

18. S. R. Arridge and J. C. Hebden, "Optical imaging in medicine: II. Modelling and reconstruction," Phys Med Biol **42**, 841-53 (1997).

19. H. Dehghani, B. W. Pogue, J. Shudong, B. Brooksby, and K. D. Paulsen, "Three-dimensional optical tomography: resolution in small-object imaging," Appl Optics **42**, 3117-28 (2003).

20. P. K. Yalavarthy, B. W. Pogue, H. Dehghani, and K. D. Paulsen, "Weight-Matrix Structured Regularization Provides Optical Generalized Least-Squares Estimate in Diffuse Optical Tomography," Med Phys **34**, 2085-98 (2007).

21. R. B. King, A. Deussen, G. M. Raymond, and J. B. Bassingthwaighte, "A vascular transport operator," Am J Physiol **265**, H2196-208 (1993).

22. B. R. Rosen, J. W. Belliveau, J. M. Vevea, and T. J. Brady, “Perfusion Imaging with NMR Contrast Agents,” Magn Reson Med **14**, 249-265 (1990).

23. P. Vaupel, F. Kallinowski, and P. Okunieff, “Blood Flow, Oxygen and Nutrient Supply, and Metabolic Microenviroment of Human Tumors: A Review,” Cancer Res **49**, 6449-6465 (1989).

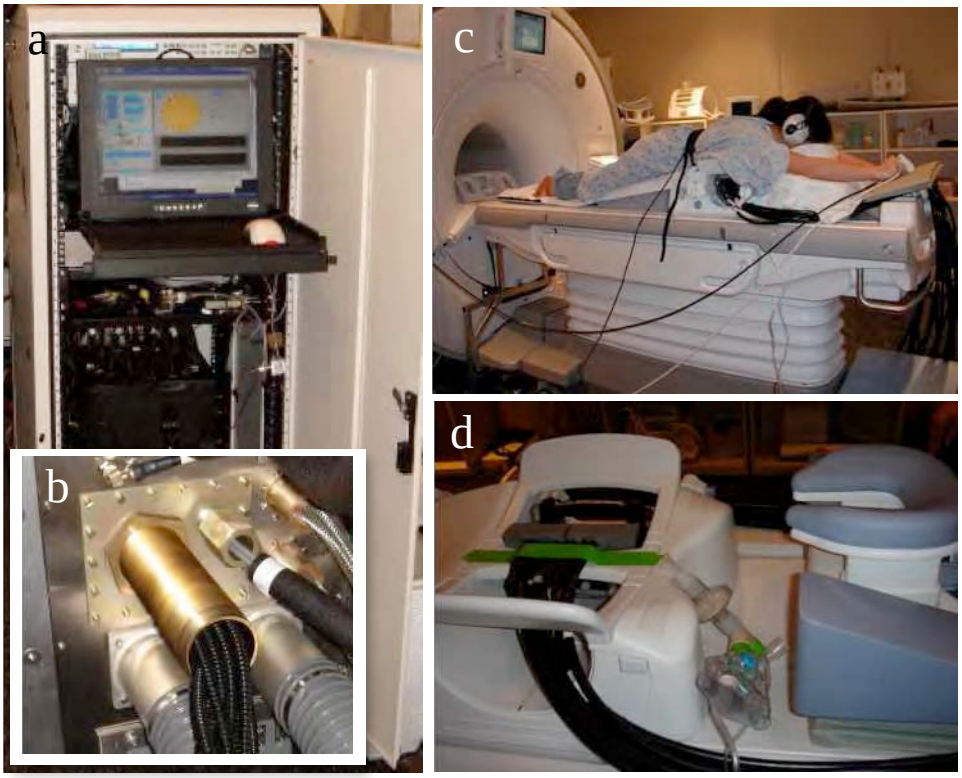

Figure 1: (a) The optical imaging instrument was operated within the MR equipment room. (b) The optical fibers entered the MR room through a shielded conduit in the wall, and (c,d) coupled to a custom interface within a MR breast coil. The respiratory apparatus is shown in (d) without the subject in place. The 3T magnet was used to provide anatomical reference, and was also used in a simultaneous study to measure BOLD changes in the breast (see text).

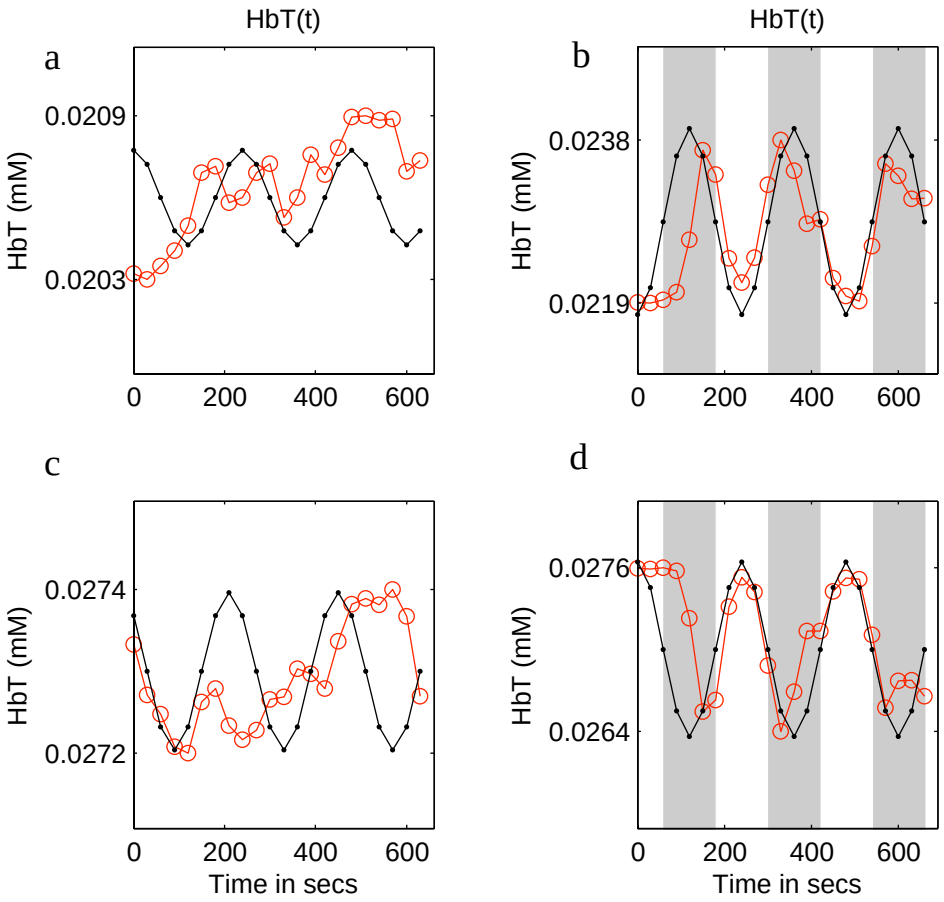

Figure 2: (a,b) Modulation of total hemoglobin in the healthy fibroglandular tissue (red, open circles) during (a) air/air breathing, and during (b) oxygen/carbogen breathing, compared to a best fit sinusoidal (black, closed circles). In (c,d), the total hemoglobin from just the tumor tissue (red, open circles) during (a) air/air breathing, and during (b) oxygen/carbogen breathing, compared to a best fit sinusoidal (black, closed circles).

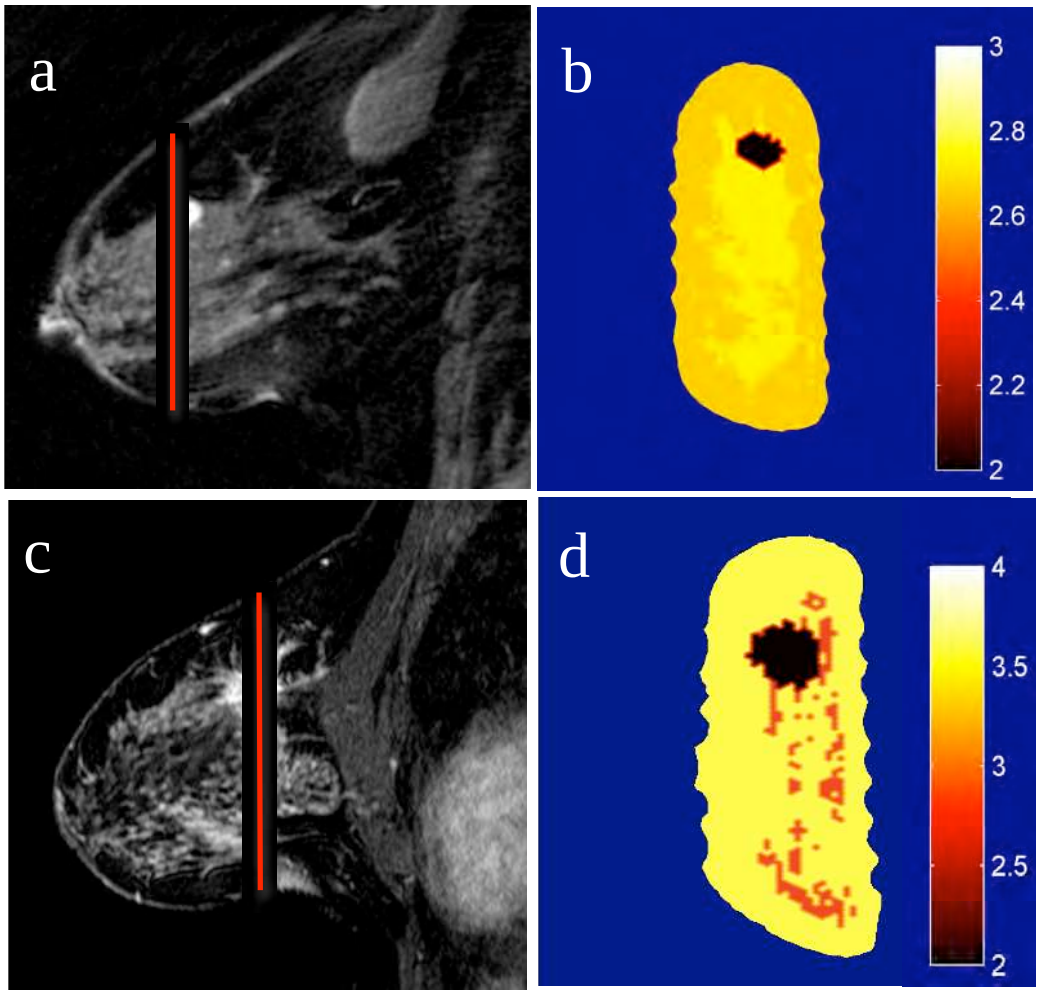

Figure 3: (a) CE-MR images of subject 1 and (c) subject 2 with invasive ductal carcinoma of the breast. The red vertical line indicates the coronal data collection plane sampled by the optical imaging system. In (b) and (d) are correlation images of total hemoglobin for subject 1 and subject 2, respectively. The tumor tissue shows lower Gas to AIR change than the background tissue.

MRI-guided near-infrared spectroscopy of breast tumors

C. M. Carpenter
S. Jiang
S. Srinivasan
B.W. Pogue
K. D. Paulsen

Thayer School of Engineering, Dartmouth College, Hanover, NH, USA.

Method has a unique ability to map hemoglobin, water and lipid content in tissue.

Image-guided near-infrared spectral tomography was developed for the detection and characterization of breast cancer because of its unique ability to map hemoglobin, water, and lipid content in tissue. The method uses measurements of light transmitted through the breast at multiple wavelengths to quantify the spectral absorption and elastic scattering properties of tissue.

Breast cancers have been shown to have higher hemoglobin and water content and lower lipid fraction relative to normal parenchyma [1-5]. Because of its modest cost and use of non-ionizing radiation, the technique can be applied to monitor tissue without safety concerns, and integrates with magnetic resonance (MR) breast imaging. Introduction of near-infrared spectroscopy (NIRS) into an existing 3T Achieva MR scanner is demonstrated and representative case studies are presented that show results for intrinsic tumor spectroscopy.

NIRS shows potential for both breast screening and treatment monitoring.

In addition to its potential in breast screening [6], NIRS may hold promise in monitoring the effectiveness of chemotherapy [7]. Cerussi et al, [8] showed that breast monitoring with near infrared light was able to predict chemotherapy response in 11 patients within the first week of treatment. In particular, the absolute concentration of total hemoglobin in tumors and the relative differences in deoxyhemoglobin and water in tumors versus normal tissue demonstrated significant separation of treatment responders from non-responders among the women enrolled in the study.

Cost-effectiveness studies of this approach indicate that the technology should be beneficial in the individualization of neoadjuvant chemotherapy, as long as the initial treatment is less than 90% effective and the cure rate can be increased by as little as 1% through a change to an alternate therapy [9].

Admittedly, optical/NIRS imaging of the breast has exhibited limited success in the screening and diagnostic settings. In several clinical trials, improvements in specificity have been reported because of better lesion characterization [10, 11]. Unfortunately, optical mammography has been unable to characterize small lesions (less than 6 mm) when used alone because of its spatial resolution limitations, which are caused by the excessive light scatter in all tissue.

Indeed, both of the larger breast optical imaging studies described in the literature have either noted the poorer characterization of lesions less than 6 mm [11], or excluded lesions smaller than 8 mm altogether [10]. As a result, the focus on breast cancer screening with NIRS has not led to a technology that has gained clinical acceptance for screening. However, alternative applications continue to be explored and carefully evaluated in order to identify the best possible opportunities for NIRS in breast health care [12].

One promising avenue for NIRS is to focus on its spectroscopic strengths in characterizing tissue without requiring high spatial resolution. Image-guided NIRS makes the strategy possible by using the spatial template of the MR image upon which localized spectroscopy is superimposed. This concept was initially demonstrated for individual wavelength imaging in the breast some ten years ago [13, 14].

A more recent version of the approach has exploited multi-spectral measurements to characterize the fibro-fatty constituents within the breast [15,16]. High-resolution spatial guidance from X-ray or MR has demonstrated an improvement in both the spatial resolution and quantification accuracy of NIRS [17-19]. Initial breast cancer images have recently been reported with the approach [20, 21]. The clinical performance of these coregistered multi-

Figure 1. View of the MR guided NIRS breast interface attached to the breast coil on the MR table (left). Optical instrumentation and MR console (right).

modality methods has yet to be fully evaluated in a clinical trial. But the phantom and clinical case studies shown to date clearly indicate that MR-guided NIRS will improve upon the results obtained with stand-alone NIRS imaging.

In this paper, we briefly summarize the MR-guided NIRS system developments that have taken place at Dartmouth Hitchcock Medical Center in collaboration with Philips Research over the last several years. We present several case studies of recent results which illustrate the promise of multi-modality NIRS, not only in terms of improving the performance of optical breast imaging alone, but also in augmenting tumor detection, characterization and monitoring with breast MR.

Methods

Instrumentation

The optical instrumentation, shown in Figure 1, uses 16 fibers that sequentially deliver light from multiple sources (six separate diode lasers covering the 660-850 nm range) and channel the collected light to a bank of photomultiplier tube (PMT) detectors. Light from the six individual diode lasers is delivered through the fibers to the breast, with an intensity modulation frequency of 100 MHz. The transmitted signals are detected by PMTs matched to each fiber.

The resulting signal is mixed down to low frequency, after which its amplitude and phase are measured through A/D capture at each detector. The phase shift of the 100 MHz light is a direct measure of the scattering path-length that the light has traveled through the breast thus allowing separation of the effects of scatter from absorption using a diffusion-based spectral estimation process.

The fiber optic lines extending from the breast to the data acquisition hardware are 13 meters long, and are non-magnetic. The breast interface has been integrated within the plates of an MR breast RF coil, allowing the NIRS data to be recorded while the scanner is in operation. The patient is positioned prone inside the bore of the magnet (Philips Achieva 3T, X-series) with the breast pendant into the fiber array interface.

Early indications show MR-guided NIRS to be an improvement on stand-alone NIRS imaging.

While early work was performed with the fibers in a circular geometry, as presented here, a more advanced version of the system conforms to the standard biopsy plates to facilitate clinical workflow. The current design, consisting of 16 fibers, is a prototype that provides one coronal slice of optical measurements. It is possible to incorporate more fibers for multi-slice data acquisition as is routinely performed in standalone NIRS systems.

MRI was used to acquire anatomical features that were integrated within the NIRS image reconstruction procedure [20]. Specifically, 3D T1-weighted Spin Echo (TR/TE = 900/10, flip angle = 18°) MR images were recorded to separate adipose and fibroglandular tissue, which are expected to have distinct optical properties [16]. Regions of interest, determined by Dynamic Contrast Enhanced MR (DCE-MR), were obtained by injecting a bolus of contrast agent (Magnavist) intravenously. A series of T1-W volume images (TR/TE = 10/6, flip angle 20°) were then acquired after each minute, beginning 40 seconds post-injection.

Image reconstruction

Tissue absorption and scattering characteristics were determined by simultaneously reconstructing the NIRS data at all wavelengths. Light propagation was modeled by the diffusion equation. This accurately describes signal propagation in tissue when scattering dominates over absorption and when source-detector distances are larger than a few scattering lengths [22].

Breast interface allows recording of NIRS data while scanner operating.

To form a spectroscopic set of images, a model based estimation algorithm is used that minimizes the mismatch between the NIR data collected and the quantities computed through the diffusion equation [23, 24]. The method

Figure 2. Physiological properties imaged on the same day of a patient before undergoing chemotherapy using:

▶ Figure 2a. Non MR-guided NIRS.

▶ Figure 2b. NIRS overlaid with the T1-W coronal MR slice in the plane of the optical fibers.

▶ Figure 2c. T1-W coronal MR slice in the plane of the optical fibers.

▶▶ Figure 2d. Dynamic contrast enhanced subtraction MR slice identifying the tumor.

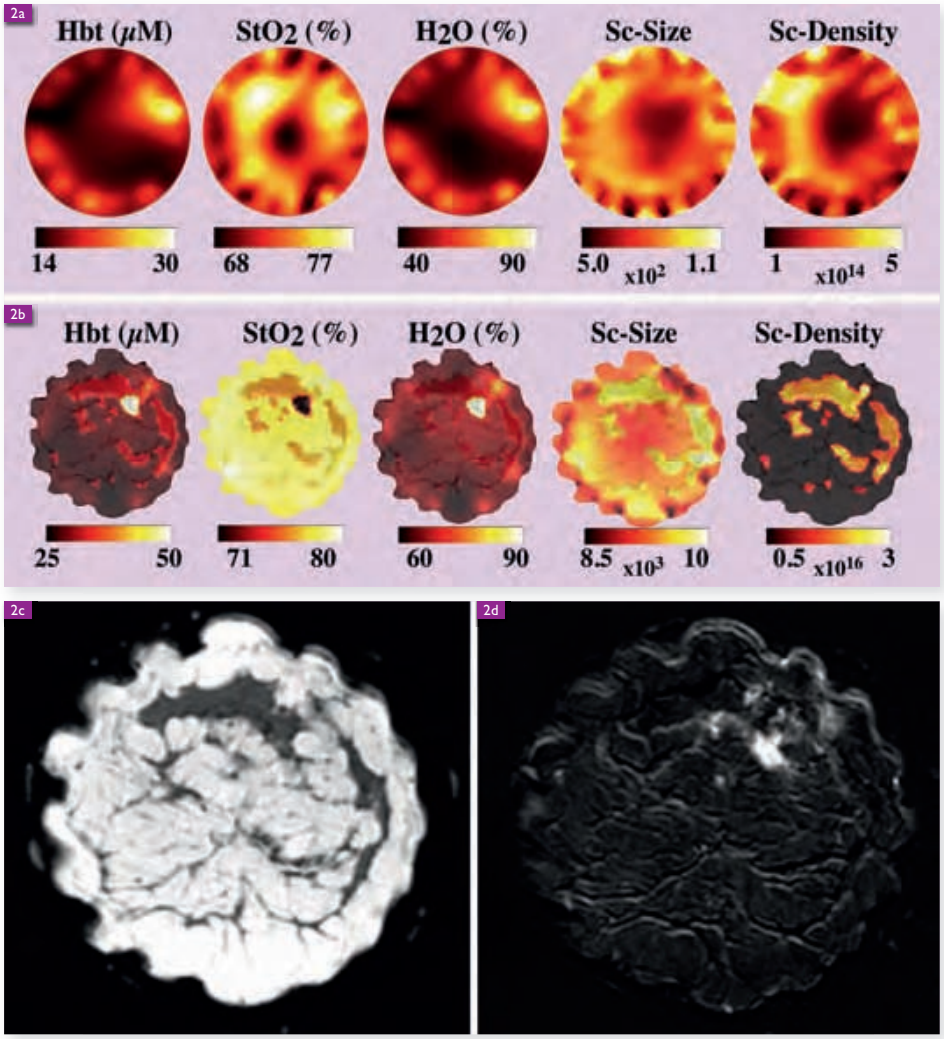

▶ **Imaging results of three patients in various stages of breast cancer treatment described.**

also recovers the tissue scattering spectrum in terms of an effective scatter size and density, since these two factors determine the dominant features associated with the scatter spectrum [25, 26].

MR structural information was incorporated into the reconstruction algorithm to constrain the recovered tissue parameters to within physiologically relevant ranges for each tissue type [18]. In addition, it reduces the number of unknowns to a set of tissue types and regions of interest (ROIs) [27]. This process has been studied extensively, although the type of constraints that should be used is still a subject of considerable research [28].

Patients

In this case-study report, imaging results from three patients are described. The patients were evaluated during various stages of neoadjuvant chemotherapy for breast cancer treatment. All subjects provided informed consent. They were then imaged according to the research study protocols approved by the Institutional Review Board at Dartmouth Hitchcock Medical Center.

Results

Image guided versus non image guided NIRS

A representative example of NIRS image improvement with MR guidance is illustrated in Figure 2. Here a patient, who was an eventual non-responder to neoadjuvant chemotherapy, was examined on the same day before treatment with a stand-alone (Figure. 2a) versus an image guided NIRS system (Figure. 2b). Image guidance leads to a dramatic improvement in contrast localization and contrast delineation of background tissue types that is not evident in the stand-alone diffuse image.

Individual cancer imaging

Three subjects undergoing neoadjuvant chemotherapy were imaged during treatment. These subjects had invasive ductal carcinomas

(IDCs) confirmed via biopsy. These examples show classic contrasts, where the cancer had higher hemoglobin and water contents because of the increased vascularity expected in tumors. Tumors also typically have a higher cellular packing density because of this vascularity, but scattering contrast was not observed in the non-responding cancer case presented below. Imaging results are shown in Figure 3 and Figure 4.

Subject 1

The subject, a 36 year old woman at the time of imaging, had a 3 cm IDC and DCIS lesion in the right breast. Imaging was performed one day after the first cycle of treatment. Results show a decrease in hemoglobin of 20 µM in the region of interest, compared to near 30 µM in the background. Interestingly, the fibroglandular tissue presented lowered hemoglobin that could be due to the large extent of collagen evident in the corresponding mastectomy slice obtained after surgery.

Oxygen saturation in the region was 60% compared to nearly 75% in the background, and water concentration was closer to 40%, compared to 60% in the background. Scattering resulted in an increased particle density near 3.5 x 10^{16}, and particle size was homogeneous near 1 µm across the image plane. The reading radiologist reported a suspicious lesion appearing in the DCE-MR exam that was not apparent on previous MR scans (lower right enhancement in Figure 3c).

Pathology performed seven weeks later revealed a complete response to chemotherapy with no viable tumor remaining. However, there was residual scar tissue in this location (see Figure 3d) that likely contributed to the lower quantities of hemoglobin, oxygenated hemoglobin, and water as compared to the background. This case is an interesting demonstration of where the NIRS findings could have significant diagnostic potential to eliminate the false positive reading from the MR exam that would have resulted in an additional MR-guided biopsy in most cases.

Subject 2

The subject, a 51 year old woman at the time of imaging, had a 7 cm IDC in her left breast. Imaging was performed seven days prior to the first cycle of chemotherapy. MR-NIRS results showed an increase in hemoglobin to greater than 180 µM compared to 40 µM in the background. Hemoglobin oxygenation was 80%, slightly lower than the 85% in the background. Water was elevated to 95% from near 60% in the background.

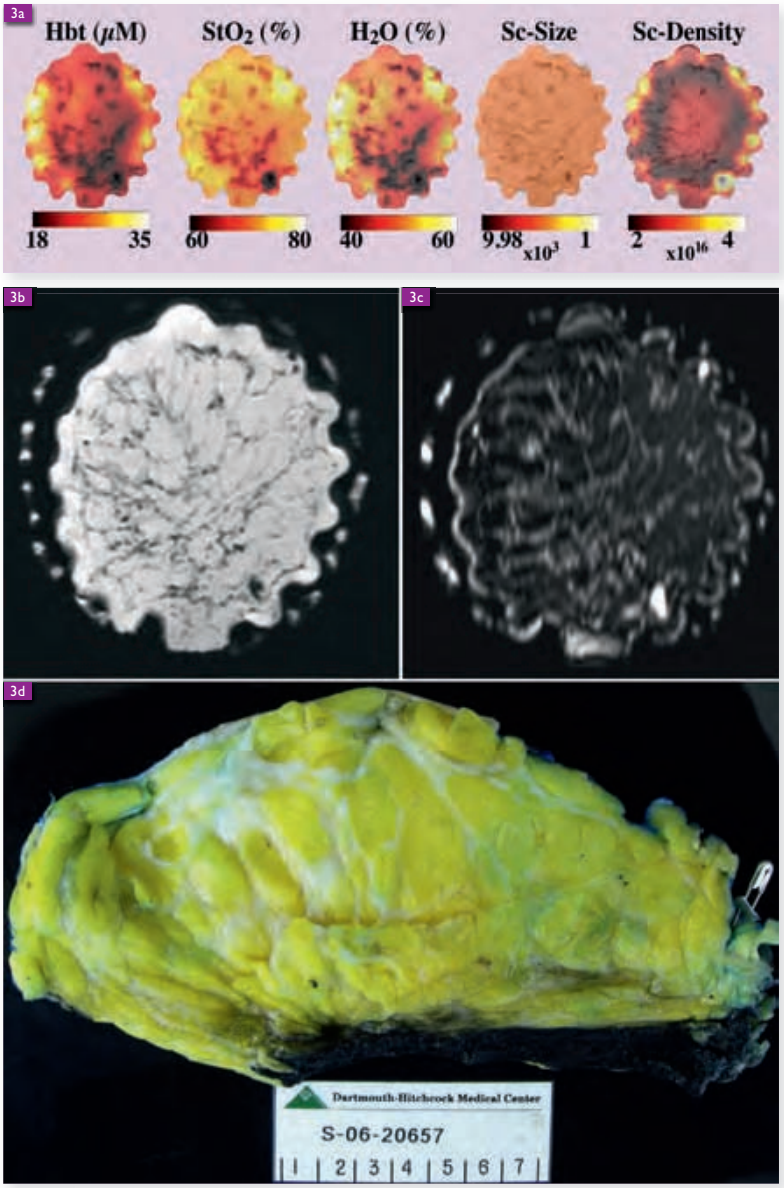

▲

Figure 3a. MR-NIR images overlaid over the T1-W MR slice in the plane of the optical fibers. There is an increase in particle number density, but no change in particle size.

Figure 3b. The T1-W MR slice in the plane of the optical fibers taken two months before surgical mastectomy of a patient who fully responded to chemotherapy. These images show a decrease in hemoglobin, oxygen saturation, and water in the region of interest with respect to the background.

Figure 3c. DCE-MR identifies a suspicious region spatially correlating to a non-fatty area in the T1-W image.

Figure 3d. Pathology showed no viable tumor.

A slight increase in effective scattering particle size to 0.95 µm compared to a background of 1 µm was found in this region, as well as a lower particle number density, around 0.5 x 10^{16} compared to nearly 1x10^{16} in the background. It is important to note that in this case the optical system was not able to fully sample the tumor

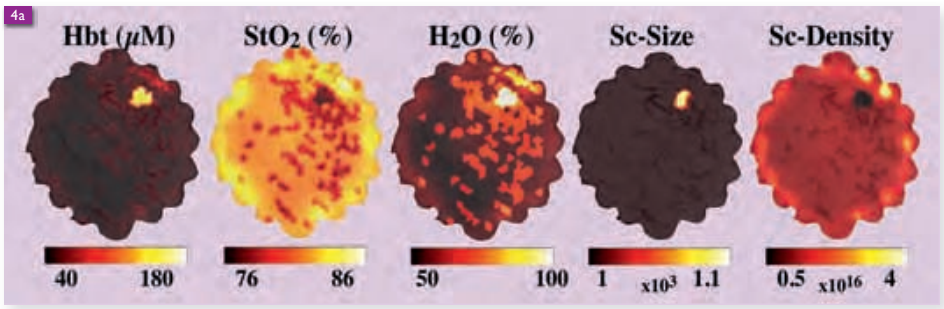

Figure 4a. MR-NIRS images from a patient with IDC in the left breast overlaid on the T1-W MR slice in the plane of the optical fibers. These images show increased hemoglobin, water, and particle size in the region of interest with respect to the background, and decreases in oxygen saturation, and particle density.

Figure 4b. T1-W MR slice in the plane of the optical fibers.

Figure 4c. DCE-MR identifying the lesion.

volume. Instead, a plane was imaged near the extreme posterior aspect of the cancer.

A full mastectomy specimen was not obtained in this case because the patient transferred to another hospital for surgery. Instead, biopsy specimens were used to confirm chemotherapy response.

Subject 3

The subject, a 36 year old woman at the time of imaging, had a 3 cm IDC with three satellite lesions in her left breast upon commencement of neoadjuvant chemotherapy. Multiple imaging sessions were performed over the course of treatment. The subject showed complete response to chemotherapy as confirmed by pathology.

Spectroscopic information shows potential for diagnostics.

The first imaging session occurred one day before her first infusion of chemotherapy. Imaging sessions thereafter were performed within 48 hours of chemotherapy. Figure 5 and Figure 6 demonstrate the volumetric changes in recovered hemoglobin contrast in the regions of interest versus the backgrounds. These MR guided NIRS images were overlaid on the respective DCE-MR views and displayed with VolView software (Kitware, Inc.).

The satellite lesions that were located in the optical fiber plane are visible as increases in hemoglobin over the background, and both are located in the fibro-glandular tissue. In the successive cycle (Figure 6), the volumes of these lesions, as well as total hemoglobin content, decreased.

A summary of the optically recovered properties from three imaging sessions performed over the course of treatment indicate that total hemoglobin decreased, from about 38 μM to about 20 μM, due to the reduction in the tumor size as a response to treatment. Water diminished in the anterior lesion from about 42% to 38%, most likely because of the reduction in functional vascular tissue in the tumor. Oxygen saturation also decreased, likely because of destruction of functioning tumor vasculature, which restricted tumor perfusion.

Discussion

This study presents MR-guided NIRS for delivery of multi-modality breast exams. The ability to obtain spectroscopic information on both the absorbers present in tissue, and the effective scattering particles, is unique, and has the potential to contribute pertinent diagnostic information. The MR-guided recovery of NIRS parameters in Subject 1 was significant because they allowed identification of lesion features that were not suggestive of cancer.

Ultimately, analysis of the tissue removed during surgery confirmed that the lesion, which was enhanced by DCE-MR, was not malignant but a fibrotic scar left after neoadjuvant chemotherapy. While this case was not in need of highly sensitive diagnostic accuracy, it was complex and the additional characterization of the breast would have helped the attending physicians recommend the best treatment option (for example, of mastectomy or not).

Subject 3 represents a case where tracking the response to chemotherapy was important because a significant change in response to neoadjuvant chemotherapy occurred in a breast which

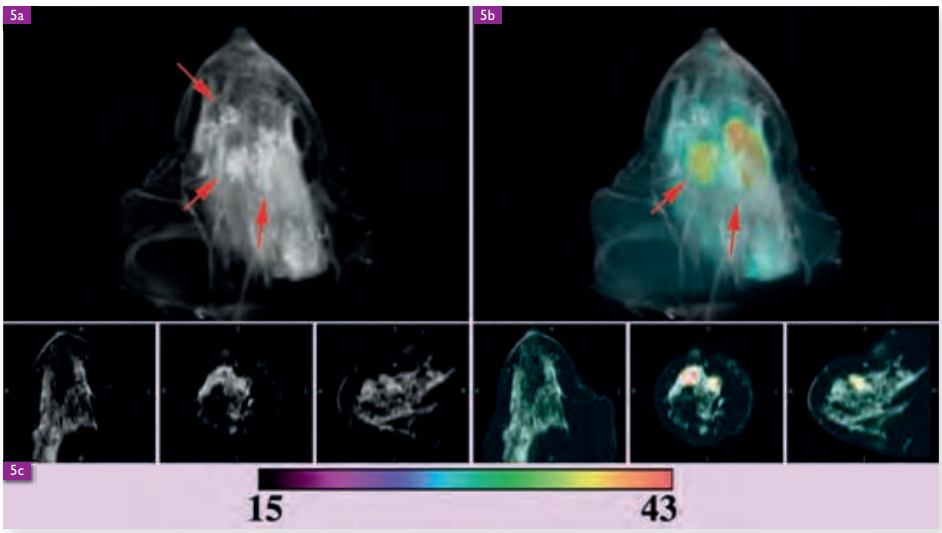

◄◄
Figure 5a. DCE MR images of a patient with an IDC acquired one day before chemotherapy show slight enhancement of one main node with three satellite lesions.

◄
Figure 5b. MR-NIRS images overlaid on 5a). The lesions that were in the plane of the optical fibers of the MR-NIR instrument show increased hemoglobin over the background.

Figure 5c. Color bar used for quantitative analysis of hemoglobin in 5b.
◄

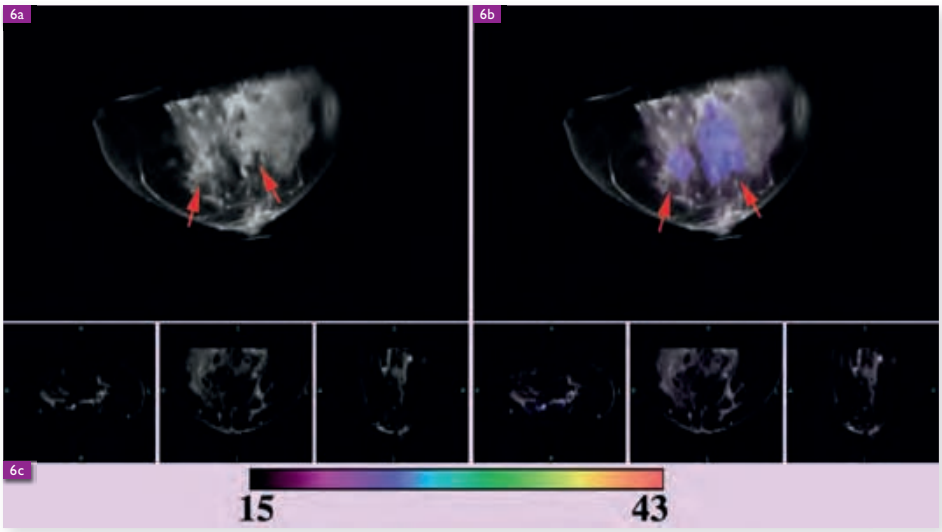

◄◄
Figure 6a. DCE MR images of the patient from Figure 5 taken within 48 hours after the second cycle of chemotherapy. It is difficult to discern here, but only two lesions enhance, indicating response to chemotherapy.
Note the decrease in hemoglobin between Figure 6b and Fig. 5b, demonstrating the response. Pathology (not shown) taken after the completion of chemotherapy indicated a complete response.

Figure 6c. Color bar has been duplicated here for comparison.
◄

presented with multiple lesions. Following each of these lesions with biopsy is not practical in many circumstances. Hence, the additional spectroscopic data can be used to inform the case management [29].

As enrollment in the study presented here is ongoing a more comprehensive summary data will be published in the future. From a system design and performance evaluation perspective, the NIRS components have little impact on MR scanner performance and exam administration. Future versions of the NIRS breast interface will have the optical fibers integrated into biopsy plates, allowing more space for positioning of the breast in the fiber array, which is of particular interest in the ongoing collaboration between Dartmouth Hitchcock Medical Center and Philips Research in Hamburg.

Acknowledgments
This work has been funded by the National Institutes of Health grants RO1CA78734 and PO1CA80139 as well as Philips Research ■

References

[1] Pogue BW, Poplack SP, McBride TO, Wells WA, Osterman Sunshine K, Osterberg UL, Paulsen KD. *Quantitative Hemoglobin Tomography with Diffuse Near-Infrared Spectroscopy: Pilot Results in the Breast.* Radiology. 2001; 218(1): 261-266.

[2] Srinivasan S, Pogue BW, Brooksby B, Jiang S, Dehghani H, Kogel C, et al. *Near-Infrared Characterization of Breast Tumors In-Vivo using Spectrally-Constrained Reconstruction*. Tech. Cancer Res. Treat. 2005; 4(5): 513-526.

[3] Fantini S, Walker SA, Franceschini MA, Kaschke M, Schlag PM, Moesta KT. *Assessment of the Size, Position, and Optical Properties of Breast Tumors in vivo by Noninvasive Optical Methods.* Applied Optics. 1998; 37(10): 1982-1989.

[4] Grosenick D, Wabnitz H, Moesta KT, Mucke J, Moller M, Stroszczynski C, et al. *Concentration and Oxygen Saturation of Hemoglobin of 50 Breast Tumors Determined by Time-Domain Optical Mammography.* Phys. Med. Biol. 2004: 47(9): 1165-1181.

[5] Cerussi A, Shah N, Hsiang D, Durkin A, Butler J, Tromberg BJ. *In vivo Absorption, Scattering, and Physiologic Properties of 58 Malignant Breast Tumors Determined by Broadband Diffuse Optical Spectroscopy.* Journal of Biomedical Optics. 2006; 11(4): 044005.

[6] Intes X. *Time-Domain Optical Mammography SoftScan: Initial Results.* Academic Radiology. 2005; 12(8): 934-947.

[7] Choe R, Corlu A, Lee K, Durduran T, Konecky SD, Grosicka-Koptyra M, et al. *Diffuse Optical Tomography of Breast Cancer during Neoadjuvant Chemotherapy: a Case Study with Comparison to MRI.* Medical Physics. 2005; 32(4): 1128-1139.

[8] Cerussi A, Hsiang D, Shah N, Mehta R, Durkin A, Butler J, Tromberg BJ. *Predicting Response to Breast Cancer Neoadjuvant Chemotherapy using Diffuse Optical Spectroscopy.* Proceedings of the National Academy of Sciences of the United States of America. 2007; 104(10): 4014-4019.

[9] Schegerin M, Kaufman PA, Tosteson ANA, Paulsen KD, Pogue BW. *Prognostic Imaging in Neoadjuvant Chemotherapy of Locally-Advanced Breast Cancer should be Cost-Effective.* Breast Cancer Research and Treatment. 2009; 114: 537-547.

[10] Chance B, Nioka S, Zhang J, Conant EF, Hwang E, Briest S, et al. *Breast Cancer Detection Based on Incremental Biochemical and Physiological Properties of Breast Cancers: A Six-Year, Two-Site Study.* Academic Radiology. 2005; 12(8): 925-933.

[11] Poplack SP, Paulsen KD, Hartov A, Meaney PM, Pogue BW, Tosteson, TD, et al. *Electromagnetic Breast Imaging - Pilot Results in Women with Abnormal Mammography.* Radiology. 2007; 243(2): 350-359.

[12] Tromberg BJ, Pogue BW, Paulsen KD, Yodh AG, Boas DA, Cerussi AE. *Assessing the Future of Diffuse Optical Imaging Technologies for Breast Cancer Management.* Med. Phys. 2008; 35(6): 2443-2451.

[13] Ntziachristos V, Ma XH, Chance B. *Time-Correlated Single Photon Counting Imager for Simultaneous Magnetic Resonance and Near-Infrared Mammography.* Review of Scientific Instruments. 1998; 69(12): 4221-4233.

[14] Ntziachristos V, Yodh AG, Schnall M, Chance B. *Concurrent MRI and Diffuse Optical Tomography of Breast after Indocyanine Green Enhancement.* Proceedings of the National Academy of Sciences of the United States of America. 2000; 97(6): 2767-2772.

[15] Brooksby B, Jiang S, Dehghani H, Pogue BW, Paulsen KD, Kogel C, et al. *Magnetic Resonance-Guided Near-Infrared Tomography of the Breast.* Rev. Sci. Instr. 2004; 75(12): 5262-5270.

[16] Brooksby B, Pogue BW, Jiang S, Dehghani H, Srinivasan S, Kogel C, et al. *Imaging Breast Adipose and Fibroglandular Tissue Molecular Signatures using Hybrid MRI-Guided Near-Infrared Spectral Tomography.* Proceedings of the National Academy of Sciences of the United States of America. 2006; 103(23): 8828-8833.

[17] Brooksby B, Jiang S, Dehghani H, Pogue BW, Paulsen KD, Weaver JB, et al. *Combining near Infrared Tomography and Magnetic Resonance Imaging to Study in vivo Breast Tissue: Implementation of a Laplacian-Type Regularization to Incorporate MR Structure.* J. Biomed. Opt. 2005; 10(5): 050504-1-10.

[18] Intes X, Maloux C, Guven M, Yazici T, Chance B. *Diffuse Optical Tomography with Physiological and Spatial a priori Constraints.* Phys. Med. Biol. 2004; 49: N155-N163.

[19] Li A, Miller EL, Kilmer ME, Brukilaccio TJ, Chaves T, Stott J, et al. *Tomographic Optical Breast Imaging Guided by Three-Dimensional Mammography.* Applied Optics. 2003; 42(25): 5181-5190.

[20] Carpenter CM, Pogue BW, Jiang S, Dehghani H, Wang X, Paulsen KD, et al. *Image-Guided Optical Spectroscopy Provides Molecular-Specific Information in vivo: MRI-Guided Spectroscopy of Breast Cancer Hemoglobin, Water, and Scatterer Size.* Optics Letters. 2007; 32(8): 933-935.

[21] Carpenter CM, Srinivasan D, Pogue BW, Paulsen KD. *Methodology Development for Three-Dimensional MR-guided Near Infrared Spectroscopy of Breast Tumors.* Optics Express. 2008; 16:17903-17914.

[22] Arridge SR, Schweiger M. *Photon-Measurement Density Functions. Part 2: Finite-Element-Method Calculations.* Appl Opt. 1995; 34: 8026-8037.

[23] Srinivasan S, Pogue BW, Jiang S, Dehghani H, Kogel C, Soho S, et al. *Interpreting Hemoglobin and Water Concentration, Oxygen Saturation, and Scattering Measured by Near-Infrared Tomography of Normal Breast In Vivo.* Proc. Nat. Acad. Sci. USA. 2003; 100(21): 12349-12354.

[24] Srinivasan S, Pogue BW, Jiang S, Dehghani H, Paulsen KD. *Spectrally Constrained Chromophore and Scattering NIR Tomography Improves Quantification and Robustness of Reconstruction.* Appl. Opt. 2004; 44(10): 1858-1869.

[25] Wang X, Pogue BW, Jiang S, Dehghani H, Song X, Srinivasan S, et al. *Image Reconstruction of Effective Mie Scattering Parameters of Breast Tissue In Vivo with Near-Infrared Tomography.* J. Biomed. Opt. 2006; 11(4): 041106.

[26] Wang X, Pogue BW, Jiang S, Song X, Paulsen KD, Kogel C, et al. *Approximation of Mie Scattering Parameters from Near-Infrared Tomography of Healthy Breast Tissue In Vivo.* J. Biomed. Opt. 2005; 10(5): 051704-1-10.

[27] Dehghani H, Pogue BW, Jiang S, Brooksby B, Paulsen KD. *Three Dimensional Optical Tomography: Resolution in Small Object Imaging.* Applied Optics. 2003; 42(1): 135-145.

[28] Yalavarthy PK, Pogue BW, Dehghani H, Paulsen KD. *Weight-Matrix Structured Regularization Provides Optimal Generalized Least-Squares Estimate in Diffuse Optical Tomography.* Medical Physics. 2007; 34(6): 2085-2098.

[29] Brooksby B, Srinivasan S, Jiang S, Dehghani H, Pogue BW, Paulsen KD, et al. *Spectral-Prior Information Improves Near-Infrared Diffuse Tomography more than Spatial-Prior.* Opt. Lett. 2005; 30(15): 1968-1970.

Methodology Development for 3 Dimensional MR-Guided Near Infrared Spectroscopy of Breast Tumors

Colin M. Carpenter, Subhadra Srinivasan, Brian W. Pogue, and Keith D. Paulsen

Thayer School of Engineering, Dartmouth College
Hanover, N.H., 03755
colinc@dartmouth.edu

Abstract: Combined Magnetic Resonance (MR) and Near Infrared Spectroscopy (NIRS) has been proposed as a unique method to quantify hemodynamics, water content, and cellular size and packing density of breast tumors, as these tissue constituents can be quantified with increased resolution and overlaid on the structural features identified by the MR. However, the choices in how to reconstruct and visualize this information can have a dramatic impact on the feasibility of implementing this modality in the clinic. This is especially true in 3 dimensions, as there is often limited optical sampling of the breast tissue, and methods need to accurately reflect the tissue composition. In this paper, the implementation and display of fully 3D MR image-guided NIRS is outlined and demonstrated using *in vivo* data from three healthy women and a volunteer undergoing neoadjuvant chemotherapy. Additionally, a display feature presented here scales the transparency of the optical images to the sensitivity of the measurements, providing a logical way to incorporate partial volume sets of optical images onto the MR volume. These concepts are demonstrated with 3D data sets using Volview software online.

OCIS codes: (170.0170) Medical optics and biotechnology, (170.3660) Light propagation in tissues, (100.3010) Image reconstruction techniques

References and links

1. B. Bone, Z. Pentek, L. Perbeck, and B. Veress, "Diagnostic accuracy of mammography and contrast-enhanced mr imaging in 238 histologically verified breast lesions.," *Acta. Radiol.*, vol. 38, no. 4 Pt 1, pp. 489–496, 1997.
2. D. Bluemke, C. Gatsonis, M. Chen, G. DeAngelis, N. DeBruhl, S. Harms, S. Heywang-Kobrunner, N. Hylton, C. Kuhl, C. Lehman, E. Pisano, P. Causer, S. Schnitt, S. Smazal, C. Stelling, P. Weatherall, and M. Schnall, "Magnetic resonance imaging of the breast prior to biopsy," *JAMA-Journal of the American Medical Association*, vol. 292, no. 22, 2004.
3. S. Orel and M. Schnall, "Mr imaging of the breast for detection, diagnosis, and staging of breast cancer," *Radiology*, vol. 220, pp. 13–30, 2001.
4. P. Hathaway, D. Mankoff, K. Maravilla, M. Austin-Seymour, G. Ellis, J. Gralow, A. Cortese, C. Hayes, and R. Mode, "Value of combined fdg pet and mr imaging in the evaluation of suspected recurrent local-regional creast cancer: Preliminary experience," *Radiology*, vol. 210, 1999.
5. C. Catana, D. Procissi, Y. Wu, M. Judenhofer, J. Qi, B. Pichler, R. Jacobs, and S. Cherry, "Simultaneous in vivo positron emission tomography and magnetic resonance imaging," *Proc. Natl. Acad. Sci. USA*, vol. 105, no. 10, 2008.
6. R. Sinkus, K. Siegmann, T. Xydeas, M. Tanter, C. Claussen, and M. Fink, "Mr elastography of breast lesions: Understanding the solid/liquid duality can improve the specificity of contrast-enhanced mr mammography," *Magnet. Reson. Med.*, vol. 58, 2007.

7. E. Van Houten, M. Doyley, F. Kennedy, J. Weaver, and K. Paulsen, "Initial in vivo experience with steady-state subzone-based mr elastography of the human breast," *JMRI-J. Magn. Reson. Im.*, vol. 17, 2002.
8. V. Ntziachristos, A. G. Yodh, M. Schnall, and B. Chance, "Concurrent mri and diffuse optical tomography of breast after indocyanine green enhancement," *Proc. Natl. Acad. Sci. USA*, vol. 97, no. 6, pp. 2767–72, 2000.
9. V. Ntziachristos, A. G. Yodh, M. D. Schnall, and B. Chance, "Mri-guided diffuse optical spectroscopy of malignant and benign breast lesions," *Neoplasia*, vol. 4, no. 4, pp. 347–54, 2002. Using Smart Source Parsing Jul-Aug.
10. B. Brooksby, S. Jiang, H. Dehghani, B. W. Pogue, K. D. Paulsen, C. Kogel, M. Doyley, J. B. Weaver, and S. P. Poplack, "Magnetic resonance-guided near-infrared tomography of the breast," *Rev. Sci. Instr.*, vol. 75, no. 12, pp. 5262–5270, 2004.
11. B. Brooksby, B. W. Pogue, S. Jiang, H. Dehghani, S. Srinivasan, C. Kogel, T. Tosteson, J. B. Weaver, S. P. Poplack, and K. D. Paulsen, "Imaging breast adipose and fibroglandular tissue molecular signatures using hybrid mri-guided near-infrared spectral tomography," *Proc. Natl. Acad. Sci. USA*, vol. 103, pp. 8828–8833, 2006.
12. D. Townsend and S. Cherry, "Combining anatomy and function: the path to true image fusion," *Eur. Radiol.*, vol. 11, 2001.
13. S. Srinivasan, B. W. Pogue, B. Brooksby, S. Jiang, H. Dehghani, C. Kogel, W. A. Wells, S. Poplack, and K. D. Paulsen, "Near-infrared characterization of breast tumors in-vivo using spectrally-constrained reconstruction," *Tech. Cancer Res. Treat.*, vol. 4, no. 5, pp. 513–526, 2005.
14. B. W. Pogue, S. P. Poplack, T. O. McBride, W. A. Wells, O. K. S., U. L. Osterberg, and K. D. Paulsen, "Quantitative hemoglobin tomography with diffuse near-infrared spectroscopy: Pilot results in the breast," *Radiology*, vol. 218, no. 1, pp. 261–6, 2001.
15. A. Cerrusi, N. Shah, D. Hsiang, A. Durkin, J. Butler, and B. Tromberg, "In vivo absorption, scattering, and physiologic properties of 58 malignant breast tumors determined by broadband diffuse optical spectroscopy," *J. Biomed. Opt.*, vol. 11, no. 4, 2006.
16. S. Fantini, S. A. Walker, M. A. Franceschini, M. Kaschke, P. M. Schlag, and K. T. Moesta, "Assessment of the size, position, and optical properties of breast tumors in vivo by noninvasive optical methods," *Appl. Opt.*, vol. 37, no. 10, pp. 1982–1989, 1998.
17. D. Grosenick, K. Moesta, H. Wabnitz, J. Mucke, C. Stroszczynski, R. Macdonald, P. Schlag, and H. Rinneberg, "Time-domain optical mammography: Initial clinical results on detection and characterization of breast tumors," *Appl. Opt.*, vol. 42, no. 16, 2003.
18. B. Chance, S. Nioka, J. Zhang, E. Conant, E. Hwang, S. Briest, S. Orel, M. Schnall, and B. Czerniecki, "Breast cancer detection based on incremental biochemical and physiological properties of breast cancers: A six-year, two-site study," *Acad. Radiol.*, vol. 12, no. 8, 2005.
19. S. Poplack, T. Tosteson, W. Wells, B. Pogue, P. Meaney, A. Hartov, C. Kogel, S. Soho, J. Gibson, and K. Paulsen, "Electromagnetic breast imaging: Results of a pilot study in women with abnormal mammograms," *Radiology*, vol. 243, no. 2, 2007.
20. B. Brooksby, S. Jiang, H. Dehghani, B. W. Pogue, K. D. Paulsen, J. B. Weaver, C. Kogel, and S. P. Poplack, "Combining near infrared tomography and magnetic resonance imaging to study in vivo breast tissue: implementation of a laplacian-type regularization to incorporate mr structure," *J. Biomed. Opt.*, vol. 10, no. 5, pp. 050504–1–10, 2005.
21. X. Intes, C. Maloux, M. Guven, T. Yazici, and B. Chance, "Diffuse optical tomography with physiological and spatial a priori constraints," *Phys. Med. Biol.*, vol. 49, pp. N155–N163, 2004.
22. A. Li, E. L. Miller, M. E. Kilmer, T. J. Brukilaccio, T. Chaves, J. Stott, Q. Zhang, T. Wu, M. Choriton, R. H. Moore, D. B. Kopans, and D. A. Boas, "Tomographic optical breast imaging guided by three-dimensional mammography," *Appl. Opt.*, vol. 42, no. 25, pp. 5181–5190, 2003.
23. P. Yalavarthy, B. Pogue, H. Dehghani, C. Carpenter, S. Jiang, and K. Paulsen, "Structural information within regularization matrices improves near infrared diffuse optical tomography," *Opt. Express*, vol. 15, no. 13, 2007.
24. C. Carpenter, B. Pogue, S. Jiang, H. Dehghani, X. Wang, K. Paulsen, W. Wells, J. Forero, C. Kogel, J. Weaver, S. Poplack, and P. Kaufman, "Image-guided spectroscopy provides molecular specific information in vivo: Mri-guided spectroscopy of breast cancer hemoglobin, water, and scatterer size," *Opt. Lett.*, vol. 32, no. 8, pp. 933–935, 2007.
25. H. Dehghani, B. W. Pogue, S. Jiang, B. A. Brooksby, and K. D. Paulsen, "Three-dimensional optical tomography: resolution in small-object imaging," *Appl. Opt.*, vol. 42, no. 16, pp. 3117–3128, 2003.
26. T. O. McBride, B. W. Pogue, E. Gerety, S. Poplack, U. L. Osterberg, and K. D. Paulsen, "Spectroscopic diffuse optical tomography for quantitatively assessing hemoglobin concentration and oxygenation in tissue," *Appl. Opt.*, vol. 38, no. 25, pp. 5480–90, 1999.
27. S. R. Arridge and M. Schweiger, "Photon-measurement density functions. part 2: Finite-element-method calculations," *Appl. Opt.*, vol. 34, pp. 8026–8037, 1995.
28. S. R. Arridge, S. M., and D. T. Delpy, "Iterative reconstruction of near infrared absorption images," *Proc. SPIE*, vol. 1767, pp. 372–383, 1992.
29. A. Corlu, R. Choe, T. Durduran, K. Lee, M. Schweiger, S. R. Arridge, E. M. Hillman, and A. G. Yodh, "Diffuse optical tomography with spectral constraints and wavelength optimization," *Appl. Opt.*, vol. 44, no. 11, pp. 2082–

93, 2005. Using Smart Source Parsing Apr 10.
30. S. Srinivasan, B. W. Pogue, S. Jiang, H. Dehghani, and K. D. Paulsen, "Spectrally constrained chromophore and scattering NIR tomography improves quantification and robustness of reconstruction," *Appl. Opt.*, vol. 44, no. 10, pp. 1858–1869, 2004.
31. T. O. McBride, B. W. Pogue, S. Jiang, U. L. Osterberg, and K. D. Paulsen, "Development and calibration of a parallel modulated near-infrared tomography system for hemoglobin imaging in vivo," *Rev. Sci. Instr.*, vol. 72, no. 3, pp. 1817–1824, 2001.
32. P. Yalavarthy, B. Pogue, H. Dehghani, and K. Paulsen, "Weight-matrix structured regularization provides optical generalized least-squares estimate in diffuse optical tomography," *Med. Phys.*, vol. 34, no. 6, 2007.
33. M. Schweiger, I. Nissila, D. Boas, and S. Arridge, "Image reconstruction in the presence of coupling errors," *Appl. Opt.*, vol. 46, no. 14, 2007.
34. J. Zhang, J. Sullivan, H. Yu, and Z. Wu, "Image-guided multimodality registration and visualization for breast cancer detection," in *SPIE* (R. Gallowat and K. Cleary, eds.), vol. 5744, pp. 123–133, 2005.
35. S. Fantini, M. A. Francheschini, A. Cerussi, J. S. Maier, S. A. Walker, B. Barbieri, B. Chance, and E. Gratton, "The effect of water in the quantitation of hemoglobin concentration in a tissue-like phantom by near-infrared spectroscopy," *Biophys. J.*, vol. 70, no. 2, pp. WP343–WP343, 1996. Part 2.
36. T. O. McBride, B. W. Pogue, S. Jiang, U. L. Osterberg, K. D. Paulsen, and S. P. Poplack, "Multi-spectral near-infrared tomography: a case study in compensating for water and lipid content in hemoglobin imaging of the breast," *J. Biomed. Opt.*, vol. 7, no. 1, pp. 72–79, 2001.
37. A. E. Cerussi, D. Jakubowski, N. Shah, F. Bevilacqua, R. Lanning, A. J. Berger, D. Hsiang, J. Butler, R. F. Holcombe, and B. J. Tromberg, "Spectroscopy enhances the information content of optical mammography," *J. Biomed. Opt.*, vol. 7, no. 1, pp. 60–71, 2002. Using Smart Source Parsing Jan.
38. A. Li, G. Boverman, Y. Zhang, D. Brooks, E. Miller, M. Kilmer, Q. Zhang, E. Hillman, and D. Boas, "Optical linear inverse solution with multiple priors in diffuse optical tomography," *Appl. Opt.*, vol. 44, no. 10, 2005.
39. S. Merritt, S. Gulsen, G. Chiou, Y. Chu, C. Deng, A. Cerussi, A. Durkin, B. Tromberg, and O. Nalcioglu, "Comparison of water and lipid content measurements using diffuse optical spectroscopy and mri in emulsion phantoms," *Tech. Cancer Res. Treat.*, vol. 2, no. 6, 2003.

1. Introduction

The current standard of care in breast cancer imaging, consisting of ultrasound, xray, and MR mammography, only provides a fraction of the total available information that could be obtained diagnostically. It is not surprising then, that there has been considerable effort in identifying new approaches which attempt to improve upon the unsatisfactory specificity [1–3] of breast cancer imaging. The ideal approach would add additional contrast to these systems to discriminate malignant tumors from the surrounding benign or healthy tissue [4–8]. The integration of optics into standard breast cancer imaging systems is one promising area. Optical imaging provides functional information which should improve lesion characterization, thereby reducing unnecessary breast biopsies. Innovations to improve its capabilities have included better instrumentation, more sophisticated computational algorithms, contrast agents, and more recently, image guided approaches which integrate the higher resolution of a complimentary modality into optical imaging to improve contrast recovery [9, 10]. While several pilot studies using this method have been carried out [9, 11], a major factor limiting more comprehensive studies has been the lack of a practical approach to combine these modalities. This paper discusses the latest software tools and methodology which have enabled 3 dimensional MR-guided diffuse optical imaging of breast cancer *in vivo* to become a practical procedure.

A synergistic multimodal approach is possible when one modality provides good structural feature identification, while the other provides functional or molecular information about the features [12]. MR imaging has encouraged perhaps more multimodality interest than xray mammography recently because its extremely high sensitivity might enable a complimentary technology to aid in specificity. Diffuse optical tomography (DOT) can fill this need because it gives information about tissue health by providing images of total hemoglobin, hemoglobin oxygen saturation, water content, lipid content, and scattering properties. Breast cancers have been shown in select studies to have higher hemoglobin and water content than normal tissue, and lower lipid content [13–17]. This technique has shown varying degrees of success, depending

on study protocol [18, 19], and generally improves upon the specificity of breast characterization. However, the accuracy of optical mammography with small lesions below the resolution limit of $\sim \frac{1}{2}$ cm is limited, as both larger-scale studies either noted poorer characterization of lesions ($<$ 6mm) [19], or excluded them altogether [18]. It has been shown that the inclusion of high resolution spatial guidance from xray or MR improves the spatial resolution and quantification of optical imaging [20–22], often by as much as 35%, depending on technique [23].

To date, most clinical studies of optical mammography involving the use of multimodality spatial guidance have been focused on planar acquisitions limited to two dimensions for practical reasons. Yet optical imaging in three dimensions is critical because of the more accurate models of light propagation in 3D, and the difficulty in positioning the optical probes directly over the region of interest with planar or sparse data sampling, especially when the lesion is not palpable. Additionally, there is a need to modify 3D visualization tools to appropriately weight the display of optical data to the sensitivity of the measurements, so that clinicians are not mislead about reconstructed tissue contents which may lie far outside the sampling volume.

The main reason for this limitation in technique has to date been the computational burden of volumetric reconstruction, as shown in Figure 1, and the effects of poorly sampled tissues on the inverse problem. It is clear that when advancing DOT or simultaneous MR-DOT to three dimensions, the number of unknowns grows by orders of magnitude. However, by using the MR to guide the separation of unique tissue types which can be characterized spectroscopically (MRg-NIRS), this modality becomes much more practical, and yet preserves the spatial fidelity of the original MR images. This paper presents the methodology and implementation of reconstruction and visualization of MR-guided NIRS in three dimensions, and results from phantom experiments and female breast tissue *in vivo*.

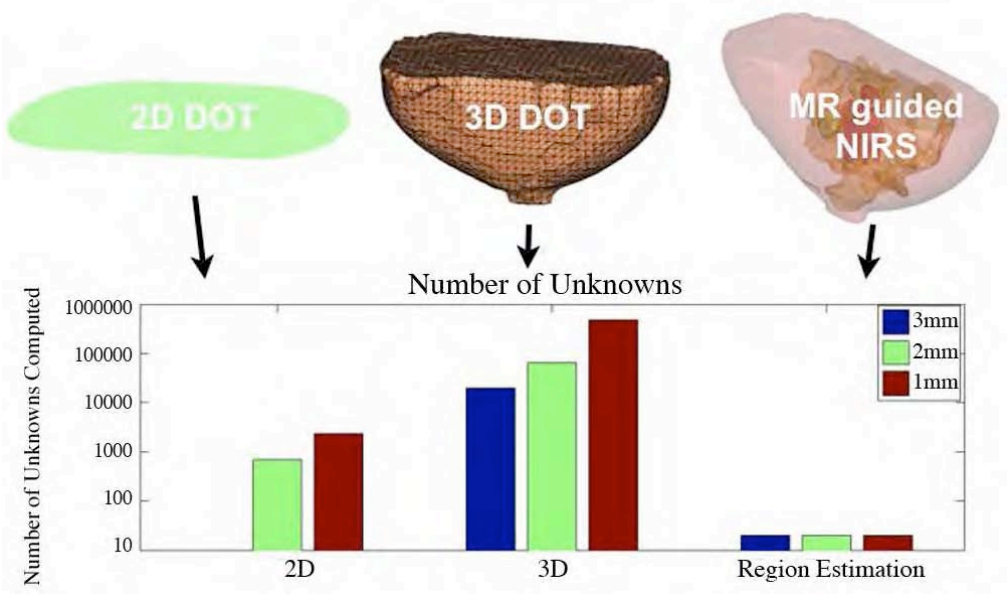

Fig. 1: Comparison of the number of chromophores to be computed for 2D DOT, 3D DOT, and MR guided DOT.

2. Methods

2.1. Instrumentation

The MR-NIRS system uses 6 intensity modulated laser diodes in the near infrared spectrum to illuminate the breast tissue. Sixteen fiber bundles are bifurcated so that the source and detector fibers are housed in the same optodes which are in contact with the skin. Source positions are moved sequentially around the breast while the amplitude and phase of transmitted light is detected with photomultiplier tubes at 15 detector locations for each source position. Fiber bundles pass through a conduit from the MR console room into the MR scanner room and into a patient interface which clips on to a commercial breast MR coil. More details about the instrumentation can be found in [10].

This study used a 3 Tesla Philips Achieva magnet to acquire anatomical and contrast enhanced images used in the optical image reconstruction procedure [24]. Specifically, T1-weighted Spin Echo (TR/TE = 900/10, flip angle = 90°) MR images are taken to differentiate between adipose and fibroglandular tissue. Dynamic Contrast Enhanced MR (DCE-MR) is acquired by injecting an MR contrast agent (Magnavist, Schering) intravenously, and taking sets of T1-W Gradient Echo volume images (TR/TE = 10/6, flip angle 20°) each minute. Contrast subtraction images are formed by subtracting the post contrast dynamic images from the pre contrast images. These images are used to identify suspect lesions, which are also confirmed as suspicious by a radiologist (S.P., R.D-A).

Coregistration between the optical and MRI domains requires knowledge of the location of the optical fibers in the MR anatomical images. Because the optical and MRI data are taken simultaneously, these modalities can be accurately coregistered to within 1mm. Accuracy in optode placement less than 2-3 cm is essential to assure high quality reconstructions. The optical fibers can be located in the MR image by identifying the displacement of the tissue caused by the contact between the tissue and the fibers, which extend beyond the breast immobilization plate by 1mm. MR radiological fiducial markers are also used to identify various points of reference in the MR domain.

2.2. Image Formation

A model based image reconstruction algorithm has been used which minimizes the mismatch between the amplitude and phase data collected from the system and a diffusion based model for three-dimensional light propagation in tissue [25] [26]. The lossy diffusion equation, which describes light fluence (Φ) in tissue from source S with frequency ω, has been well studied in turbid media such as tissue, and is an acceptable approximation if scattering (μ_s') dominates over absorption (μ_a), and if source detector distances are more than a few scattering distances apart [27].

$$-\nabla \cdot D\nabla\Phi(r,\omega) + \big(\mu_a + \frac{i\omega}{c}\big)\Phi(r,\omega) = S(r,\omega) \tag{1}$$

Here, D is the diffusion coefficient, defined as $\frac{1}{(3(\mu_s'+\mu_a))}$. Since parameter estimation problems are non-linear, the image formation algorithm, shown below in equation (2), uses an iterative procedure based on a Newton-type minimization method [28] to find the best estimate for the physiological parameters c: oxy hemoglobin, deoxy hemoglobin, water, scatter power, and scatter amplitude [29, 30]. Here, J is the Jacobian matrix, I is the Identity matrix, and δ is the difference between the collected data and the model data produced by (1).

$$\big(J^T J + \lambda I\big)\Delta c = J^T \Delta\delta \tag{2}$$

This equation is known to be ill-posed and is often underdetermined. This is especially true in 3D, and many strategies have been introduced to alleviate the associated effects by constraining

the allowed solution space. We use an iterative Tikhanov optimization routine which adds a regularization parameter, λ, to eliminate improbable solutions [31]. This parameter requires information on both the noise of the system and limitations on the contrast of the imaging domain, and is highly influential on the solutions [32]. This term can be problematic and may seem somewhat arbitrary, as coupling errors which introduce noise are difficult to quantify [33], and determining limitations on contrast is a problem which is case and situation specific.

The incorporation of MR information into the reconstruction algorithm helps solve the dependence of the solution on this parameter, because it alleviates the ill-posed nature of the problem by reducing the parameter space to a set number of tissue types and regions of interest (ROIs). This reduces the unknown parameter space considerably. Additionally, because the high structural resolution is kept intact, this spectroscopic approach is advantageous over other image guided techniques which use the tissue regions only to infer information about tissue contrast [21, 22]. This technique also reduces the burden of reconstructing for features which are so far from the imaging plane that they have no contribution to the data. Reduction in parameters is done by summing the contributions from unknowns in each region in the jacobian; the technique is explained in more detail in a previous publication [25]. Using this technique, solutions are less affected by noise. In this study, image reconstructions were calculated with a regularization parameter of 10. However, recovered values were quite immune to changes in the regularization parameter. With the addition of the high resolution structural information provided by the MR, the imaging procedure becomes a volumetric spectroscopy problem.

2.3. From MR Images to Computational Domains

Incorporating MR images into the image reconstruction is non-trivial in 3D, and much effort has gone into processing these irregular shaped domains. The steps from image segmentation to volumetric meshing and region labeling are overviewed in Figure 2. Tissue types were identified in 3D with a commercial software package (Mimics, Materialise NV). Structural MR (T1-W) images were taken to separate the adipose tissue from the fibroglandular tissue. Dynamic contrast enhanced MR was used to delineate suspect regions of interest from the background. These MR images were all taken in the same geometry, so volumes segmented from the DCE-MR could be imported directly into the structural MR image. The outer surface of the adipose layer was input into a software package MIVA [34] to create a volumetric finite element mesh required to solve equation (1). This mesh was imported back into Mimics and tagged with tissue material region labels for use in the image reconstruction algorithm. The meshes used in this study had an average of 2.5 mm/node resolution, which usually formed meshes of 40,000 nodes.

2.4. 3-Dimensional Image Visualization

The images presented in this paper show recovered contrast in each MR-defined tissue type. However, images presented in this way can be misleading because of the decrease in sensitivity of the detectors to contrasts at distance. The distance limit on contrast recovery depends on both the intrinsic contrast and the system properties. Therefore, the volumes presented in this work have used a transparency setting which is proportional to the sensitivity of the measurements to the contrast in each tissue voxel. This relation, the Jacobian, is shown in equation 3, where β is a scaling parameter which is adjusted so that the transparency is zero 1 cm above the center fiber array, and Φ is the amplitude for absorbing and phase for scattering chromophores, c. By scaling the transparency to the Jacobian matrix values, tissue properties far outside the imaging plane will not be seen and misinterpreted as true contrasts.

$$\alpha = \beta \frac{\partial \Phi}{\partial c} \tag{3}$$

2.5. *Human Subject Imaging*

Imaging protocol for the subject examinations was approved by the Committee for the Protection of Human Subjects at Dartmouth Hitchcock Medical Center. Written consent was obtained from all subjects. The subjects were positioned in the MR breast coil on the MR table and optical fibers in a slab type geometry were brought into contact with the tissue. Because of the desire for light compression, some optical fibers on some exams did not contact the breast, but at least 14 of 16 were in contact for all exams. Optical fibers were located on MR images taken in the sagittal or axial geometries with the aid of fiducial markers placed on the optical interface. Optical exams were performed simultaneously with MR exams, and usually took about 15 minutes. MR exams were completed within 45 minutes.

3. Results

3.1. *Phantom Imaging Results*

The accuracy of MR guided NIRS in 3D was tested on a gelatin phantom with a cylindrical inclusion 1.6 cm in diameter in a slab (12 x 6.4 cm). For the background, porcine blood was mixed at the appropriate concentration into a solution of Phosphate Buffered Saline (PBS), gelatin, and titanium oxide particles once the temperature of the stirring mixture cooled sufficiently. This solution was cooled in a refrigerator with a test tube sunk near the boundary until the solution set into a hard phantom. A mixture of PBS, intralipid, and porcine blood was added to the hole remaining from the extracted test tube. The inclusion had an expected value for total hemoglobin of 0.02 milliMolar (mM), and the background of 0.01 mM, for an expected contrast of 2:1. There was no contrast expected in water, which was quantified using MRI 3-Point Dixon water fat separation. There was no expected contrast in scatter, as the

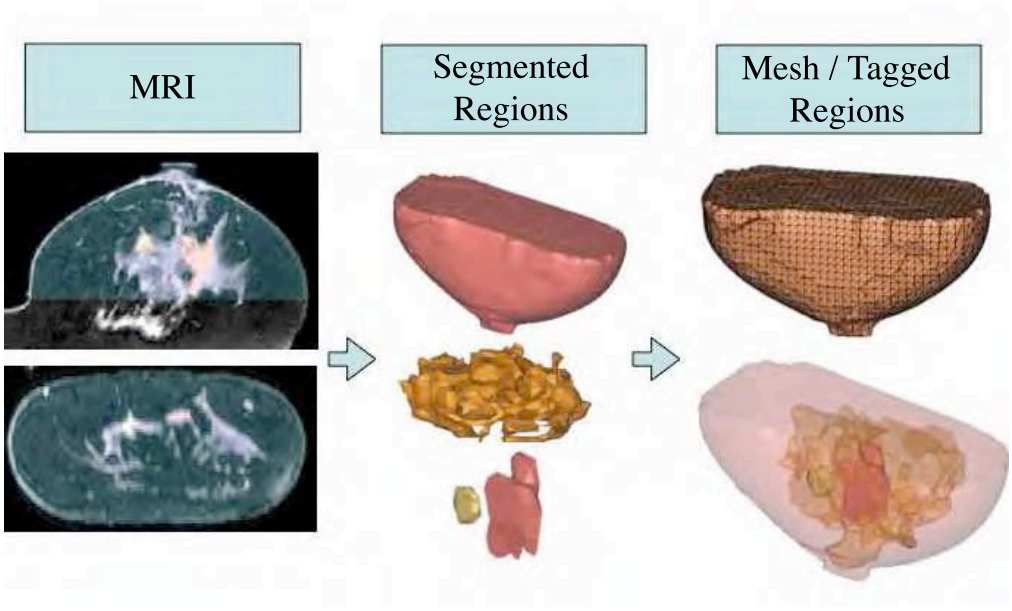

Fig. 2: Transforming MRI images for computational use requires 1) Segmentation of tissue types into adipose, fibroglandular, and suspicious lesions, 2) Creating a finite element mesh of the volume from surface rendering, and 3) Tagging the mesh with tissue regions.

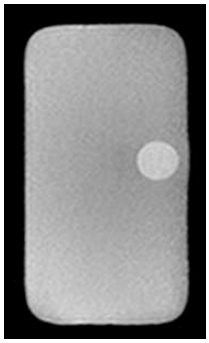

(a) MR image of the gelatin phantom.

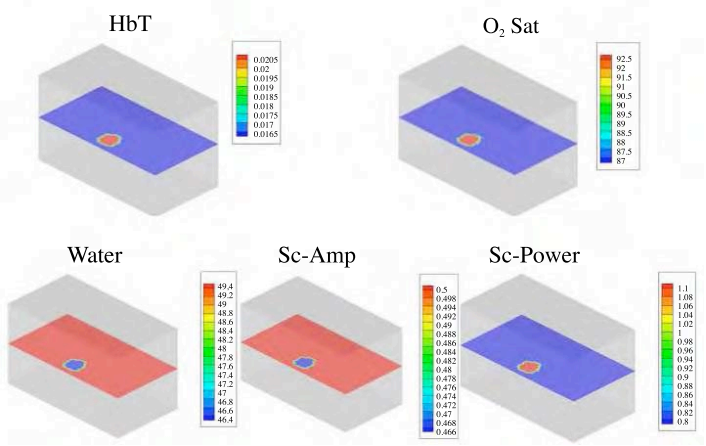

(b) Total hemoglobin (in mM), Oxygen Saturation (in %), Water (in %), Scatter-Amplitude, and Scatter Power.

Fig. 3: 3D gelatin phantom results.

appropriate amount of intralipid was added to match the scattering of the background, as confirmed by imaging of the bulk solution in the system. Figure 3a shows a T2-W MR image of the phantom. The reconstructed results shown in Figure 3b show that total hemoglobin in the inclusion reaches the expected value. The background total hemoglobin is elevated by about 60% over the expected contrast. This could be explained from the crosstalk between water and oxy-hemoglobin which is expected because of the limitation of the PMT optical detectors in the long wavelengths above 850nm as discussed below. However, this crosstalk is expected to be greater in this phantom than in human tissue because gelatin mixtures have nearly twice the water of human tissue. The variations in oxygen saturation and water were just over 6%, and the variations for scatter amplitude and power were just over 8% and 37%.

3.2. Human Breast Imaging Results

3D imaging of breast tissue was applied to data from three healthy subjects. The patient interface was adjusted to apply light compression to the breast so that the optodes were in contact with the breast. Figure 4 shows the results which are comparable to previously published 2D results of 11 subjects with the same system [11], and are in the range typically found in the breast. It is expected that total hemoglobin and water both increase in the fibroglandular tissue compared to the adipose tissue because of the increase in vasculature in the fibroglandular tissue.

A 33 yr old patient undergoing neo-adjuvant chemotherapy was scanned with the system 1 day after the second cycle of chemotherapy and 4 months before surgery. This patient had a 3cm invasive ductal carcinoma with 3 satellite lesions as identified by DCE-MR shown in Figure 5a. Because this patient responded to chemotherapy, the recovered contrasts between the tumors and the fibroglandular tissue in the optical imaging plane were reduced compared to earlier in the treatment cycle, but were still evident at this stage. Optical and MR results from a later date (not shown) show very little contrast compared to the fibroglandular tissue. Recovered chromophore values are shown in Figure 5b.

The values of total hemoglobin in the 2 tumor masses in the imaging plane were about 20 μM in the main lesion and about 19 μM in the satellite lesion in the plane of the opti-

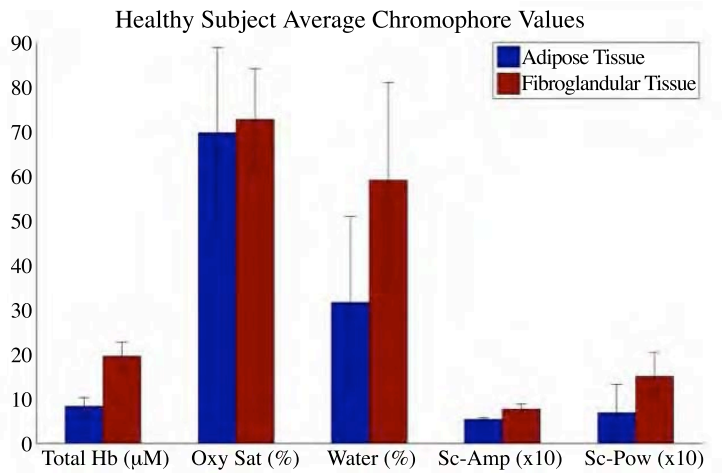

Fig. 4: Mean and standard devation chromophore values for 3D recovered optical contrasts for 3 healthy subjects.

cal fibers. These values are elevated compared to the fibroglandular tissue at 17 μM, and the adipose layer at 16 μM. This trend is expected in breast cancer because of the increased vasculature that is inherent to tumors, although the contrast in this imaging session is lower, most likely due to the response to chemotherapy treatment. The decrease in oxygen saturation from 75% in the fibroglandular tissue to 52% in the tumor masses are also expected because of the increase in metabolic activity related to growth. In previous work, water has been shown to be elevated in tumor tissue to values above 50% compared to the background [13, 15, 24]. In this case, the main lesion is slightly higher at 52% compared to 51% and 48% in the surrounding tissue. Interestingly, the satellite lesion is at the same water content as the fibroglandular, at 49%, perhaps indicating less inflammation than the main lesion. However, this result should be interpreted with less certainty because of the limitations in water recovery demonstrated in phantom imaging. Contrast is found in scattering amplitude in both lesions compared to the surrounding tissue, but not in scattering power. Scattering has been shown to correlate to microvascular density, and differences in microvascular density are expected in tumor tissue. These results were also compared to imaging results from a standalone optical tomography system (not shown), and quantification appears to be quite similar, although the spatial resolution of the standalone system is poorer because of the lack of MR guidance. Further investigations are underway to determine the benefits of using MR-NIRS for monitoring neoadjuvant chemotherapy.

Figure 6 shows examples of 3D interactive images of total hemoglobin, oxygen saturation, water, and scattering properties overlaid on the MR image for this subject. A closer inspection of the effect of scaling the transparency to the Jacobian can be seen in Figure 7. These datasets may be viewed interactively with Volview software, for further investigation.

4. Discussion

Diffuse optical tomography is inherently a 3D problem, and 3D models describe light propagation with more accuracy than 2D models. Additionally, radiologists and clinicians are accustomed to assessing lesions in 3 dimensions. However, non image-guided 3D-DOT is limited in its accuracy due to the ill-posed nature of the inversion problem and the fact that the problem is highly under-determined. Reducing the imaging problem to a NIR spectroscopy problem

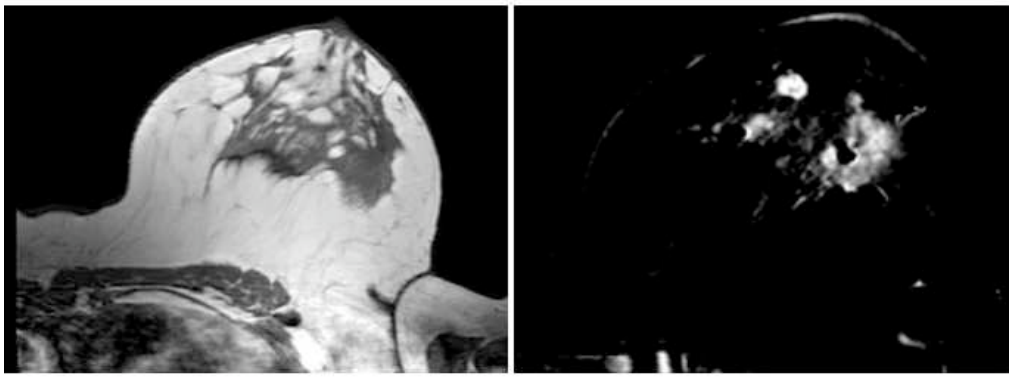

(a) Images of a malignant tumor with three satellite lesions (2 in plane):T1-W Spin Echo MRI image and DCE-MR subtraction image.

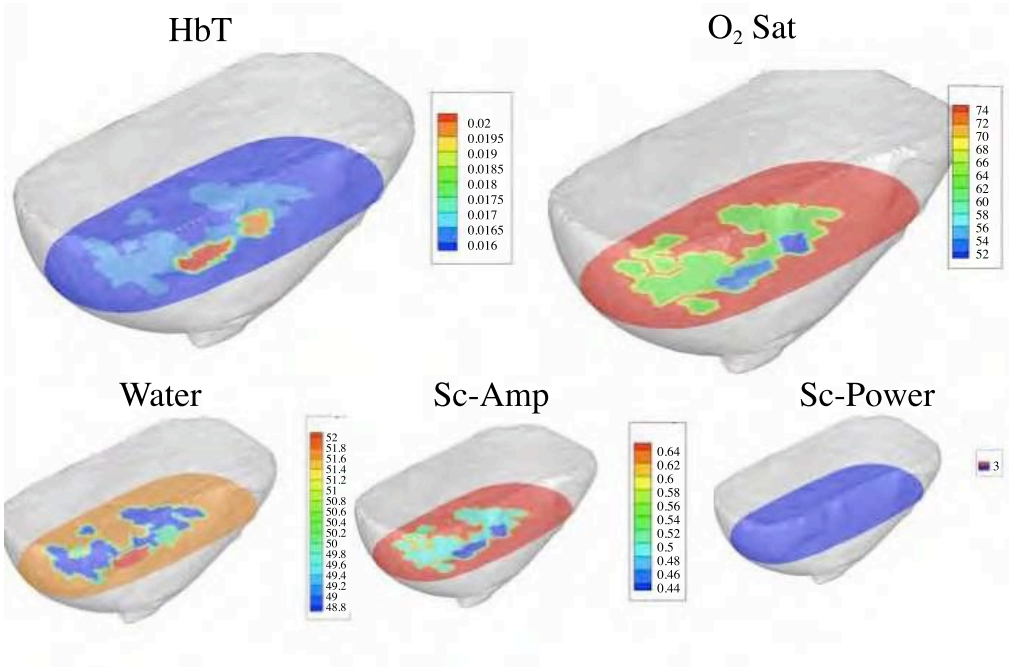

(b) Images of a malignant tumor with three satellite lesions (2 in plane) Total hemoglobin, Oxygen Saturation, Water, Scatter Amplitude, and Scatter Power.

Fig. 5: 3D Reconstructed results of multi-focal IDC of the left breast.

makes the solution more tractable and improves quantification. The MR-guided regionization process demonstrated here provides a huge reduction in memory usage and allows the overlay of optical data onto the MR scan without affecting the image resolution.

This paper has shown several examples of 3D image guided NIRS *in vivo*, with a goal of identifying the optimal way to visualize the data using tools which conform to existing radiological conventions. Phantom studies were completed to validate the contrast recovery, and show reasonable recovery of total hemoglobin in the inclusion. The recovered values for the subjects are within the physiologically expected range. These are the first published 3D MR

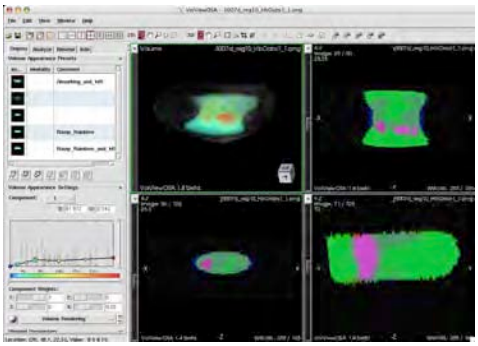

(a) Composite image of Optical absorbing images.

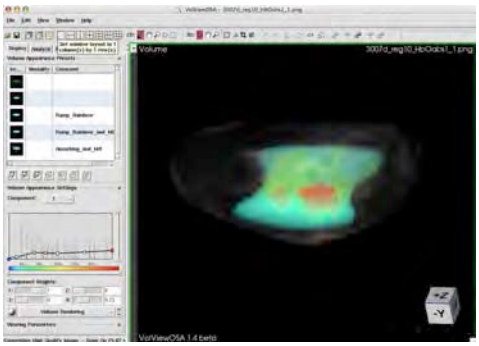

(b) Total Hemoglobin, Oxygen Saturation, Water, Scatter Amplitude, and Scatter Power images.

Fig. 6: Optical and MR overlays of subject from Figure 5.

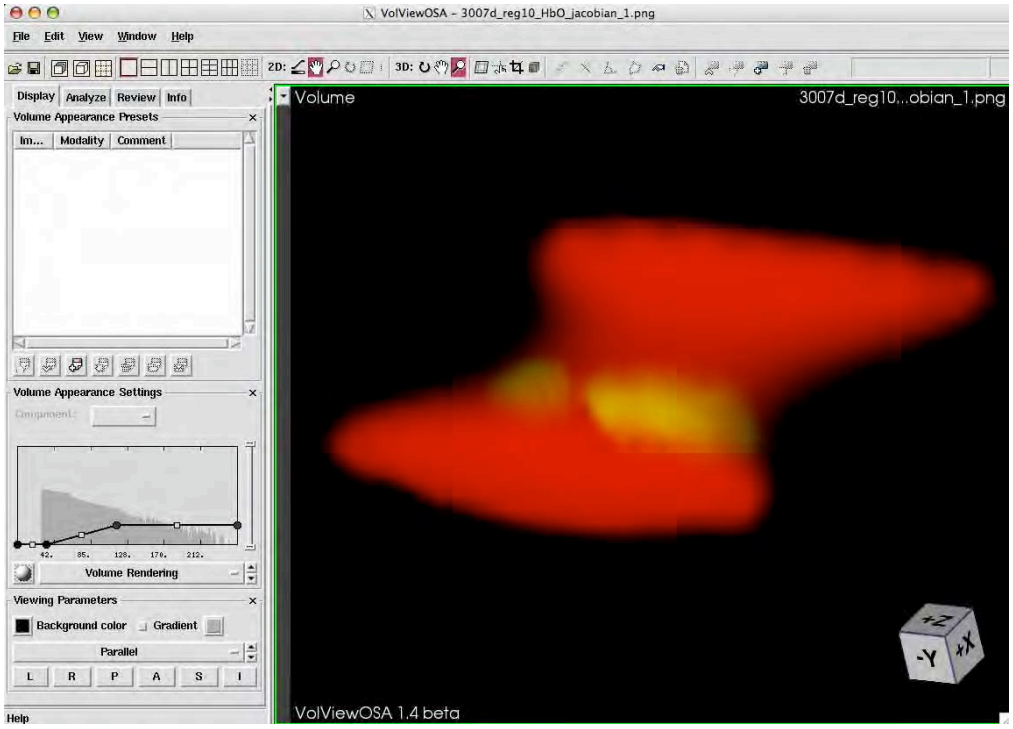

Fig. 7: Effect of scaling the transparency of the recovered properties to the Jacobian. Interactive volume.

guided optical images of healthy tissue and breast cancer, and the results in the malignancy show the expected increase in total hemoglobin and decrease in oxygen saturation.

An important exception to the expected values is the inaccuracy in the recovery of water concentration. This limitation is well known [35] [36] [37], and arises from the exclusion of longer wavelength diodes above 900nm which would better quantify the water spectrum. However, the photomultiplier tubes necessary for this application which need fast temporal response and high

gain are not uniformly sensitive from 650nm – 950nm. This limitation yeilds crosstalk between water and oxyhemoglobin. Two approaches are currently underway to address this issue. One involves the use of spectrometers which are sensitive to these longer wavelengths and detect CW light. Coupling these detectors to PMTs would yield valuable quantification of water and lipids. The other approach is to use the MRs ability to separate water and fat. Assuming that the MR and optical are sensitive to the same water and fat, MR water quantification could be coupled to optical methods to further improve the accuracy of physiological parameters [38]. Previous studies [39] prove that this is true in oil/water phantoms.

5. Conclusions

This paper has presented the methodology of 3D segmentation, meshing, spectral fitting, and 3D visualization which enable optical imaging to become a viable, practical tool in the clinic, and was validated with phantoms and healthy and abnormal subjects. The main goal of MR-NIRS is to help radiologists characterize suspicious lesions which have been located *a priori* with DCE-MRI. The steps transforming these MRI images into computational space have been presented and evaluated, with a key addition being a method of displaying the confidence in the optical recovery by scaling the transparency to the Jacobian matrix values in the 3D image. This visualization overlay conforms the optical contrasts to a fused MR dataset to appropriately display the tissue contrasts.

6. Acknowledgements

The authors gratefully thank the contributing radiologists Dr. Steven P. Poplack and Dr. Roberta M. diFlorio-Alexander, and the MRI technicians, Jorge A. Forero and Michael A. Pearl for their time and expertise. This work was funded by the Department of Defense Breast Cancer pre-doctoral fellowship (BC073418) and the National Cancer Institute (P01CA80139).